2012

The effect of sulfur on structure and conversion of bioactive borate glasses

Ali Mohammadkhah

Department:

THE EFFECT OF SULFUR ON STRUCTURE AND CONVERSION OF BIOACTIVE BORATE GLASSES

by

ALI MOHAMMADKHAH

A THESIS

Presented to the Faculty of the Graduate School of the

MISSOURI UNIVERSITY OF SCIENCE AND TECHNOLOGY

In Partial Fulfillment of the Requirements for the Degree

MASTER OF SCIENCE IN MATERIALS SCIENCE AND ENGINEERING

2012

Approved by

Delbert E. Day, Advisor
Richard K. Brow
Mohamed N. Rahaman
Roger F. Brown

PUBLICATION THESIS OPTION

This thesis has been prepared in the style utilized by the Journal of American Ceramic Society. Pages 1-49 and 50-113 will be submitted for publication in that journal. Supplementary data added as an appendix at the end of each paper for the purposes normal to thesis writing.

ABSTRACT

The effect of sulfur on glass structure and the conversion process of bioactive CaO-Li_2O-B_2O_3 glasses were studied. One glass without and two glasses with different amounts of sulfur were made using conventional melting and dry quenching techniques. These glasses reacted with a phosphate solution and converted to hydroxyapatite. Particles (150-355μm) were reacted in 0.25 and 0.5 molar K_2HPO_4 solutions at 37°C for 2 to 96 hours. The weight loss of the particles and the final pH of the solution were measured. The weight loss measurements indicated that the reaction rate increases with increasing the sulfur content. Sulfur was released from the glass, causing the pH of the solution to decrease, but was absent in the reacted layer.

In the *in-vivo* studies, the effect of sulfur and phosphorus on the conversion of two different bioactive borate glasses was studied, *in-vivo*. Discs made from two sulfur-free glasses (CaLB-0 and 93B3-0) and two sulfur-containing glasses (CaLB-12 and 93B3-6) were implanted in a subcutaneous site in rats for 2, 4, and 12 weeks. Each rat remained healthy during the experiment and there were no sign of infection or necrosis at the implantation site.

The CaLB glass discs reacted with the body fluids and formed a thin calcium phosphate reacted layer on their surface, but the 93B3 glass discs reacted to form a thicker calcium phosphate reacted layer with an onion-skin structure. Compared the phosphorus-free CaLB implants to phosphorus-containing 93B3 implants the CaLB implants absorbed 2 times more phosphorus from the body fluids to form the calcium phosphate reacted layer.

Compared to the CaLB implants, the connective tissue attached to the 93B3 implants was ~3 times thicker, and contained more blood vessels and collagen. For all of the sulfur-containing implants sulfur released to the body fluids and was not presented in the reacted materials.

ACKNOWLEDGMENTS

First, I would like to thank my advisor, Dr. Delbert Day, for his guidance throughout my masters' studies. I am very grateful to have had such a patient and supportive advisor. He has stood beside me to the last moment and helped me by giving me advice and guidance. Dr. Day has taught me a lot about glass science and the application of glass as a biomaterial during last two years, but it has been the life lessons that he has passed on that are the most priceless. Dr. Day, simply put, changed the way I see the world. It was my pleasure to be his student.

I would like to thank my committee because of their endless help. Dr. Brow for sharing his knowledge of glass science, Dr. Rahaman for sharing his resources, and Dr. Brown for his comments and help with all *in-vivo* experiments. I would also like to thank Dr. Kimberly Henthorn. She was the reason that I decided to come to Missouri S&T and helped me a lot when I first started my graduate studies. She supported me and encouraged me, enthusiastically, in the pursuit of my ambitions.

To my friends and colleagues, especially Dr. Brow's and Dr. Rahaman's groups, I also wish to extend my thanks for their help with my experiments and tests. Also, a special thanks to the Material Research Center (MRC) and Material Science and Engineering Department staff for all of the help they provided.

Last, but not least, my most sincere thanks and regards for my family, which are my inspiration in life. Although they were not with me during this time in my life, they have always supported me and encouraged me to continue my journey. My Dad inspired me to continue my education to higher levels. My Mom, despite any misgivings, encouraged me to pursue my dreams. She is the reason that I have succeeded-her love and her prayers have kept me going. My sister has been my closest friend throughout my life. She was always there for me when I needed someone to talk to. I would not be here without their love and support. I love them and they are always with me in my heart.

TABLE OF CONTENTS

Page

PUBLICATION THESIS OPTION iii

ABSTRACT iv

ACKNOWLEDGMENTS v

LIST OF ILLUSTRATIONS ix

LIST OF TABLES xiv

PAPER

1: The Effect of Sulfur on Structure and Conversion of Bioactive Borate Glasses. Part I: *In-vitro* Studies 1

Abstract 1

I. Introduction 2

II. Experimental Procedure 5

(1) Glass Compositions and Preparation 5

(2) XRF Measurements 6

(3) Density and Molar Volume 7

(4) Differential Thermal Analysis (DTA) 7

(5) Scanning Electron Microscopy (SEM) and Energy Dispersive Spectroscopy (EDS) 7

(6) X-Ray Diffraction 8

(7) Micro-Raman Spectroscopy 8

(8) Glass Conversion in Phosphate Solution 8

III. Results 9

(1) Glass Formation, Composition, and Properties 9

(2) Glass Micro-Raman Analysis 10

(3) DTA and Crystallization 11

(4) Conversion in Phosphate Solution 12

(5) Phase Identification 12

a. X-Ray Diffraction 12

b. Micro-Raman 13

(6) SEM and Energy Dispersive Spectroscopy (EDS) 13

IV. Discussion 14

(1) Sulfur in the Glass and Glass Structure 14

(2) Glass Conversion 16

V. Conclusion 21

References 23

APPENDIX: SUPPLEMENTARY DATA FOR PAPER 1 42

2: The Effect of Sulfur on Structure and Conversion of Bioactive Borate Glasses. Part II: *In-vivo* Studies 50

Abstract 50

I. Introduction 51

II. Experimental Procedure 54

(1) Glass Compositions and Preparation 54

(2) In-vivo Experiment 55

a. Implant Preparation and Sterilization 55

b. Subcutaneous Implantation in Rats 55

c. Implant Removal and Processing 56

(3) Sample Analysis 57

a. X-Ray Diffraction 57

b. Micro-Raman 58

c. Scanning Electron Microscopy (SEM) and Energy Dispersive Spectroscopy (EDS) 58

d. Histology 59

(4) In-vitro Experiment 59
III. Results 60
(1) Implant Recovery and Tissue Examination 60
(2) SEM and EDS 60
a. Backscattered Electron Microscopy 61
b. Elemental Mapping Analysis 61
(3) Micro-Raman Analysis 63
(4) XRD 64
(5) Histology- Stained Tissue Sections 64
a. H&E Staining 65
i. CaLB Glasses 65
ii. 93B3 Glasses 65
b. CD31 Staining 66
c. Trichrome 67
IV. Discussion 67
(1) Reaction of Glasses In-Vivo 67
a. Reaction Rate and Reacted Layer Structure 67
b. Effect of Sulfur 69
c. Role of Phosphorus 71
(2) Biological Response 75
V. Conclusion 78
References 79
APPENDIX: SUPPLEMENTARY DATA FOR PAPER 2 108
VITA 114

LIST OF ILLUSTRATIONS

PAPER 1

Figure 1. Micro-Raman spectra for CaLB-0%, CaLB-12%, and CaLB-22% glasses. 31

Figure 2. Typical DTA spectra for CaLB-0%, CaLB-12%, and CaLB-22% glasses. T_g = Glass transition temperature, T_x = Crystallization temperature, T_m = Melting, Heating rate=10°C/min....32

Figure 3. Percent weight loss for a sample CaLB glass reacted in (A) 0.25M and (B) 0.5M K_2HPO_4 solutions at 37°C with initial pH= 10. The final pH of the solution after ~96 hours of reaction is given for each glass. The lines are for guidance. The arrows for each glass point to the weight loss after reaction for ~96 hrs. The error bars are estimates based on weighing measurements....33

Figure 4. XRD pattern for the CaLB-0%, CaLB-12%, and CaLB-22% glass particles (150-355μm) after reaction in the 0.5M K_2HPO_4 solution at 37°C for 96 hours. 34

Figure 5. Micro-Raman spectra of particles (150-355μm) reacted in a 0.5M K_2HPO_4 solution at 37°C for 96 hours. Bottom curve is HA (Fisher Scientific St Louis MO- Cat#: C133-212)....35

Figure 6. Phase mapping analysis for calcium (Ca), oxygen (O), phosphorus (P), and sulfur (S) for a CaLB-12% glass particle that had reacted in the 0.5M K_2HPO_4 solution at 37°C for 96 hours. 36

Figure 7. Schematic of incorporation of sulfate ions in the borate glass structure. (A) Shows how vitreous B_2O_3 converts to a cross-linked 3 dimensional structure with No non-bridging oxygen ion at 33 mol% R_2O+RO. (B) Shows how 66.67 B_2O_3. 33.33 R_2O+RO structure converts to 50 B_2O_3. 50 R_2O+RO structure (The CaLB glasses). (C) Adding sulfur to 50 B_2O_3. 50 R_2O+RO structure (The sulfur-containing CaLB glasses). R= Alkali or alkali earth metal. O= Bridging oxygen, O^-=Non-bridging oxygen, S= Sulfur, B= Boron 37

Figure 8. Schematic of the conversion process of CaLB glasses to Hydroxyapatite....38

Figure 9. Reaction kinetic modeling of sulfur-containing CaLB glasses reacted in (A) 0.25M and (B) 0.5M K_2HPO_4 solution at 37°C with initial pH= 10. Horizontal axis is time (hours) and vertical axes are CVM and 3D Diffusion model equations. The normalized weight loss is "α". The equation for each fitted line is provided along with the coefficient of determination for linear regression (R^2). 39

Figure 10. Comparison of the measured weight loss at 48 hours for CaLB glasses reacted in 0.25 and 0.5 molar K_2HPO_4 solution at 37°C with their theoretical weight loss (assuming stoichiometric HA forms). 40

Figure 11. SEM image of the cross section of a CaLB-0% (A and B), CaLB-12% (C), and CaLB-22% particle reacted in 0.5M K_2HPO_4 solution at 37°C for 96 hrs. (B) is a magnified image of the black box showed in (A).....41

APPENDIX: SUPPLEMENTARY DATA FOR PAPER 1

Figure 1. XRD spectra for (A) CaLB-0% glass particles crystallized at 598°C and (B) CaLB-12% glass particles crystallized at 608°C. 43

Figure 2. XRD spectra for (A) CaLB-22% glass particles crystallized at 559°C and (B) CaLB-22% glass particles crystallized at 653°C. 44

Figure 3. Two typical DTA spectra for CaLB-12% glass showing that this spectrum is reproducible. The endothermic peaks ~700°C and the endothermic peak ~950°C is repeated after running this sample again using the same DTA.....45

Figure 4. XRD pattern for the CaLB-0%, CaLB-12%, and CaLB-22% glass particles (150-355μm) after reaction in the 0.25M K_2HPO_4 solution at 37°C for 96 hours. 46

Figure 5. Micro-raman spectra of particles (150-355μm) reacted in a 0.25M K_2HPO_4 solution at 37°C for 96 hours. Bottom curve is HA (Fisher Scientific St Louis MO- Cat#: C133-212).....47

Figure 6. Phase mapping analysis for calcium (Ca), oxygen (O), and phosphorous (P) for a CaLB-0% glass particle that had reacted in the 0.5M K_2HPO_4 solution at 37°C for 96 hours. 48

Figure 7. Phase mapping analysis for calcium (Ca), oxygen (O), and phosphorous (P) for a CaLB-22% glass particle that reacted in the 0.5M K_2HPO_4 solution at 37°C for 96 hours. 49

PAPER 2

Figure 1. Schematic figure showing the subcutaneous site, where one sample of each glass was implanted in six rats. 89

Figure 2. A schematic figure of the disc removed from the subcutaneous site of a rat showing the reacted surface layer and unreacted glass in the cross section of the disc. 90

Figure 3. Appearance of the as made implants before removal after 2, 4, and 12 weeks in a subcutaneous site in a rat. The view shows the implant surface adjacent to the muscle tissue. 91

Figure 4. Appearance of the as made implants before removal after 2, 4, and 12 weeks in a subcutaneous site in a rat. The view shows the implant surface adjacent to the muscle tissue. 92

Figure 5. Backscattered SEM image of the cross section of the glass implants after 12 weeks in a rat. (A): CaLB-0, (B): CaLB-12, (C,E): 93B3-0, (D,F): 93B3-6. A thin layer of soft tissue (ST) is faintly visible between the reacted layer (RL) and the PMMA (PM). The unreacted glass is designated as G. 93

Figure 6. Elemental mapping analysis of the CaLB-0 and CaLB-12 implants after reaction in the subcutaneous site of a rat for 12 weeks and impregnated with PMMA (PM). SE= Secondary Electron, Ca= Calcium, P= Phosphorus, C= Carbon, S= Sulfur, RL= Reacted Layer, G= Unreacted Glass. Dark lines in PMMA regions are formed during the EDS scan due to degradation of PMMA..... 94

Figure 7. Elemental mapping analysis of 93B3-0 reacted in subcutaneous site of a rat for 12 weeks impregnated with PMMA (PM). SE= Secondary Electron, Ca= Calcium, P= Phosphorus, C= Carbon, Na= Sodium, K= Potassium, Mg= Magnesium, RL= Reacted Layer, and G= Unreacted Glass. 95

Figure 8. Elemental mapping analysis of 93B3-6 reacted in subcutaneous site of a rat for 12 weeks impregnated with PMMA (PM). SE: Secondary Electron, Ca: Calcium, P: Phosphorus, C: Carbon, Na: Sodium, K: Potassium, Mg: Magnesium, PM: PMMA, RL: Reacted Layer, and G: Unreacted Glass. 96

Figure 9. Optical micrograph (100X) of the polished cross-section of the CaLB-0 implanted subcutaneously in a rat for 12 weeks (A). Micro-Raman spectra (B) were collected for the point showed with squares. Carbonate ion (CO_3^{2-}) has 2 peaks at 711 cm^{-1} and 1085 cm^{-1}. Phosphate ion (PO_4^{3-}) represents HA which has 3 major peaks at 420 cm^{-1}, 570 cm^{-1}, and 960 cm^{-1}. The HA spectrum showed as a reference. The lines across the cross section are due to polishing. G: Unreacted Glass, RL: Reacted Layer, ST: Soft Tissue, PM: PMMA, HA: Hydroxyapatite..... 97

Figure 10. Optical micrograph (100X) of the polished cross-section of the CaLB-12 implanted subcutaneously in a rat for 12 weeks (A). Micro-Raman spectra (B) were collected for the point showed with squares. Carbonate ion (CO_3^{2-}) has 2 peaks at 711 cm^{-1} and 1085 cm^{-1}. Phosphate ion (PO_4^{3-}) represents HA which has 3 major peaks at 420 cm^{-1}, 570 cm^{-1}, and 960 cm^{-1}. The sulfate ion (SO_4^{2-}) has a primary peak at 1000 cm^{-1}. The HA spectrum showed as a reference. G: Unreacted Glass, RL: Reacted Layer, ST: Soft Tissue, PM: PMMA, HA: Hydroxyapatite 98

Figure 11. X-Ray diffraction patterns for the glass implants after 12 weeks in the subcutaneous site in a rat. The spectra were collected from 10 to 80 degrees, but only that portion from 25 to 70 degrees are presented here. 99

Figure 12. X-Ray diffraction patterns for glass discs reacted *in-vitro* in nSBF for 1 week at 37°C. 100

Figure 13. H&E stained sections of the tissue attached to a CaLB-0 and a CaLB-12 implant after 2 and 4 weeks in a rat. (A): CaLB-0, 2W, (B): CaLB-0, 4W, (C) CaLB-12, 2W, (D): CaLB-12, 4W. G: Unreacted (decalcified) Glass. Black arrows point to blood vessels. 101

Figure 14. H&E stained sections of the tissue attached to 93B3-0 and 93B3-6 implants after 2 and 4 weeks in a rat. (A,AA): 93B3-0, 2W, (B,BB): 93B3-0, 4W, (C,CC): 93B3-6, 2W, (D): 93B3-6, 4W. G: Unreacted (decalcified) Glass. Black arrows point to blood vessels. 102

Figure 15. CD31 (A) and H&E (B) stained section of 93B3-0 after 4 weeks in a rat. A sample of 4 blood vessels selected and identified by arrows with assigned numbers. Brown in CD31 section shows platelets or endothelial cells. CD31 identified that these are blood vessels because they stained brown. This confirms that the regions marked with black arrows in the H&E stained section are indeed blood vessels. G= Unreacted (decalcified) Glass. 103

Figure 16. CD31 stained sections of CaLB and 93B3 glasses after 4 weeks in the subcutaneous site in a rat. (A): CaLB-0, (B): CaLB-12, (C): 93B3-0, (D): 93B3-6. Brown color denotes endothelial cells or platelets in CD31 staining and blue is connective tissue. G: Unreacted (decalcified) Glass. 104

Figure 17. Masson's Trichrome stained sections of the tissue attached to each glass after 2 (left column) and 4 (right column) weeks in a subcutaneous site in a rat. (A,B): CaLB-0, (C,D): CaLB-12, (E,F): 93B3-0, (G,H): 93B3-6. Red= Keratin, Muscle Fibers, Cytoplasm, and Blue= Collagen 105

Figure 18. Line-scan (white line) EDS analysis for Ca (red) and P (green) across the reacted layer for a (A) CaLB-0 and (B) 93B3-0 glass implanted subcutaneously for 12 weeks in a rat. G= Unreacted Glass, RL= Reacted Layer, ST= Soft Tissue, and PM= PMMA. The figure shows the intensity of the signal for Ca and P is shown along the scanned line. Ca/P ratio for each region is shown in blue and circled. 106

Figure 19. Proposed determination of the source and amount of phosphorus (P) in the reacted layer on CaLB-0 and 93B3-0 implants after subcutaneous implantation for 12 weeks in a rat. 107

APPENDIX: SUPPLEMENTARY DATA FOR PAPER 2

Figure 1. Elemental mapping analysis of the CaLB-0 and CaLB-12 implants after reaction in the subcutaneous site of a rat for 4 weeks and impregnated with PMMA (PM). SE= Secondary Electron, Ca= Calcium, P= Phosphorus, C= Carbon, S= Sulfur, RL= Reacted Layer, G= Unreacted Glass. Dark lines in PMMA regions are formed during the EDS scan due to degradation of PMMA.....109

Figure 2. Elemental mapping analysis of 93B3-0 and 93B3-6 reacted in subcutaneous site of a rat for 4 weeks impregnated with PMMA (PM). SE: Secondary Electron, Ca: Calcium, P: Phosphorus, C: Carbon, Na: Sodium, K: Potassium, Mg: Magnesium, PM: PMMA, RL: Reacted Layer, and G: Unreacted Glass.....110

Figure 3. Optical micrograph (10X) of the polished cross-section of the 93B3-0 implanted subcutaneously in a rat for 12 weeks (A). Micro-Raman spectra (B) were collected for the point showed with squares. Carbonate ion (CO_3^{2-}) has 2 peaks at 711 cm^{-1} and 1085 cm^{-1}. Phosphate ion (PO_4^{3-}) represents HA which has 3 major peaks at 420 cm^{-1}, 570 cm^{-1}, and 960 cm^{-1}. G: Unreacted Glass, RL: Reacted Layer, PM: PMMA, HA: Hydroxyapatite 111

Figure 4. Optical micrograph (10X) of the polished cross-section of the CaLB-12 implanted subcutaneously in a rat for 12 weeks (A). Micro-Raman spectra (B) were collected for the point showed with squares. Carbonate ion (CO_3^{2-}) has 2 peaks at 711 cm^{-1} and 1085 cm^{-1}. Phosphate ion (PO_4^{3-}) represents HA which has 3 major peaks at 420 cm^{-1}, 570 cm^{-1}, and 960 cm^{-1}. The sulfate ion (SO_4^{2-}) has a primary peak at 1000 cm^{-1}. G: Unreacted Glass, RL: Reacted Layer, PM: PMMA, HA: Hydroxyapatite 112

Figure 5. X-Ray diffraction patterns for the CaLB-0 and CaLB-12 glass implants after 2 weeks in the subcutaneous site in a rat. The spectra were collected from 10 to 80 degrees, but only that portion from 20 to 70 degrees are presented here.....113

LIST OF TABLES

PAPER 1

Table 1. As-Batched composition, analyzed* (XRF) composition, density (ρ) and molar volume (Vm) for glasses melted at 1100°C for one hour. The values in ( ) are Mol%. 29

Table 2. DTA data. Minor phases formed at Tx1 for CaLB-0% and CaLB-12% and at Tx2 for CaLB-22%. 30

PAPER 2

Table 1. As-Batched composition for the CaLB and 93B3 glasses in wt%. The values in ( ) are in Mol%. 86

Table 2. Ion concentration (mM) of human blood plasma, nSBF, and Kokubo-SBF. 87

Table 3. Reaction rate (μm/week) as calculated from the thickness of the reacted layer and time, in-vivo. The thickness of the reacted layer was measured on the flat surface of each implant where the thickness is relatively uniform as opposed to the corners where the thickness varies (see Fig 5). 88

PAPER

1: The Effect of Sulfur on Structure and Conversion of Bioactive Borate Glasses. Part I: *In-vitro* Studies

Ali Mohammadkhah,[†] Delbert E. Day,[†] Richard K. Brow, [†] Mohamed N. Rahaman, [†]

Roger F. Brown[§]

† Department of Materials Science and Engineering, Center for Bone and Tissue Repair and Regeneration, Missouri

University of Science and Technology, Rolla, Missouri 65409

§ Department of Biological Sciences, Center for Bone and Tissue Repair and Regeneration, Missouri

University of Science and Technology, Rolla, Missouri 65409

Abstract

The effect of sulfur on glass structure and the conversion process of bioactive CaO-Li_2O-B_2O_3 glasses were studied. One glass without and two glasses with different amounts of sulfur were made using conventional melting and dry quenching techniques. Calcium lithium borate glasses containing dissolved sulfur were made by substituting $CaSO_4$ for $CaCO_3$ in the glass batch. Using $CaSO_4$ improved glass formation. Sulfur containing glasses formed without crystallization or phase separation.

X-ray fluorescence was used to measure the sulfur content of each glass. Up to 22 wt% sulfur in the form of sulfate ions was incorporated in the glass structure. Micro-Raman analysis identified SO_4^{2-} units in the sulfur-containing glasses and showed that substituting more $CaSO_4$ increased the dissolved sulfur content in the borate glass. Sulfur

was found to participate in the glass structure by reacting with non-bridging oxygens and cross-linking the boron-oxygen network.

These glasses reacted with a phosphate solution and converted to hydroxyapatite. Particles (150-355μm) were reacted in 0.25 and 0.5 molar K_2HPO_4 solutions at 37°C for 2 to 96 hours. The weight loss of the particles and the final pH of the solution were measured. The weight loss measurements indicated that the reaction rate increases with increasing the sulfur content. Sulfate was released from the glass, causing the pH of the solution to decrease, but was absent in the reacted layer.

I. Introduction

Inorganic glasses were introduced for biomedical use with the discovery of the 45S5 glass by Hench et al. in 1971[1]. The 45S5 glass is a bioactive and biocompatible silicate glass with silica content of 45 wt%. It has been studied extensively *in-vitro* and *in-vivo* over decades[2-6]. Despite several good properties, 45S5 does not have a wide working range and it crystallizes quickly when sintered above ~700°C. Bone healing and regeneration varies with several parameters (i.e. type of bone, age, etc.) so matching the degradation rate of the glass implant to the bone for regeneration becomes critical. There have been many efforts to control the conversion rate of bioactive glasses[5-10] by changing the composition of the glass.

Borate glasses are known to react faster both in *in-vitro* and *in-vivo* as compared to silicate glasses[8-13] and in biomedical applications they have been found to provide good biological activity and compatibility[9; 13-15]. The difference between borate and silicate glasses in the way they dissolve is that silicate glasses follow selective leaching

dissolution and form a silica-rich layer, but borate glasses dissolve more rapidly by bulk dissolution[6; 7].

Modifying the composition of borate glasses can also control their reaction rate. Adding more CaO to the glass causes the glass to react more slowly in phosphate solutions[16]. It has been shown that increasing the local calcium content, *in-vivo*, in bone regeneration can have a positive effect on the differentiation of osteoblasts[17]. Also, in making hydroxyapatite (HA) microspheres by reacting borate glasses in a phosphate solution, a higher calcium content could enhance the mechanical strength of the microspheres since solid HA rather than hollow microspheres can be formed[16; 18; 19]. Having more calcium in the glass could be promising in enhancing the mechanical properties of the converted borate glass reacted either *in-vitro* or *in-vivo*. Higher CaO could also improve the *in-vivo* biological response, but it reduces the reaction rate. Increasing the over-all reaction rate of the glass by other compositional changes to compensate for the higher CaO content could be very beneficial.

Sulfur is the key in three amino acids in the human body; two essential amino acids cysteine, methionine, and one non-essential amino acid, taurine. Sulfur also found in many other compounds in the body i.e. heparin, insulin, thiamin, and biotin[20]. Sulfur has a long history in the treatment of different dermatological disorders[21; 22]. One of the most important roles of sulfur in the body is forming disulfide bridges. A disulfide bridge is a strong covalent bond of two sulfur-containing groups, which is responsible for the rigidity and toughness of hair and nails. Keratin, which contains a large amount of cysteine, is the key component of skin, hair, and nail. Sulfur helps in wound healing via the formation keratin[22].

Sulfate (SO_4^{2-}) also has a long history in biomedical science. Calcium sulfate ($CaSO_4$) is a FDA approved material that was one of the first materials used in orthopedic surgery, over 100 years ago. Calcium sulfate is an effective bone graft material, and is completely resorbed by the body in 5 to 7 weeks[23; 24]. It does not cause inflammation, foreign body reaction or rejection of the implant. Calcium sulfate is an osteoconductive and angiogenic material, which makes it a good candidate for bone scaffolds[24; 25]. It has been reported that when $CaSO_4$ is used as a *in-vivo* bone regeneration implant, it reduces the local pH and makes the environment more acidic by releasing sulfate. This causes the adjacent bone to demineralize and release matrix-bound bone growth factor, which stimulates bone growth[26].

Sulfur has been used as a refining agent and melt accelerant in glass technology for years[27-29]. For instance, adding sulfur to a silicate glass accelerates its melting since in the silica rich region, sulfates decompose and release sodium (assuming sulfate added as Na_2SO_4) which reacts with silica particles and forms sodium metasilicate which is a fluid liquid[29]. Usually it is not possible to add more than 1-2 wt% sulfur to a silicate glass. Sulfate released in the batch during the melting stage stirs the melt and homogenizes the melt. Also, when gasses form in the melt they help remove small bubbles by consolidating them on their way to the surface[29].

The addition of sulfur to a borate glass is easier due to its more open structure as compared to a silicate glass. Adding sulfur to a glass in the form of $CaSO_4$ is assumed to not only increase the reaction rate, but to also improve the glass formation tendency of compositions of higher calcium content compared to conventional bioactive glasses like 45S5 (24.5 wt% CaO).

A main goal of this work was to determine how much sulfur could be incorporated into a $CaO\text{-}Li_2O\text{-}B_2O_3$ glass by gradually replacing portions of the $CaCO_3$ raw material by $CaSO_4$. The effect of sulfur on the structure of lithium borate glasses was also investigated. In addition, the effect of sulfur on the conversion rate and formation of hydroxyapatite was studied *in vitro*. Lithium borate glasses were chosen because their physical, chemical, and biological properties have been studied previously[16; 18; 19]. These glasses have been shown to convert to hydroxyapatite in phosphate solutions at 37°C[16; 18; 19], which should make them biocompatible. By adding sulfur to the glass, it was expected to be more reactive. It was also expected that if the sulfur was released to the solution during the reaction of the glass, the pH of the solution would be reduced (more acidic) if H_2SO_4 was formed.

II. Experimental Procedure

(1) Glass Compositions and Preparation

The compositions of the $CaO\text{-}Li_2O\text{-}B_2O_3$ glasses investigated are shown in Table 1. The CaLB glasses are identified as CaLB-X% where X denotes the SO_3 content in weight percent. For instance, the calcium lithium borate glass containing 12.5 wt% SO_3 is identified as CaLB-12%.

The raw materials used were reagent grade H_3BO_3, Li_2CO_3, $CaCO_3$, and $CaSO_4$, which was the source of sulfur in the sulfur-containing glasses. For CaLB-12% one quarter and for CaLB-22% half of CaO supplied from $CaSO_4$ and the rest supplied from $CaCO_3$.

When $CaSO_4$ reacts in the batch, it decomposes to CaO and SO_3. The SO_3 ideally dissolves in the glass so the composition of the glass changes by considering the sulfur as a batch component. Glasses with higher sulfur content, $CaSO_4$ was substituted for 3/4 and all of the $CaCO_3$, were also attempted, but when the melt was quenched between copper plates crystallization could not be prevented so these compositions were not investigated.

To improve the homogeneity, of the batch materials they were mixed wet using acetone. The slurry was dried overnight at 90°C, crushed and mixed again using a mortar and pestle. The CaLB glasses were melted in a platinum crucible at 1100°C in an electric furnace for 1 hour, air atmosphere. The melt was then poured and quenched between copper plates. Pieces of the quenched glass were crushed using mortar and pestle and particles between 150 to 355 μm were separated by screening. These particles were used for *in-vitro* experiments in a phosphate solution.

(2) XRF Measurements

Glass particles, 150 to 355 μm in diameter, were chemically analyzed by XRF (Spectro Xepos ED X-Ray Fluorescence)[1]. The sulfur and calcium content of each glass (in wt%) was measured by XRF in terms of absolute values and were not standardized to 100 wt%. The estimated error in the CaO and SO_3 content is ± 5%. Elements like boron and lithium cannot be detected by XRF, so the assumption was made that none of these elements were lost during the melting process.

---

[1] Mo-Sci Corporation Rolla MO

(3) Density and Molar Volume

The density of each glass was measured by the Archimedes technique. The samples were weighed using a Mettler Toledo X5105 Dual Range scale. Water at room temperature (~22°C) was used as the suspension media and the density of at least 10 separate pieces were measured for each glass. The density reported in Table 1 is the average density and the measured error (standard deviation) is ±0.01 g/cm^3.

The molar volume (V_m) of each glass was calculated from equation (1),

$$V_m = \frac{\rho}{M_w} \tag{1}$$

Where ρ is the average density and M_w is the molecular weight of the glass, as calculated from the batch composition.

(4) Differential Thermal Analysis (DTA)

The glass transition temperature (T_g) and crystallization temperature (T_x) for each glass was measured using a Perkin Elmer DTA7 (Perkin Elmer Life and Analytical Sciences Inc., Waltham, MA). Each glass was heated from room temperature to 1050°C at a rate of 10°C/min. To identify the phases crystallizing from the glass, particles were heated at 10°C/min to their crystallization temperature (T_x) and held at T_x for 20 minutes.

(5) Scanning Electron Microscopy (SEM) and Energy Dispersive Spectroscopy (EDS)

A Field Emission Hitachi S-4700 SEM was used for microstructural analysis. This microscope was equipped with a Silicon Drift Detector (SDD) (EDAX Inc. Mahwah, NJ)

which was used for elemental and phase mapping analysis of the glass particles reacted in the phosphate solution. All samples were coated with carbon to reduce charging and the accelerating voltage ranged from 5 to 15 kV.

(6) X-Ray Diffraction

The identification of crystalline phases was done using a Philips X-Pert with Cu K_α of (λ= 0.15405 nm) radiation and a 2θ step size of 0.025° from 10 to 70 degrees. The absence of crystalline phases in the quenched glass was determined by XRD.

(7) Micro-Raman Spectroscopy

To identify vibrational modes associated with sulfur, phosphorus, and boron bond with oxygen in the samples, the micro-Raman spectrum of at least 10 pieces of each CaLB glasses was measured (LabRAM ARAMIS, Horiba Jobin Yvon) from 200 to 3000 cm^{-1}. The device was calibrated prior to measuring the spectra of each CaLB glass with a silicon wafer. The intensity of the micro-Raman peaks depends on several variables, but if the device settings are kept constant, the intensity of the peaks should be approximately proportional to the concentration of the species producing it. The micro-Raman spectra for each glass were collected at the same instrument settings in order to compare the concentration of sulfur and bridging and non-bridging oxygen in the borate glass.

(8) Glass Conversion in Phosphate Solution

Particles (150-355 μm) of each glass were reacted in a phosphate solution at 37°C for up to 96 hours. The phosphate solution was made by dissolving reagent K_2HPO_4 (Fisher Scientific, Pittsburgh PA) in deionized (DI) water to produce 0.25 and 0.5 M K_2HPO_4

solutions. Two molar NaOH was added to the phosphate solution to adjust the pH to 10.0. A 0.25 M phosphate solution was chosen based on previous studies[15; 16] while a 0.5 M solution was chosen to study the effect of phosphate solution concentration.

Glass particles ranging from 150-355 μm were washed with acetone prior to being placed in phosphate solution to remove any small fragments adhering to the larger particles. The glass particles were reacted with the phosphate solutions in either plastic or glass containers in the amount of 5 mg of glass/ml of solution (250 mg of glass in 50 ml of solution). The containers holding the phosphate solution were placed on a sand-bath at 37°C that provided agitation through an orbital shaker set at 40 rpm. All experiments were done in duplicates.

After reaction, the pH of the solution was measured at 37°C and then the particles were filtered from the phosphate solution. The particles were washed three times with DI water and dehydrated by washing twice with ethanol. Then they placed in an oven and dried overnight at 110°C.

The weight of the particles after being dried in the oven was measured and the difference in weight compared to the initial weight (~250 mg) was calculated as the percent weight loss.

III. Results

(1) Glass Formation, Composition, and Properties

It was difficult to prevent crystallization of the sulfur-free melt (CaLB-0%) except by quenching it between copper plates. Replacing a portion of the $CaCO_3$ in the batch with

$CaSO_4$ reduced the crystallization tendency and a glass was obtained when the melt quenched between copper plates.

The absolute calcium (CaO) and sulfur (SO_3) content of each glass was measured using XRF. It was assumed that no B_2O_3 or Li_2O was lost during the melting. The total amount of CaO and SO_3 measured by XRF was subtracted from 100 and the difference was assumed to be the amount of B_2O_3 plus Li_2O. The amount of B_2O_3 and Li_2O were then calculated by assuming the Li_2O to B_2O_3 ratio (wt/wt) was 1:7 as in the starting batch.

As an example, the amount of CaO and SO_3 measured by XRF for the CaLB-12% glass was 11.4 and 35.7 wt%, respectively. The B_2O_3 plus Li_2O would be 52.9 wt% (100-(11.4 + 35.7)). Since Li_2O/ B_2O_3 ratio is 1:7 then Li_2O would be 1/8 and B_2O_3 would be 7/8 of this amount or 6.6 and 46.3 wt%, respectively.

The XRF measurements show that sulfur was present in the two glasses when $CaSO_4$ was substituted for $CaCO_3$ in the batch, see Table 1. The density and molar volume of the glasses did not change significantly with increasing sulfur content.

(2) Glass Micro-Raman Analysis

Sulfur can be incorporated in a glass as SO_4^{2-}, SO_3, S^{2-}, etc.[30-37]. Micro-Raman spectroscopy of each glass was used to identify sulfur dissolved in the CaLB glasses. The spectra in Fig 1 show three distinguishable peaks, at 1000, 620, and 460 cm^{-1} which have been attributed to sulfur in a glass as tetrahedral SO_4^{2-} groups[3; 34; 36; 37]. The peak at 1000 cm^{-1} (ν_1) is S-O stretching, the peak at 460 cm^{-1} (ν_2) is symmetric O-S-O bending, and the peak at 620 cm^{-1} (ν_4) is asymmetric O-S-O bending mode[36]. Another peak at 1100 cm^{-1}

(ν_3), has been attributed to asymmetric S-O stretching vibration[35], but this peak was not detected in the two CaLB sulfur-containing glasses. The broad peak from 1250 to 1600 cm^{-1} in Fig 1 is related to B-O^- bond (O^- = Non-Bridging Oxygen)[38; 39].

(3) DTA and Crystallization

Figure 2 shows the DTA pattern for each glass. With the addition of sulfur to the glass the glass transition temperature (T_g) shifted by 25°C to a higher temperature, see Fig 2. The crystallization temperature (T_x) also shifted higher in the sulfur containing glasses and a peak (T_{x1}), associated with the crystallization of $CaSO_4$ appeared in the spectra for the CaLB-22% glass. Table 2 shows the crystalline phases present after the glasses were heat treated at T_{x1} and T_{x2} for 20 minutes. X-ray diffraction spectra for each crystalized glass are given in Fig 1 and 2 of the appendix.

An endothermic peak, attributed to melting, is present in the spectra at ~800°C for the CaLB-0% and CaLB-22% glasses, see Fig 2. This peak could not be related to the melting of any particular crystal that had formed during the crystallization of these glasses. However, crystalline $LiBO_2$ and $Li_2B_4O_7$ melt around 850°C and 915°C respectively[40-42]. For unknown reasons, no endothermic peak is seen around 800°C in the DTA pattern for the CaLB-12% glass in Fig 2. The DTA measurement was repeated for this glass and the spectrum in Fig 2 was reproduced, see Fig 3 in the appendix. Neither $LiBO_2$ nor $Li_2B_4O_7$ was identified by XRD, even as a minor phase, in the CaLB-12% glass when it was crystalized.

(4) Conversion in Phosphate Solution

The weight loss data of the glass particles as they reacted in the 0.25M and 0.5M K_2HPO_4 solutions are shown in Fig 3.

The two glasses containing sulfur (CaLB-12% and CaLB-22%) undergo a greater weight loss at any given time compared to that for the sulfur-free glass, CaLB-0%. Also, the CaLB-22% glass has a greater weight loss in both solutions than the CaLB-12% glass. It can be seen that the sulfur-containing glasses react faster compared to the sulfur-free glass and the weight loss becomes nearly constant after ~48 hours. When reacted in the 0.5M K_2HPO_4 solution at 37°C for 48 hours, the weight loss for the CaLB-12% and CaLB-22% compositions is more than 4 and 6 times greater, respectively, than the weight loss for the CaLB-0%, the sulfur-free glass.

(5) Phase Identification

a. X-Ray Diffraction

XRD was used to identify the crystalline phases in the particles after they had reacted in the phosphate solutions, see Fig 4. All of these glasses formed hydroxyapatite ($Ca_{10}(PO_4)_6(OH)_2$) in either 0.25M or 0.5M phosphate solution, although the degree of crystallinity of these particles is different. The XRD spectra for the particles reacted in 0.25M K_2HPO_4 solution are given in Fig 4 in the appendix.

b. Micro-Raman

In Fig 5 the micro-Raman spectra of particles reacted in 0.5 M phosphate solution for 96 hours is shown along with the spectrum for crystalline HA (Fisher Scientific, St Louis Mo). The micro-Raman spectra for particles reacted in 0.25 M phosphate solution are given in Fig 5 in the appendix.

Hydroxyapatite has four bands related to PO_4^{3-} vibrations (see bottom curve in Fig 5), doubly degenerate bending of O-P-O bending is ν_2 at ~420 cm^{-1}, triply degenerate bending of O-P-O bending bond is ν_4 at ~560 cm^{-1}, symmetric stretching of P-O is ν_1 at ~960 cm^{-1}, and asymmetric stretching of P-O bond is ν_3 at ~1018 cm^{-1}.

The micro-Raman spectra for the sulfur-containing glasses reacted in the 0.5M phosphate solution for ~96 hours (Fig 5) do not contain any peaks related to sulfate but contain all four peaks related to PO_4^{3-}. The spectrum in Fig 5 for the sulfur-free glass after being in the 0.5M phosphate solution for ~96 hours, is identical to the unreacted glass spectrum in Fig 1, the only slight difference is the barely detected peak at ~960 cm^{-1} which is related to phosphate ν_1.

(6) SEM and Energy Dispersive Spectroscopy (EDS)

It is of interest to track the sulfur when the sulfur-containing glasses react in the phosphate solution. Energy dispersive spectroscopy technique was used to map the different elements present in the reacted particles. Fig 6 shows EDS results for a CaLB-12% particle reacted in the 0.5M phosphate solution for 96 hours. A glass particle starts reacting from its outer surface inward as shown in Fig 6, the center of the CaLB-12%

particle examined is composed of un-reacted glass as indicated by the presence of Ca and sulfur. The indicated reacted layer of the particle in Fig 6 contains Ca and P indicating that Ca from the glass has reacted with P in the solution to form a hydroxyapatite material (HA), no sulfur (< 2 At%) is present in the reacted HA layer. Energy dispersive analysis of CaLB-0% and CaLB-22% reacted in 0.5 M phosphate solution for 96 hours are given in Fig 6 and 7 of the appendix, respectively.

IV. Discussion

(1) Sulfur in the Glass and Glass Structure

a. Sulfur in the Glass

The CaLB-0% composition was difficult to obtain as a glass except by quenching between copper plates due to the amount of Li_2O and CaO in the glass (56.1 mol%). Sulfur dissolved in the glass improved the glass-forming tendency compared to the CaLB-0%. As sulfur was added to the composition, the relative amount of Li_2O and CaO decreased in the glass (47.4 mol% in CaLB-22%) and this change helped improve glass formation.

There are many studies[65; 66; 76; 77] describing the dissolution of sulfur in silicate and borosilicate glasses, although the sulfur concentration in these glasses is below 1 or 2 wt%[35; 36]. Based on the XRF data (Table 1) and the micro-Raman (Fig 1) measurements much larger amounts of sulfur (up to 22wt% SO_3) were present in the CaLB glasses and more than 90% of the sulfur in the batch was present in the glass. The sulfur content of the glass also directly depends on how much of CaO in the glass was supplied by $CaSO_4$.

Sulfur can be dissolved in a glass in several different forms [30-37]. Micro-Raman spectroscopy showed that the sulfur was present as SO_4^{2-} units in the CaLB glasses (Fig 1). When $CaSO_4$ decomposes to CaO and SO_3 during the melting process the SO_3 dissolves in the glass and is present as a SO_4^{2-} tetrahedron.

b. Borate Glass Structure

Vitreous boron oxide is composed of 3-coordinated boron (BO_3 triangles) which are connected at all three corners by B-O bonds to form a three dimensional, cross-linked network[29]. Adding R_2O or RO to a borate glass causes 3-coordinated boron to change to 4-coordinated boron (BO_4 tetrahedral) up to 33 mol% alkali or alkaline earth, Fig 7 (A). This increases the network connectivity and leads to an increases in a property like T_g[43]. This is called the borate anomaly.

Adding more R_2O or RO (>33 mol%) to the glass eventually causes non-bridging oxygen ions to form. When the alkali concentration reaches 75 mol% it is assumed that all of the BO_4 units ideally converted to BO_2O^- groups (Fig 7 (B)), which are boron oxygen triangles with one or more NBO (O^-). As soon as the NBOs start forming, the change in properties reverses i.e. T_g decrease.

c. CaLB Glasses Structure

The CaLB glasses studied in the present work contain more than 50 mol% Li_2O plus CaO, which means that these glasses contain BO_4 tetrahedra and BO_3 triangles with NBOs.

Fig 7 (C) shows the structure of these glasses without sulfur and how sulfur is incorporated in the structure as SO_4^{2-} units. When $CaSO_4$ decomposes to CaO and SO_3, the latter is dissolved in the melt and combines with a NBO to form a SO_4^{2-} tetrahedron. In this case, some of the Li^+ or Ca^{2+} ions, which were associated with the NBOs, balance the charge by forming BO_4 groups.

In the micro-Raman spectra of these glasses (Fig 1), the intensity of the NBO bands (1250 to 1500 cm^{-1}) decreases with increasing sulfur content of the glass; which suggests that the NBOs are converting to bridging oxygens. The conversion of NBO to BO causes the glass network to become more cross-linked, which could explain the slightly higher T_g for the sulfur containing glasses.

(2) Glass Conversion

A schematic of the conversion process for a CaLB glass is shown in Fig 8. When a CaLB glass is immersed in a phosphate solution it begins to react. Unlike silicate glasses with the dissolution of single species, dissolution of borate glasses is controlled by bulk dissolution[6; 7] with an equivalent loss of B, Li, and Ca. That is also why borate glasses react faster than silicate glasses.

Borate glasses in a phosphate solution (K_2HPO_4) undergo a dissolution-precipitation reaction. In this process, all of the ions are released to the solution, which produces a weight loss. However, when the Ca^{2+} ions are released, they react with either PO_4^{3-} and/or OH^- in the solution and form an insoluble amorphous calcium phosphate (ACP) on the surface of the glass particle, which produces a weight gain.

Eventually the amorphous calcium phosphate layer crystallizes to form a porous layer of hydroxyapatite ($Ca_{10}(PO_4)_6(OH)_2$) as the solution continues to penetrate through the HA and ACP layer, the conversion process continues until all of the starting glass has reacted/converted. After 96 hours in the 0.5 M phosphate solution, the reacted layer on the CaLB-0% glass particles (150-355μm) was only 10-15μm thick. For the same time (96 hours), more of the CaLB-22% particles were fully reacted compared to the CaLB-12% particles.

Overall, the weight loss of the glass exceeds the weight gain due to the formation of HA. So the net result is a weight loss is shown as Fig 3.

In hydroxyapatite some of the Ca^{2+}, PO_4^{3-}, or OH^- can be replaced by other ions. Sulfur was not present in the HA layer (see Fig 6) nor did it precipitate as another phase. Phase mapping analysis (Fig 6) confirms that there is little, if any, sulfur in the reacted layer. The peaks due to sulfur are absent in the micro-Raman spectra of the reacted particles (Fig 5) and the spectra are identical to the HA spectrum.

Therefore, the results suggest that the sulfur in the glass is released to the solution during the glass conversion reaction. The pH of the phosphate solution for the sulfur-free glass increased while the pH stayed constant or decreased slightly for the solution containing the CaLB-12% and CaLB-22% glasses, respectively due to release of sulfate ions.

To determine the reaction kinetics of the CaLB glasses in the phosphate solution the normalized weight loss (α) was compared to several reaction models including Contracting Volume Model (CVM) and 3D diffusion model for the glasses reacted in 0.25M and 0.5M K_2HPO_4 at 37°C.

The normalized weight loss (α) defined as the weight loss over the maximum weight loss that measured during the experiment. It was assumed that the reaction was complete, where the maximum weight loss occurs, which in this set of experiments was 48 hours for CaLB-0% and CaLB-22% and 96 hours for CaLB-12%.

Comparing different models for the reaction kinetic (data not shown here), the contracting volume model was the best fit for glasses reacted in the phosphate solution, while the 3D diffusion model fits to the weight loss data very closely to the CVM. For the CVM and 3D diffusion, α was calculated using these equations:

CVM: $1-(1-\alpha)^{1/3}= kt$

3D Diffusion Model: $(1-(1-\alpha)^{1/3})^2 = kt$

in which the "k" is the reaction rate constant and "t" is time. In this equation the relation of $(1-(1-\alpha)^{1/3})$ or $(1-(1-\alpha)^{1/3})^2$ with "t" should be linear with the slope of "k".

The results are shown in Fig 9 for the sulfur-containing CaLB glasses reacted in 0.25M and 0.5M K_2HPO_4 at 37°C. The results for the sulfur-free CaLB-0% was not shown because the sulfur-free CaLB-0% did not react compared the sulfur-containing CaLB glasses so the measured weight loss varies in a very small range and the reaction model does not fit the normalized weight loss data points. In another words the data for the

sulfur-free CaLB-0% glass is not suitable for the modeling purposes due to the slow reaction. The analysis was done just for the first 24 hours of the reaction because it was assumed that the phosphate solution properties like pH and concentration of different ions might affect the reaction rate/mechanism.

However, the reaction mechanism for sulfur-containing glasses could be fitted to either CVM or 3D diffusion model. Previously[8], it was shown that the reaction mechanism for the borate glasses reacted in K_2HPO_4 solution fits the CVM better during the span of the experiment while the silicate or borosilicate glasses show a deviation in reaction mechanism after ~48 hours of reaction from CVM to the 3D diffusion model and could be due to the formation of thick silica gel layer.

In this work, as it can be seen in Fig 9, the CVM model fits the normalized weight loss data of CaLB-22% reacted in either 0.25M or 0.5M phosphate solution, but for the CaLB-12% reacted in 0.25M phosphate solution the 3D diffusion model provide a better match compared to the CVM while the CVM fits the reaction in 0.5M phosphate solution. The rate constant for CaLB-22% is 2 times bigger than that for the CaLB-12% showing that the reaction rate for the glass with 22 wt% is 2 times higher than the glass with 12 wt% sulfur.

It has been reported that the reaction rate of similar borate glasses increased with decreasing calcium content of the glass[16]. Adding ~12 and ~22 wt% sulfur to the glass reduced the CaO content from 39.9% to 35% and from 39.9% to 31.1 wt%, respectively for the CaLB-12% and CaLB-22% glasses (Table 1). This small reduction in CaO content could also explain the greater reaction rate for the sulfur-containing CaLB glasses.

In theory, all the B^{3+} and Li^{+} ions in the glass were released and all the calcium in the glass reacted with phosphate and hydroxide ions in the solution to form stoichiometric hydroxyapatite $Ca_{10}(PO_4)_6(OH)_2$ (Ca/P= 1.67) following these reactions:

$$HPO_4^{2-} \rightarrow PO_4^{3-} + H^+$$
$$10Ca^{2+} + 6PO_4^{3-} + 2OH^- \rightarrow Ca_{10}(PO_4)_6(OH)_2$$

Knowing how much CaO is in the glass, the weight of the HA resulting from the above reaction can be calculated thus the change in weight could be calculated. This change would be a weight loss, which called the theoretical weight loss. In most cases, the glass reacting in a phosphate solution does not attain its theoretical weight loss. One reason is that a perfectly stoichiometric HA is not formed. Usually calcium deficient HA (CaDHA) is formed which has essentially the same XRD pattern as stoichiometric HA, but has a lower Ca/P ratio (1.2-1.4).

The theoretical weight loss values calculated for the CaLB glasses are shown in Fig 10 along with the weight loss measured after 48 hours in the 0.25 and 0.5 M K_2HPO_4 solutions at 37°C. The difference between the theoretical weight loss and the measured weight loss for the CaLB-0% glass is due to incomplete reaction. Fig 11 (A) shows a SEM image of a CaLB-0% glass particle reacted in the 0.5 M K_2HPO_4 solution for 96 hours at 37°C. A high magnification image, Fig 11 (B), of the CaLB-0% glass particle shows that not more than 10μm of the particle reacted (d= 150-355μm).

On the other hand, while most of the CaLB-12% and CaLB-22% glass particles are completely reacted there are some particles that have an unreacted glass core, see Fig 11 (C). The weight loss curve becomes nearly constant after 48 hours of reaction. The

difference between the measured and theoretical weight loss could be due to the formation CaDHA with lower Ca/P compared to synthetic HA. Sulfur-containing glasses reacted more compared to the sulfur-free glass but they formed CaDHA.

The Ca/P ratio of a CaLB glass similar to CaLB-22% reacted in K_2HPO_4 solution (pH=9) at 37°C has been measured previously[16] and reported a value of ~1.6. The difference could be because of difference in sulfur content of the glass or the reaction parameters like pH.

Another reason for the difference between the measured and theoretical weight loss for CaLB-12% and CaLB-22% glasses could be that not all B^{3+} and Li^{+} ions are released to the solution. In the other words, the sulfur-containing CaLB glasses did not react completely with the phosphate solution.

V. Conclusion

Substituting $CaSO_4$ for $CaCO_3$ in the batch materials improved the glass-forming tendency of the CaLB glass containing 40 wt% CaO. XRF analysis showed that sulfur (as SO_3) was present in the CaLB glasses at concentration up to 20 wt% SO_3. Micro-Raman spectra also indicated that sulfur was present in glass in the form of SO_4^{2-} groups.

The base glass (CaLB-0%) contains more CaO and Li_2O (56.1 mol%) compared to the sulfur-containing CaLB glasses (<51 mol%) so, ideally, the glass network contains more BO_3 triangles with one NBO. The dissolved sulfur in the borate glass converts some of the NBOs to BOs as the sulfate tetrahedrons are formed. This way SO_4^{2-} cross-linked with boron-oxygen network and reduces NBOs. Sulfate ions in the glass structure did not affect the density or molar volume, but did increase T_g slightly.

Sulfur-containing glasses (CaLB-12% and CaLB-22%) reacted 4 to 6 times faster than the sulfur-free glass (CaLB-0%). The reaction rate also depends on sulfur content of the glass. The sulfur-containing CaLB-22% reacts 2 times faster than the other sulfur-containing glass CaLB-12%.

Sulfur was not detected by EDS, or micro-Raman in the reacted layer and no sulfur-containing phase was identified using XRD after the reaction in the K_2HPO_4 phosphate solution. During reaction the sulfur in the glass was released to the phosphate solution as indicated by the decrease in pH.

Hydroxyapatite formed for both sulfur-free and sulfur-containing glasses reacted in the K_2HPO_4 solution at 37°C. Sulfur-containing glasses developed a reacted layer with a lower Ca/P ratio (~1.2±0.2) compared to the sulfur-free glass (~1.5±0.2), which is an indication of CaDHA.

In the biomedical application, increasing the reaction rate of the glass could be beneficial in hard tissue (bone) regeneration when there is a time constraint like pediatrics orthopedics or athletic injuries or soft tissue regeneration (wound healing) for skin burns when the healing time is crucial. Sulfur participates in different biological

processes so a glass that releases sulfur in the *in-vivo* environment could be helpful in different dermatological and orthopedic applications.

References

[1]L. L. Hench, R. J. Splinter, W. C. Allen, and T. K. Greenlee, "Bonding Mechanisms at the Interface of Ceramic Prosthetic Materials," *J. Biomed. Mater. Res.,* **5**[6] 117-41 (1971).

[2]L. L. Hench, "Bioceramics," *J. Am. Ceram. Soc.,* **81**[7] 1705-27 (1998).

[3]I. B. Leonor, A. Ito, K. Onuma, N. Kanzaki, Z. P. Zhong, D. Greenspan, and R. L. Reis, "In Situ Study of Partially Crystallized Bioglass and Hydroxylapatite in Vitro Bioactivity Using Atomic Force Microscopy," *J. Biomed. Mater. Res.,* **62**[1] 82-88 (2002).

[4]Q. Z. Chen, I. D. Thompson, and A. R. Boccaccini, "45s5 Bioglass Derived Glass-Ceramic Scaffolds for Bone Tissue Engineering," *Biomaterials,* **27**[11] 2414-25 (2006).

[5]A. Yao, D. Wang, W. Huang, Q. Fu, M. N. Rahaman, and D. E. Day, "In Vitro Bioactive Characteristics of Borate-Based Glasses with Controllable Degradation Behavior," *J. Am. Ceram. Soc.,* **90**[1] 303-06 (2007).

[6]W. Huang, D. E. Day, K. Kittiratanapiboon, and M. N. Rahaman, "Kinetics and Mechanisms of the Conversion of Silicate (45S5), Borate, and Borosilicate Glasses to Hydroxyapatite in Dilute Phosphate Solutions," *J. Mater. Sci.: Mater. Med.,* **17**[7] 583-96 (2006).

[7]W. Huang, M. N. Rahaman, D. E. Day, and Y. Li, "Mechanisms for Converting Bioactive Silicate, Borate, and Borosilicate Glasses to Hydroxyapatite in Dilute Phosphate Solution," *Phys. Chem. Glasses: Eur. J. Glass Sci. Technol., Part B,* **47**[6] 647-58 (2006).

[8]S. B. Jung and D. E. Day, "Conversion Kinetics of Silicate, Borosilicate, and Borate Bioactive Glasses to Hydroxyapatite," *Phys. Chem. Glasses: Eur. J. Glass Sci. Technol., Part B,* **50**[2] 85-88 (2009).

[9]Q. Fu, M. N. Rahaman, B. S. Bal, L. F. Bonewald, K. Kuroki, and R. F. Brown, "Silicate, Borosilicate, and Borate Bioactive Glass Scaffolds with Controllable Degradation Rate for Bone Tissue Engineering Applications. Ii. In Vitro and in Vivo Biological Evaluation," *J. Biomed. Mater. Res., Part A,* **95**[1] 172-79 (2010).

[10]Q. Fu, M. N. Rahaman, H. Fu, and X. Liu, "Silicate, Borosilicate, and Borate Bioactive Glass Scaffolds with Controllable Degradation Rate for Bone Tissue Engineering Applications. I. Preparation and in Vitro Degradation," *J. Biomed. Mater. Res., Part A,* **95**[1] 164-71 (2010).

[11]D. E. Day, J. E. White, R. F. Brown, and K. D. McMenamin, "Transformation of Borate Glasses into Biologically Useful Materials," *Glass Technol.,* **44**[2] 75-81 (2003).

[12]X. Han and D. E. Day, "Reaction of Sodium Calcium Borate Glasses to Form Hydroxyapatite," *J. Mater. Sci.: Mater. Med.,* **18**[9] 1837-47 (2007).

[13]X. Zhang, W. Jia, Y. Gu, W. Xiao, X. Liu, D. Wang, C. Zhang, W. Huang, M. N. Rahaman, D. E. Day, and N. Zhou, "Teicoplanin-Loaded Borate Bioactive Glass Implants for Treating Chronic Bone Infection in a Rabbit Tibia Osteomyelitis Model," *Biomaterials,* **31**[22] 5865-74 (2010).

[14]N. W. Marion, W. Liang, G. C. Reilly, D. E. Day, M. N. Rahaman, and J. J. Mao, "Borate Glass Supports the in Vitro Osteogenic Differentiation of Human Mesenchymal Stem Cells," *Mech. Adv. Mater. Struct.,* **12**[3] 239-46 (2005).

[15]H. Fu, Q. Fu, N. Zhou, W. Huang, M. N. Rahaman, D. Wang, and X. Liu, "In Vitro Evaluation of Borate-Based Bioactive Glass Scaffolds Prepared by a Polymer Foam Replication Method," *Mater. Sci. Eng., C,* **29**[7] 2275-81 (2009).

[16]K. P. Fears, "Formation of Hollow Hydroxyapatite Microspheres " Master of Science, Materials Science & Engineering Department, University of Missouri-Rolla (2001).

[17]M. Yamauchi, T. Yamaguchi, H. Kaji, T. Sugimoto, and K. Chihara, "Involvement of Calcium-Sensing Receptor in Osteoblastic Differentiation of Mouse Mc3t3-E1 Cells," *Am. J. Physiol.,* **288**[3 51-3] E608-E16 (2005).

[18]G. S. Sandhu, "Synthesis and Characterization of Microspheres for Controlled Release," MS, Mechanical Engineering Department, Missouri University of Science and Technology (2010).

[19]H. Fu, M. N. Rahaman, D. E. Day, and R. F. Brown, "Hollow Hydroxyapatite Microspheres as a Device for Controlled Delivery of Proteins," *J. Mater. Sci.: Mater. Med.,* **22**[3] 579-91 (2011).

[20]D. H. Baker, "Utilization of Isomers and Analogs of Amino Acids and Other Sulfur-Containing Compounds," *Prog. Food Nutr. Sci.,* **10**[1-2] 133-78 (1986).

[21]N. Tarimci, S. Sener, and T. Kilinc, "Topical Sodium Sulfacetamide/Sulfur Lotion [1]," *J. Clin. Pharm. Ther.,* **22**[4] 301 (1997).

[22]A. N. Lin, R. J. Reimer, and D. M. Carter, "Sulfur Revisited," *J. Am. Acad. Dermatol.,* **18**[3] 553-58 (1988).

[23]R. Lillo and L. F. Peltier, "The Substitution of Plaster of Paris Rods for Portions of the Diaphysis of the Radius in Dogs," *Surg. Forum,* **6** 556-8 (1956).

[24]W. H. Bell, "Resorption Characteristics of Bone and Bone Substitutes," *Oral Surg. Oral Med. Oral Pathol.,* **17** 650-7 (1964).

[25]N. E. Alderman, "Sterile Plaster of Paris as an Implant in the Infrabony Environment: A Preliminary Study," *J. Periodontol.,* **40**[1] 11-3 (1969).

[26]W. R. Walsh, P. Morberg, Y. Yu, J. L. Yang, W. Haggard, P. C. Sheath, M. Svehla, and W. J. Bruce, "Response of a Calcium Sulfate Bone Graft Substitute in a Confined Cancellous Defect," *Clin. Orthop. Relat. Res.*[406] 228-36 (2003).

[27]A. R. Conroy, W. H. Manring, and W. C. Bauer, *Glass Ind.* (1966).

[28]L. Nemec, "Refining in the Glass Melting Process," *J. Am. Ceram. Soc.,* **60**[9-10] 436-40 (1977).

[29]J. E. Shelby, "Introduction to Glass Science and Technology," pp. 291 2nd ed. Royal Society of Chemistry: Cambridge, (2005).

[30]T. Chivers and C. Lau, "Raman Spectroscopic Identification of the S4n- and S3- Ions in Blue Solutions of Sulfur in Liquid Ammonia," *Inorg. Chem.,* **21**[1] 453-55 (1982).

[31]G. J. Rosasco and J. H. Simmons, "Identification of Sulfur Deposits in Bubbles in Glass by Raman Scattering Spectroscopy," *Am. Ceram. Soc. Bull.*, **54**[6] 590-91 (1975).

[32]G. J. Rosasco and J. H. Simmons, "Investigation of Gas Content of Inclusions in Glass by Raman Scattering Spectroscopy," *Am. Ceram. Soc. Bull.*, **53**[9] 626-30 (1974).

[33]W. L. Konijnendijk and J. H. J. M. Buster, "Raman-Scattering Measurements of Silicate Glasses Containing Sulphate," *J. Non-Cryst. Solids,* **23**[3] 401-18 (1977).

[34]A. A. Ahmed, N. A. Sharaf, and R. A. Condrate Sr, "Raman Microprobe Investigation of Sulphur-Doped Alkali Borate Glasses," *J. Non-Cryst. Solids,* **210**[1] 59-69 (1997).

[35]M. Lenoir, A. Grandjean, S. Poissonnet, and D. R. Neuville, "Quantitation of Sulfate Solubility in Borosilicate Glasses Using Raman Spectroscopy," *J. Non-Cryst. Solids,* **355**[28-30] 1468-73 (2009).

[36]D. A. McKeown, I. S. Muller, H. Gan, I. L. Pegg, and C. A. Kendziora, "Raman Studies of Sulfur in Borosilicate Waste Glasses: Sulfate Environments," *J. Non-Cryst. Solids,* **288**[1-3] 191-99 (2001).

[37]T. Tsujimura, X. Xue, M. Kanzaki, and M. J. Walter, "Sulfur Speciation and Network Structural Changes in Sodium Silicate Glasses: Constraints from Nmr and Raman Spectroscopy," *Geochim. Cosmochim. Acta,* **68**[24] 5081-101 (2004).

[38]B. N. Meera and J. Ramakrishna, "Raman Spectral Studies of Borate Glasses," *J. Non-Cryst. Solids,* **159**[1-2] 1-21 (1993).

[39]Y. Matsuda, M. Kawashima, Y. Moriya, T. Yamada, O. Yamamuro, and S. Kojima, "Composition Dependence of the Boson Peak and Universality in Lithium Borate Binary Glasses: Inelastic Neutron and Raman Scattering Studies," *J. Phys. Soc. Jpn.,* **79**[3] (2010).

[40]A. B. Kaplun and A. B. Meshalkin, "Phase Equilibria in the Li2o-B2o3 System," *Inorg. Mater.,* **35**[11] 1154-58 (1999).

[41]A. B. Kaplun and A. B. Meshalkin, "Phase Equilibria in the Binary Systems Li2o-B2o3 and Cs2o-B2o3," *J. Cryst. Growth,* **209**[4] 890-94 (2000).

[42]H. Yu, Z. Jin, Q. Chen, and M. Hillert, "Thermodynamic Assessment of the Lithium-Borate System," *J. Am. Ceram. Soc.,* **83**[12] 3082-88 (2000).

[43]G. N. Greaves and S. Sen, "Inorganic Glasses, Glass-Forming Liquids and Amorphizing Solids," *Adv. Phys.,* **56**[1] 1-166 (2007).

Table 1. As-Batched composition, analyzed* (XRF) composition, density (ρ) and molar volume (V_m) for glasses melted at 1100°C for one hour. The values in ( ) are Mol%.

Glass Identifier		SO_3	CaO	Li_2O	B_2O_3	ρ	V_m
		wt% (mol%)				g/cm^3	cm^3/mol
CaLB-0%	Batch	0.0 (0)	40.0 (41.5)	7.5 (14.6)	52.5 (43.9)	2.64	22.0
	XRF	0.0 (0)	39.9 (41.5)	7.5 (14.6)	52.6 (43.9)		
CaLB-12%	Batch	12.5 (9.4)	35.0 (37.6)	6.6 (13.3)	45.9 (39.7)	2.64	22.8
	XRF	11.4 (8.5)	35.7 (38.3)	6.6 (13.3)	46.3 (39.9)		
CaLB-22%	Batch	22.3 (17.3)	31.1 (34.4)	5.8 (12.0)	40.8 (36.3)	2.62	23.6
	XRF	20.5 (15.8)	32.0 (35.2)	5.9 (12.2)	41.6 (36.8)		

*** Analyzed for SO_3 and CaO only. Li_2O and B_2O_3 concentration determined by difference from 100%.**

Table 2. DTA data. Minor phases formed at T_{x1} for CaLB-0% and CaLB-12% and at T_{x2} for CaLB-22%.

Glass Identifier	T_g (°C)	T_{x1} (°C)/ Crystal	T_{x2} (°C)/ Crystal	Minor Phases Identified by XRD
CaLB-0%	477	598/ $2CaO.B_2O_3$	-	$CaO.B_2O_3$
CaLB-12%	492	608/ $CaO.B_2O_3$	-	$2CaO.B_2O_3$ $CaSO_4$ $CaSO_3$
CaLB-22%	502	559/ $CaSO_4$	653/ $CaO.B_2O_3$	$2CaO.B_2O_3$ $Li_2O.B_2O_3$ Li_2SO_4

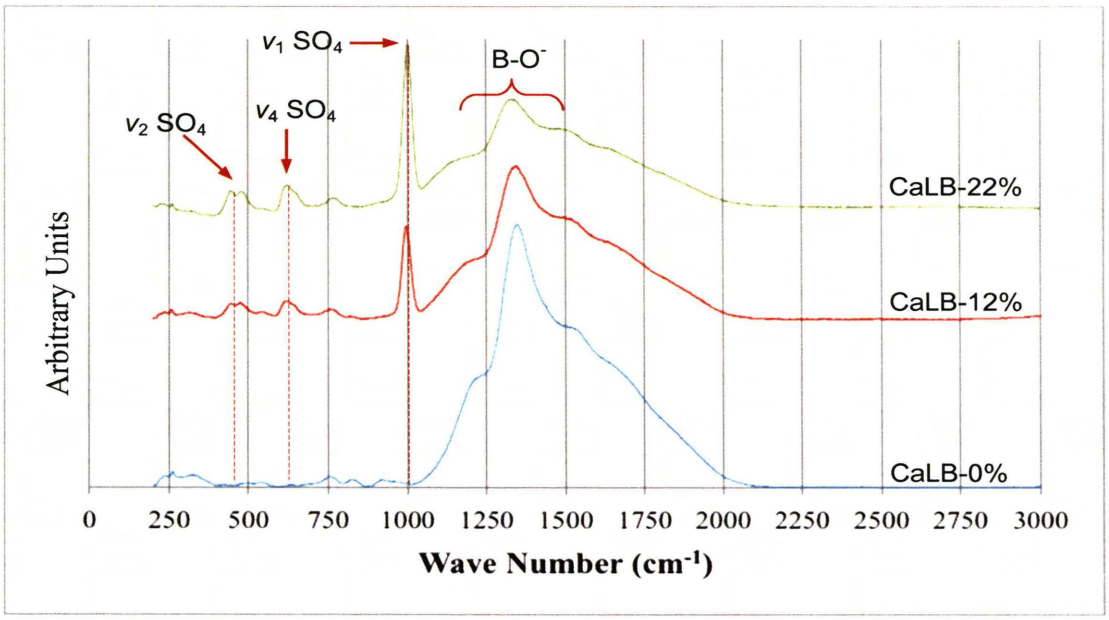

Figure 1. Micro-Raman spectra for CaLB-0%, CaLB-12%, and CaLB-22% glasses.

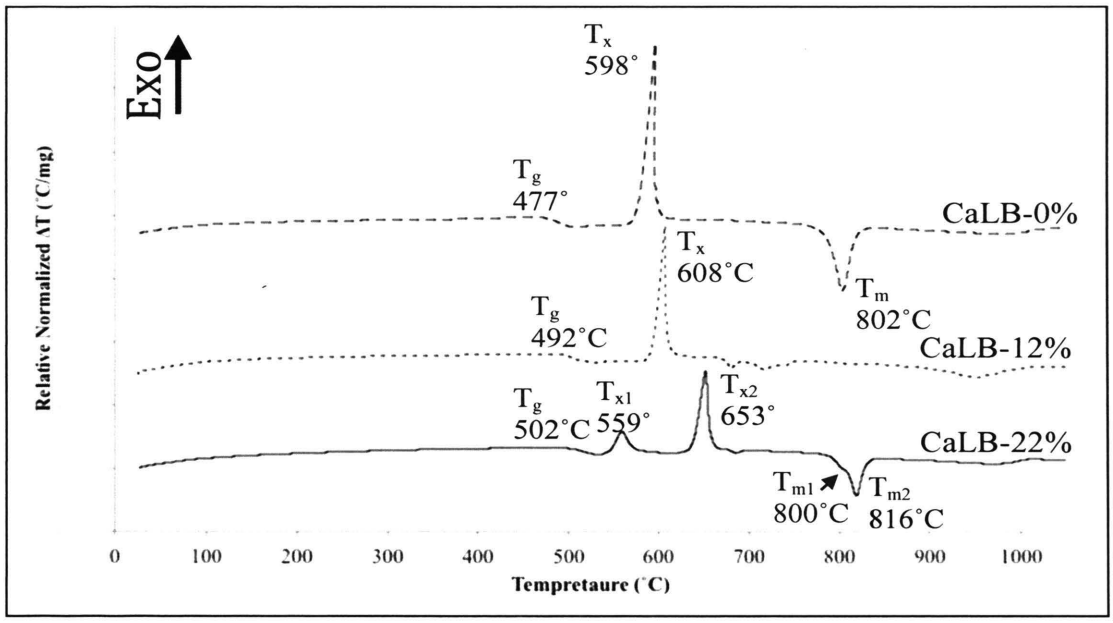

Figure 2. Typical DTA spectra for CaLB-0%, CaLB-12%, and CaLB-22% glasses. T_g = Glass transition temperature, T_x = Crystallization temperature, T_m = Melting, Heating rate=10°C/min.

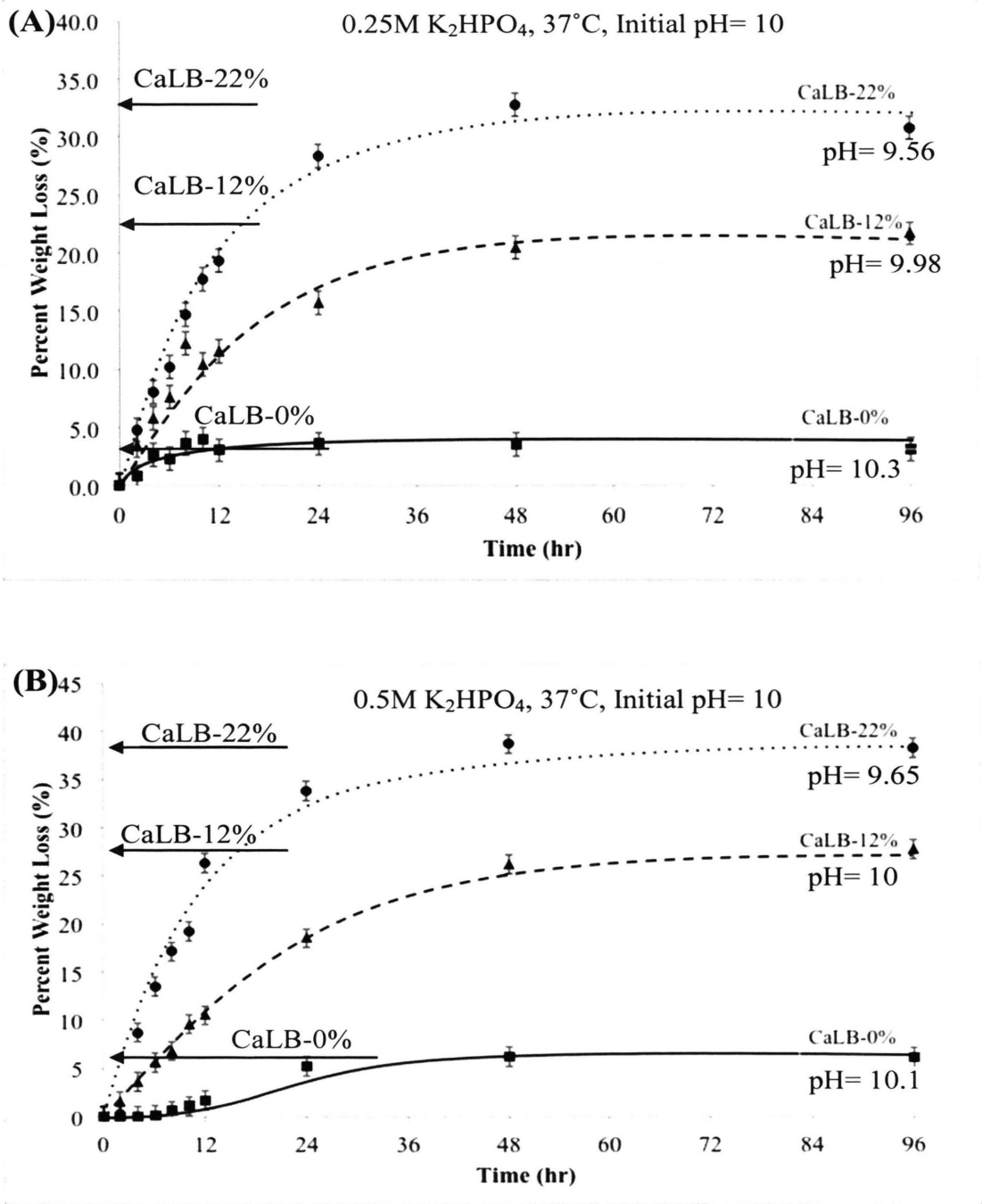

Figure 3. Percent weight loss for a sample CaLB glass reacted in (A) 0.25M and (B) 0.5M K_2HPO_4 solutions at 37°C with initial pH= 10. The final pH of the solution after ~96 hours of reaction is given for each glass. The lines are for guidance. The arrows for each glass point to the weight loss after reaction for ~96 hrs. The error bars are estimates based on weighing measurements.

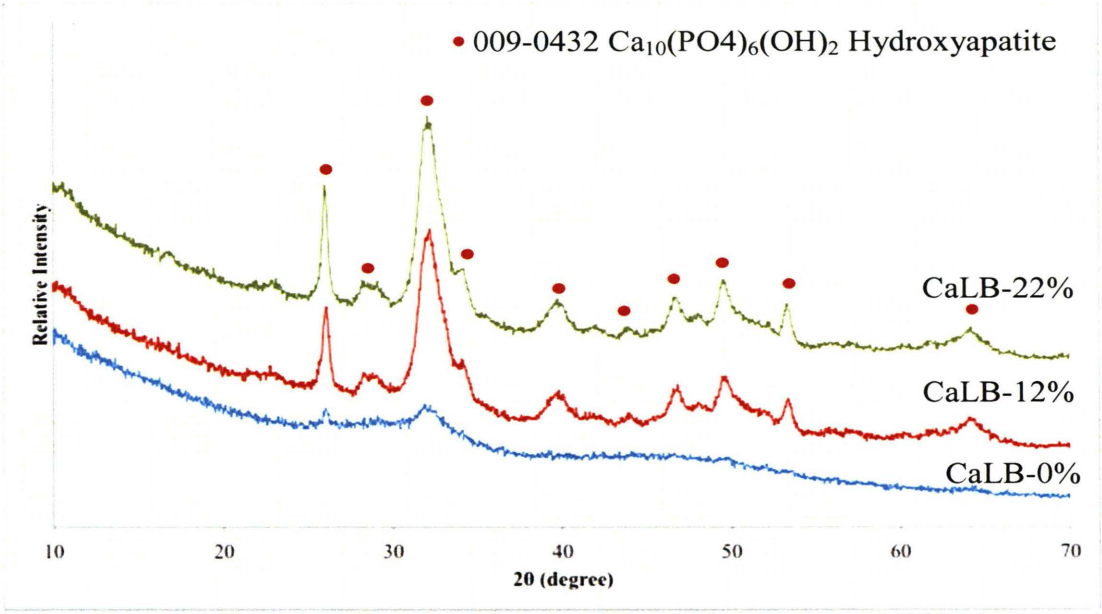

Figure 4. XRD pattern for the CaLB-0%, CaLB-12%, and CaLB-22% glass particles (150-355μm) after reaction in the 0.5M K_2HPO_4 solution at 37°C for 96 hours.

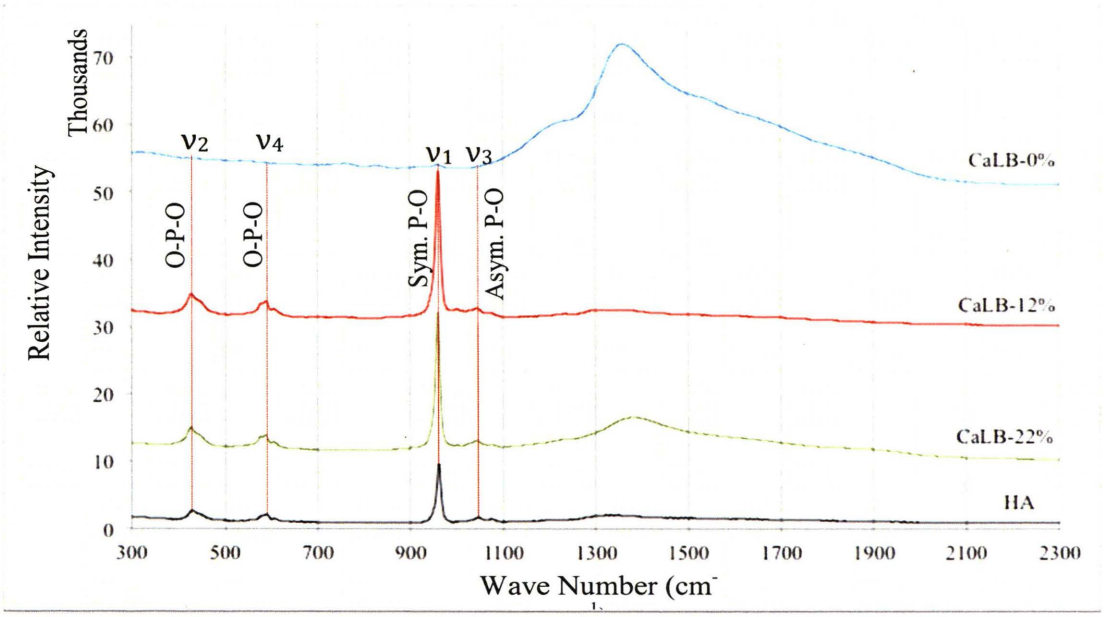

Figure 5. Micro-Raman spectra of particles (150-355μm) reacted in a 0.5M K_2HPO_4 solution at 37°C for 96 hours. Bottom curve is HA (Fisher Scientific St Louis MO- Cat#: C133-212)

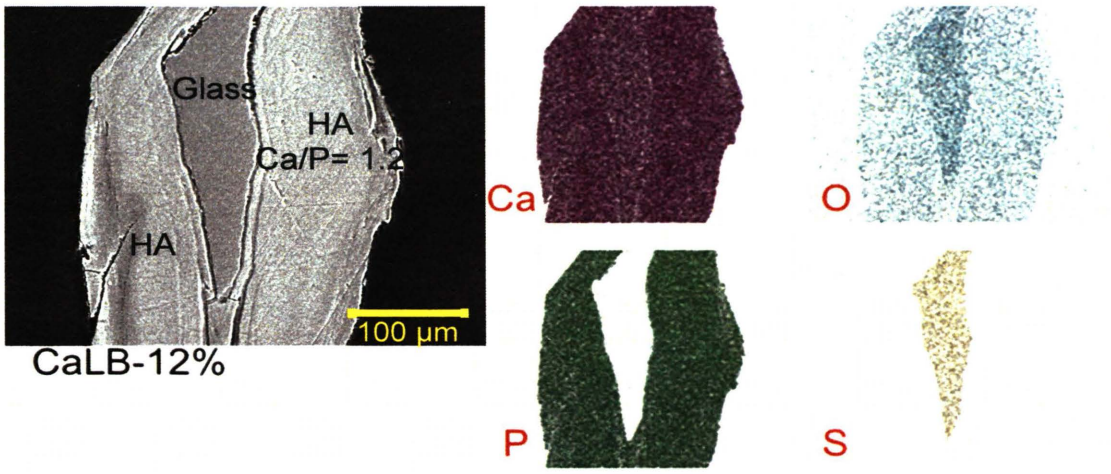

Figure 6. Phase mapping analysis for calcium (Ca), oxygen (O), phosphorus (P), and sulfur (S) for a CaLB-12% glass particle that had reacted in the 0.5M K_2HPO_4 solution at 37°C for 96 hours.

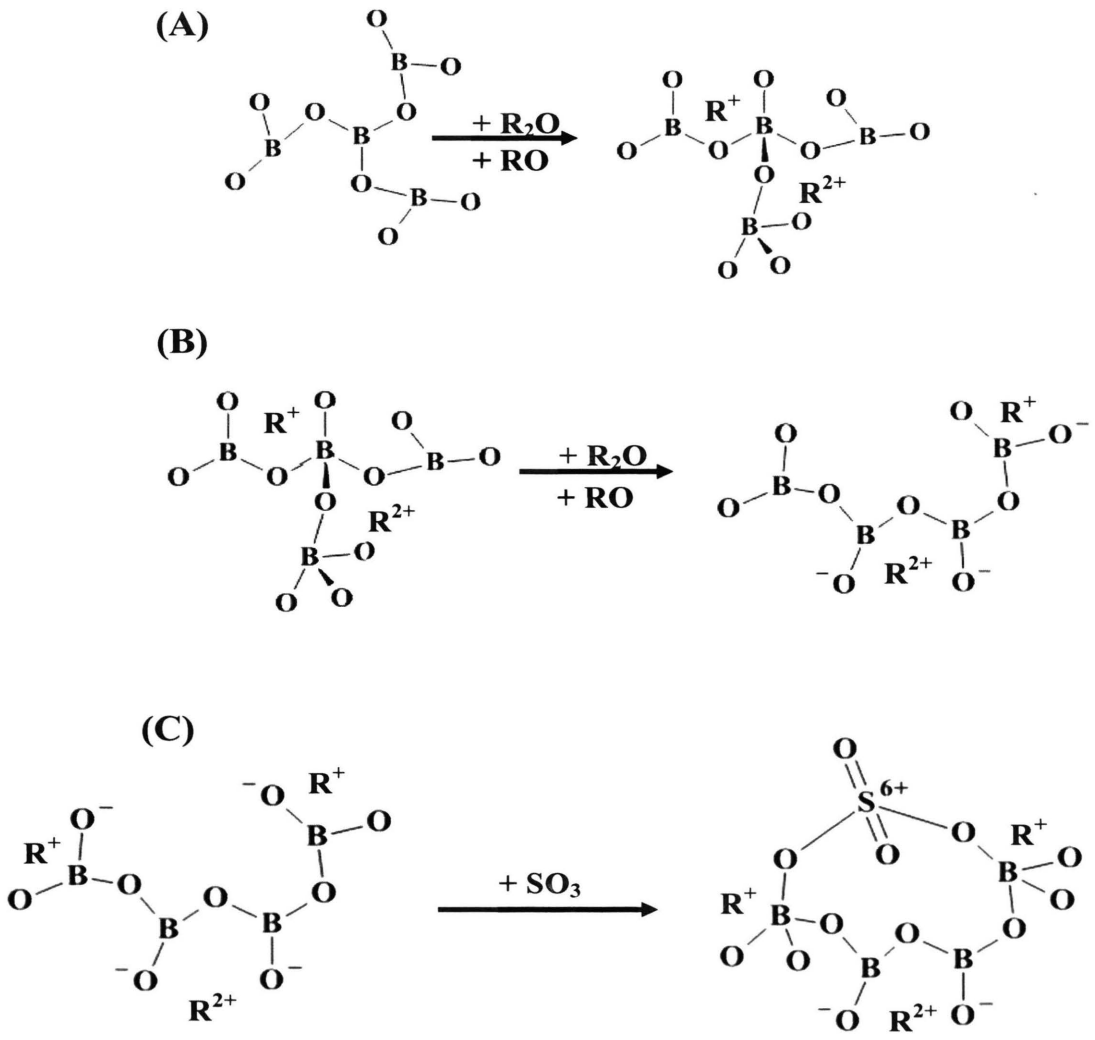

Figure 7. Schematic of incorporation of sulfate ions in the borate glass structure. (A) Shows how vitreous B_2O_3 converts to a cross-linked 3 dimensional structure with No non-bridging oxygen ion at 33 mol% R_2O+RO. (B) Shows how 66.67 B_2O_3. 33.33 R_2O+RO structure converts to 50 B_2O_3. 50 R_2O+RO structure (The CaLB glasses). (C) Adding sulfur to 50 B_2O_3. 50 R_2O+RO structure (The sulfur-containing CaLB glasses). R= Alkali or alkali earth metal. O= Bridging oxygen, O^-=Non-bridging oxygen, S= Sulfur, B= Boron

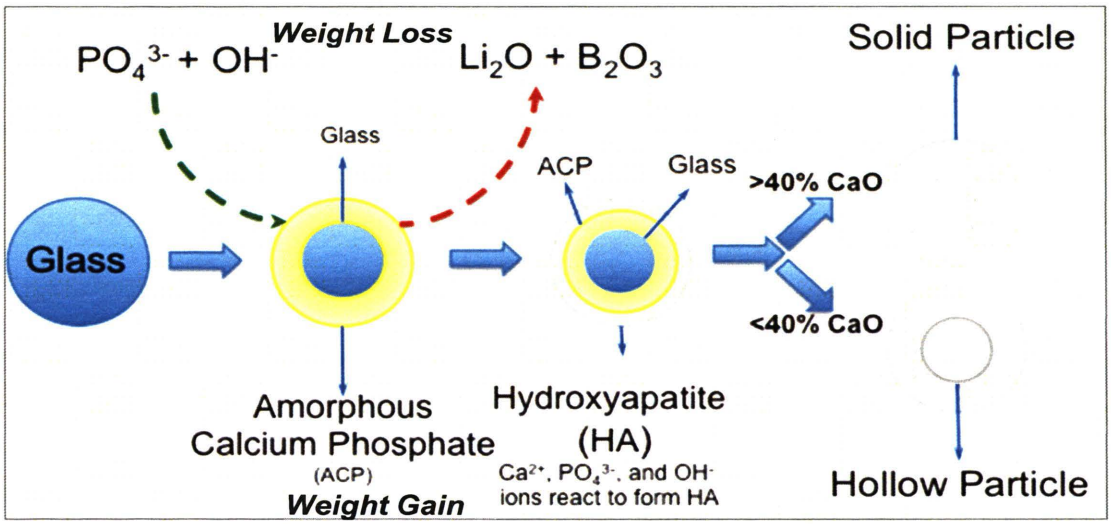

Figure 8. Schematic of the conversion process of CaLB glasses to Hydroxyapatite.

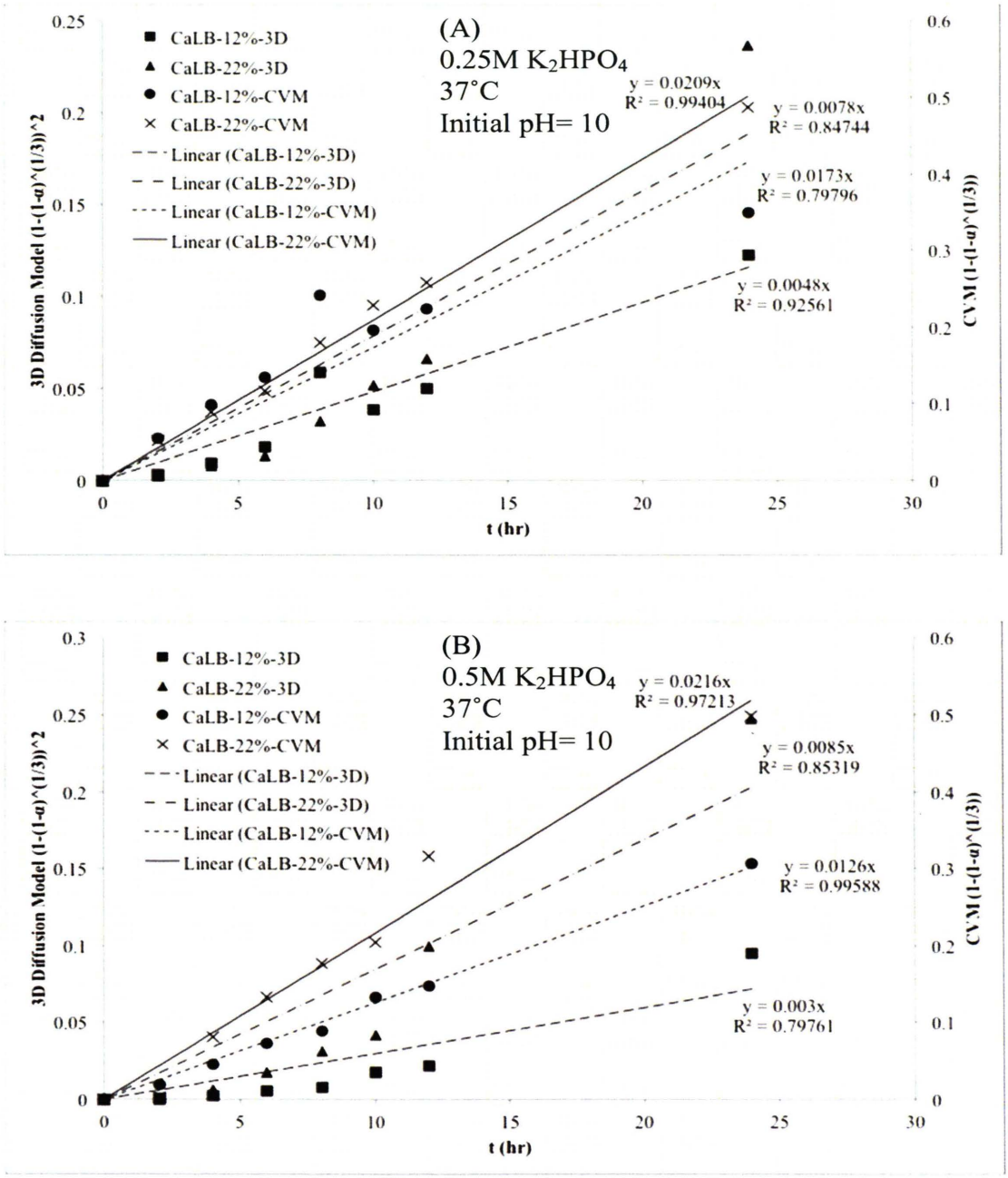

Figure 9. Reaction kinetic modeling of sulfur-containing CaLB glasses reacted in (A) 0.25M and (B) 0.5M K_2HPO_4 solution at 37°C with initial pH= 10. Horizontal axis is time (hours) and vertical axes are CVM and 3D Diffusion model equations. The normalized weight loss is "α". The equation for each fitted line is provided along with the coefficient of determination for linear regression (R^2).

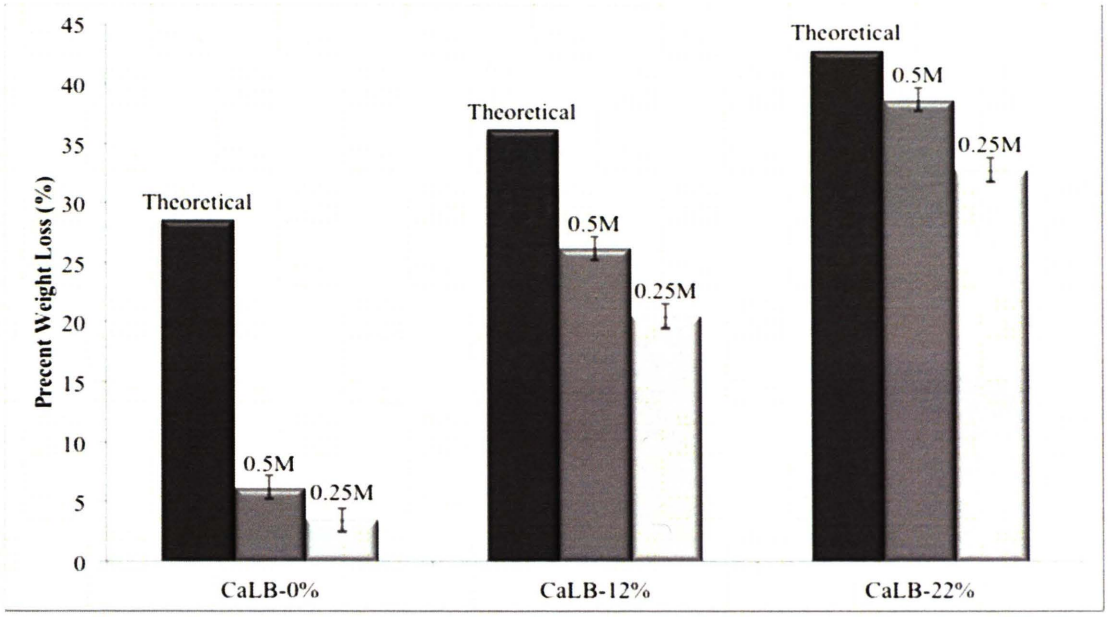

Figure 10. Comparison of the measured weight loss at 48 hours for CaLB glasses reacted in 0.25 and 0.5 molar K_2HPO_4 solution at 37°C with their theoretical weight loss (assuming stoichiometric HA forms).

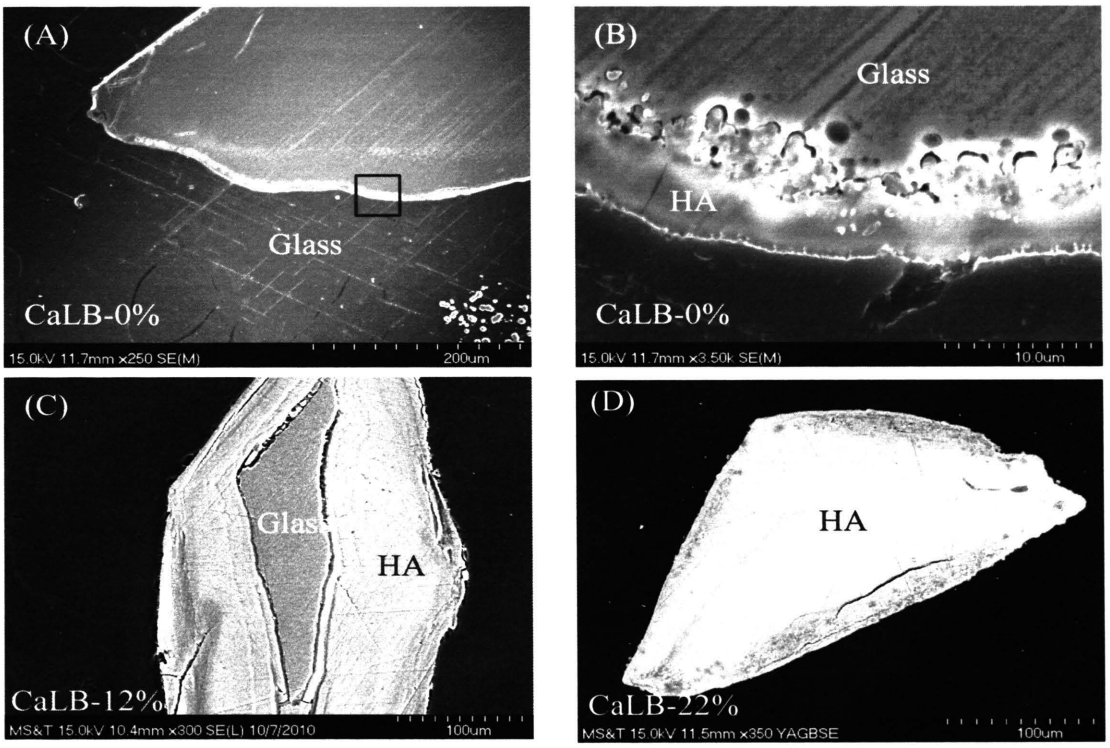

Figure 11. SEM image of the cross section of a CaLB-0% (A and B), CaLB-12% (C), and CaLB-22% particle reacted in 0.5M K_2HPO_4 solution at 37°C for 96 hrs. (B) is a magnified image of the black box showed in (A).

APPENDIX: SUPPLEMENTARY DATA FOR PAPER 1

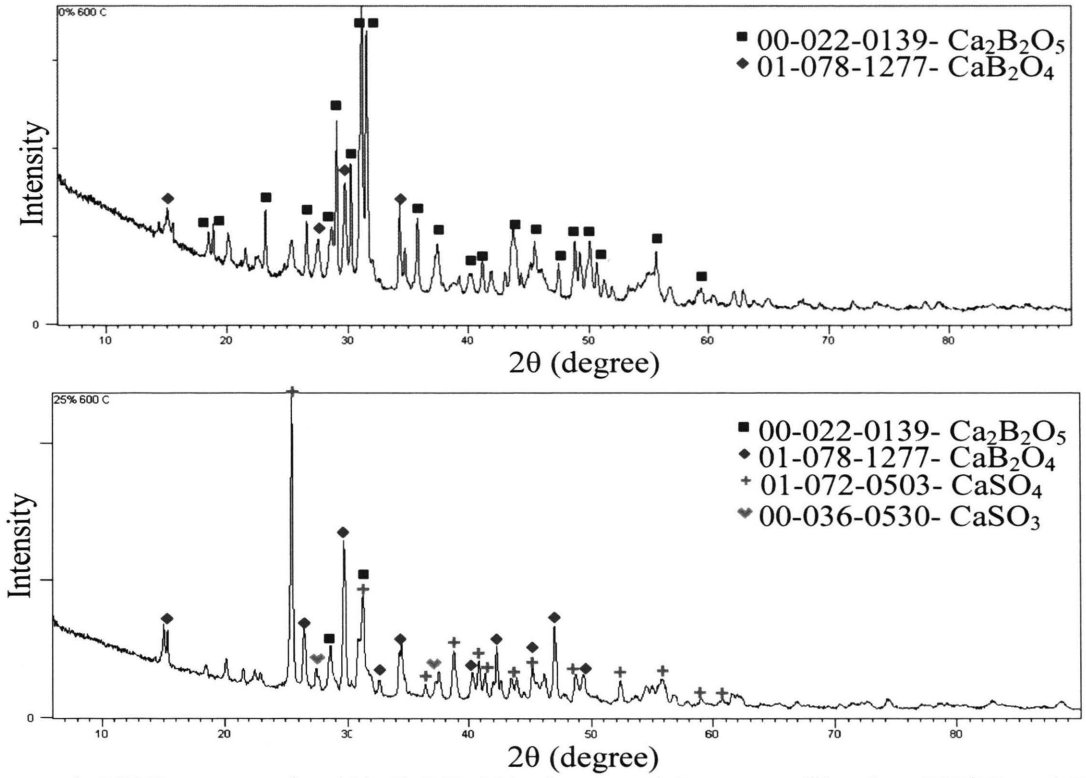

Figure 1. XRD spectra for (A) CaLB-0% glass particles crystallized at 598°C and (B) CaLB-12% glass particles crystallized at 608°C.

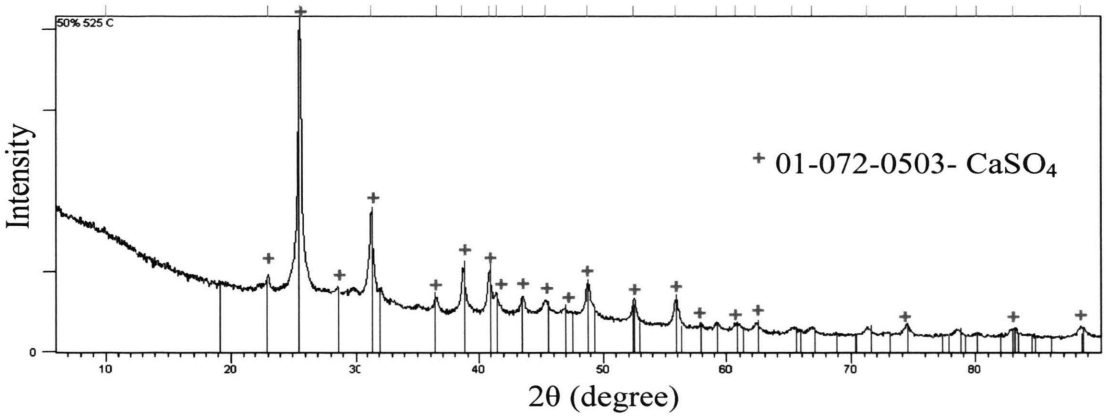

Figure 2. XRD spectra for (A) CaLB-22% glass particles crystallized at 559°C and (B) CaLB-22% glass particles crystallized at 653°C.

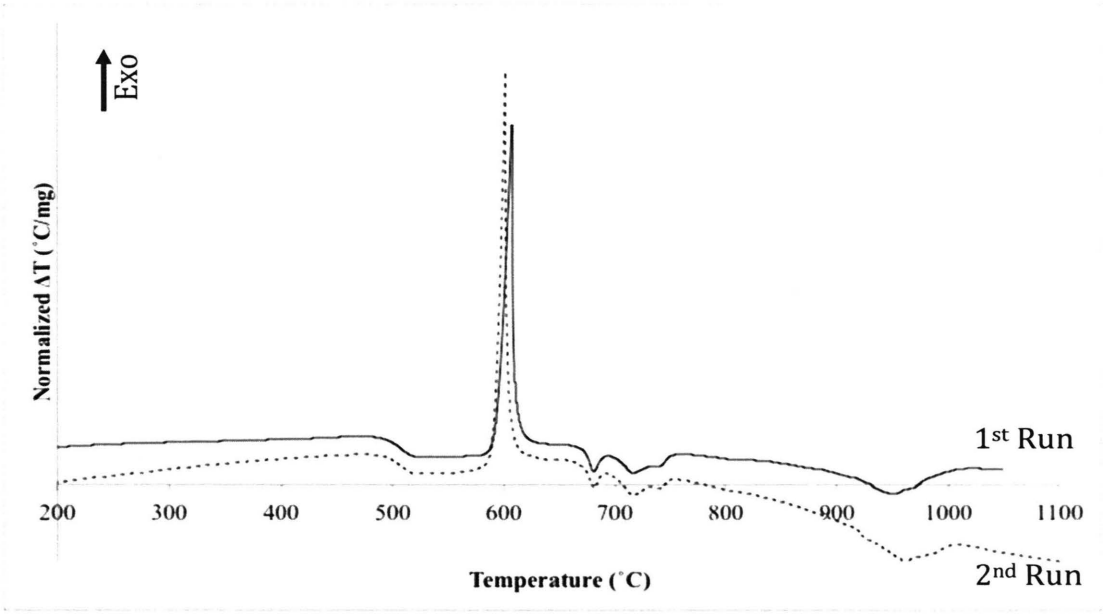

Figure 3. Two typical DTA spectra for CaLB-12% glass showing that this spectrum is reproducible. The endothermic peaks ~700°C and the endothermic peak ~950°C is repeated after running this sample again using the same DTA.

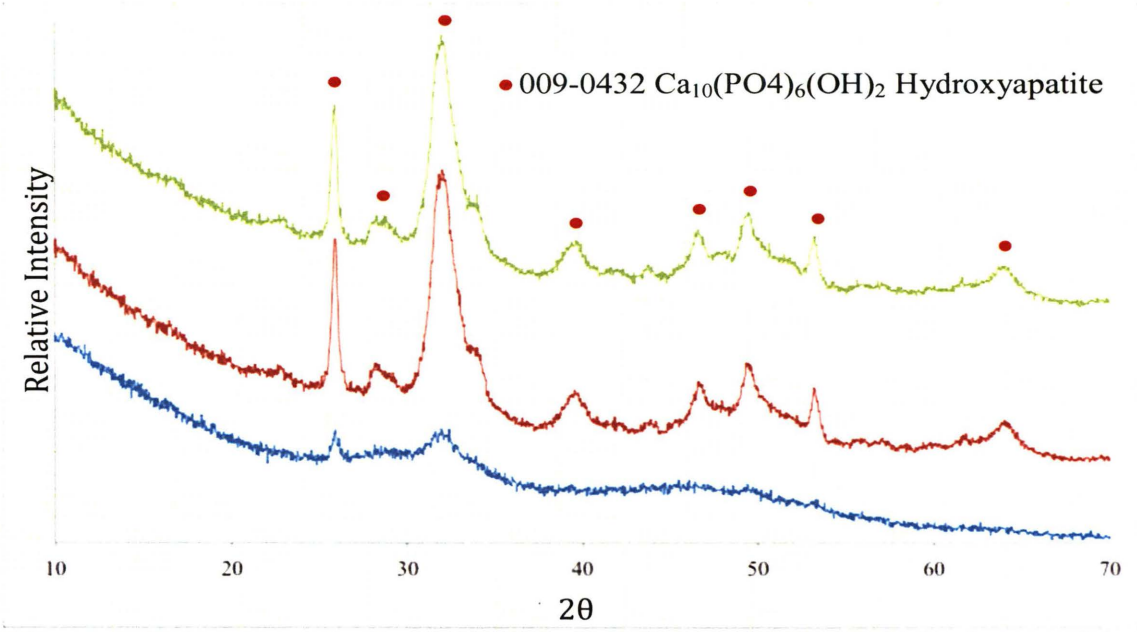

Figure 4. XRD pattern for the CaLB-0%, CaLB-12%, and CaLB-22% glass particles (150-355μm) after reaction in the 0.25M K_2HPO_4 solution at 37˚C for 96 hours.

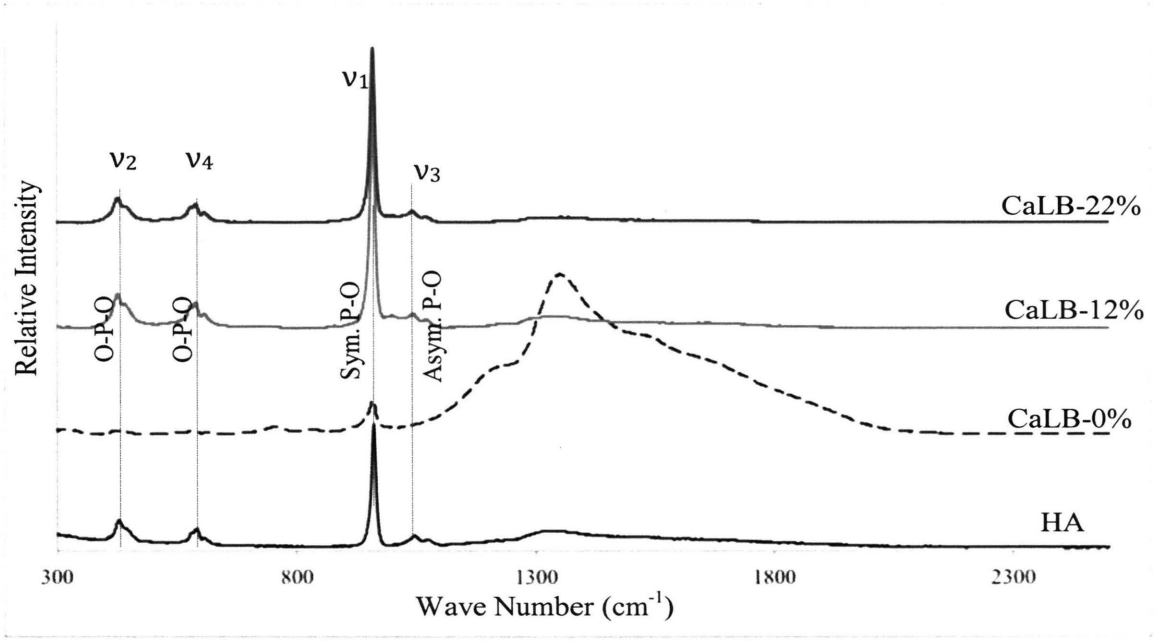

Figure 5. Micro-raman spectra of particles (150-355μm) reacted in a 0.25M K_2HPO_4 solution at 37°C for 96 hours. Bottom curve is HA (Fisher Scientific St Louis MO- Cat#: C133-212)

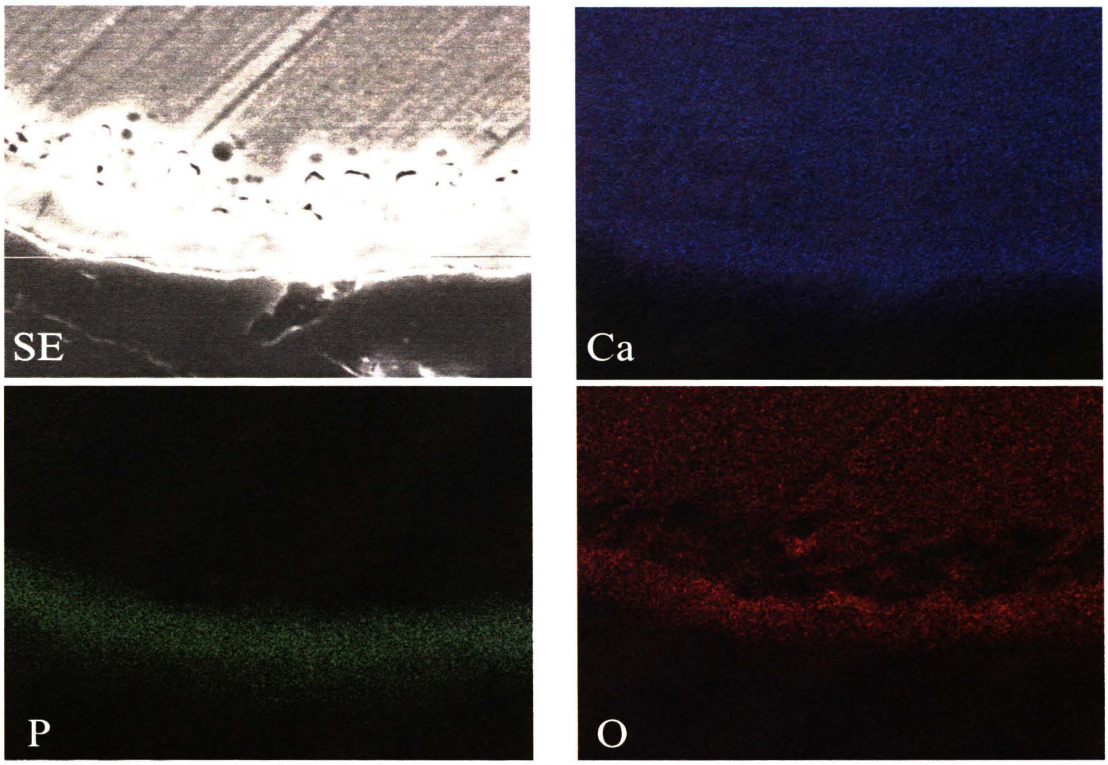

Figure 6. Phase mapping analysis for calcium (Ca), oxygen (O), and phosphorous (P) for a CaLB-0% glass particle that had reacted in the 0.5M K_2HPO_4 solution at 37°C for 96 hours.

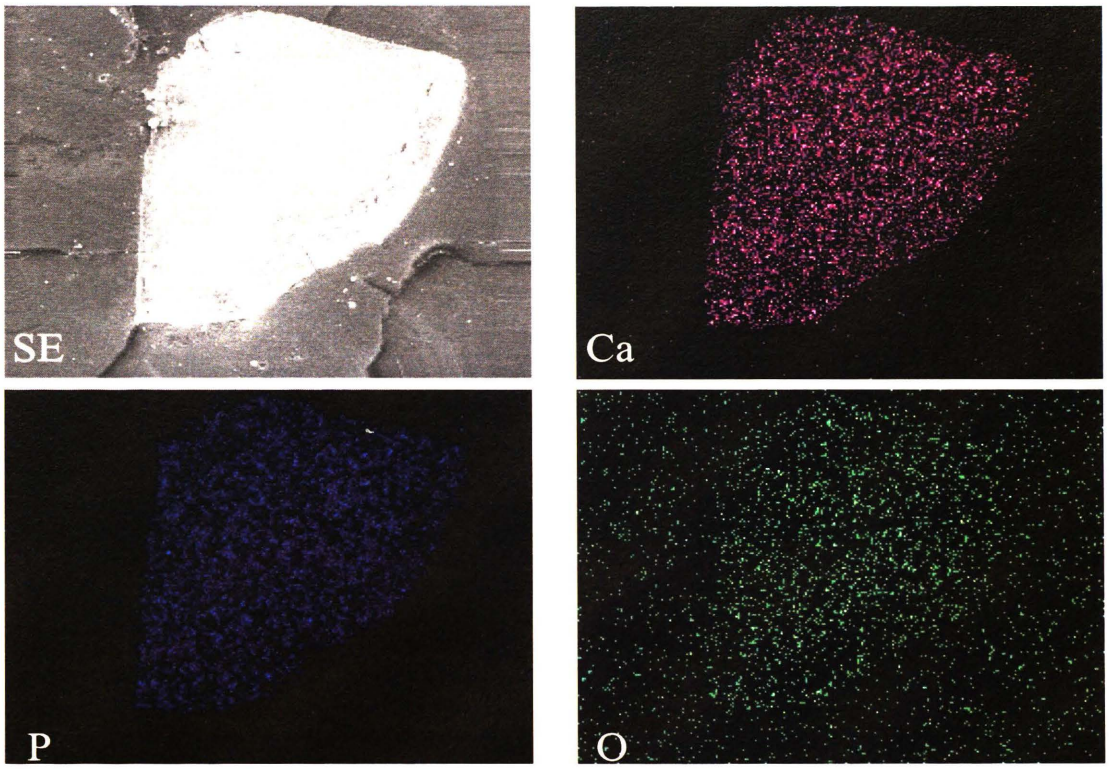

Figure 7. Phase mapping analysis for calcium (Ca), oxygen (O), and phosphorous (P) for a CaLB-22% glass particle that reacted in the 0.5M K_2HPO_4 solution at 37°C for 96 hours.

2: The Effect of Sulfur on Structure and Conversion of Bioactive Borate Glasses. Part II: *In-vivo* Studies

Ali Mohammadkhah,[†] Delbert E. Day,[†] Richard K. Brow, [†] Mohamed N. Rahaman, [†]

Roger F. Brown[§]

† Department of Materials Science and Engineering, Center for Bone and Tissue Repair and Regeneration, Missouri

University of Science and Technology, Rolla, Missouri 65409

§ Department of Biological Sciences, Center for Bone and Tissue Repair and Regeneration, Missouri

University of Science and Technology, Rolla, Missouri 65409

Abstract

The effect of sulfur and phosphorus on the conversion of two different bioactive borate glasses was studied, *in-vivo*. Discs made from two sulfur-free glasses (CaLB-0 and 93B3-0) and two sulfur-containing glasses (CaLB-12 and 93B3-6) were implanted in a subcutaneous site in rats for 2, 4, and 12 weeks. Each rat remained healthy during the experiment and there were no sign of infection or adverse reaction at the implantation site.

The CaLB glass discs reacted with the body fluids and formed a thin calcium phosphate reacted layer on their surface, but the 93B3 glass discs reacted to form a thicker calcium phosphate reacted layer with an onion-skin structure. The phosphorus-free CaLB implants compared to phosphorus-containing 93B3 implants, the CaLB implants

absorbed 2 times more phosphorus from the body fluids to form the calcium phosphate reacted layer.

Compared to the CaLB implants, the connective tissue attached to the 93B3 implants was ~3 times thicker, and qualitatively contained more blood vessels and collagen. For all of the sulfur-containing implants sulfur released to the body fluids and was not presented in the reacted materials. Sulfur had only a small effect on the *in-vivo* reaction of the CaLB glasses but the sulfur-containing 93B3-6 glass had a 2 to 3 times greater reaction rate compared to the sulfur-free 93B3-0 glass *in-vivo*.

I. Introduction

Sulfur is the key in three amino acids in the human body; two essential amino acids cysteine, methionine, and one non-essential amino acid, taurine. Sulfur also found in many other compounds in the body i.e. heparin, insulin, thiamin, biotin, and chondroitin sulfate[1]. Methionine is an essential amino acid that is not synthesized in the body so it must be supplied from external sources. Methionine is responsible for the formation of cysteine, which participates in most of sulfur-containing reactions in the body. Cysteine is a precursor in the production of antioxidant glutathione and also in the formation of disulfide bridges. A disulfide bridge is a covalent bond of two sulfur-containing groups. This is the bond that gives rigidity and toughness to human hair and nails. Keratin, which contains a large amount of cysteine, is the key component of skin, hair, and nail. Sulfur has a long history of treating different dermatological disorders[2; 3] and helps in wound healing via the formation of keratin[2].

Another sulfur-containing material, which plays an important role in cartilage and bone function, is chondroitin sulfate. Chondroitin sulfate is a major component of extracellular matrix (ECM) and cartilage. The resistance behavior of cartilage tissue to compression is because of packed sulfate groups in chondroitin sulfate.

Sulfate has a long history in biomedical science. Calcium sulfate is a FDA approved material that was one the first materials used in orthopedic surgery, more than 100 years ago. Calcium sulfate is an effective bone graft material that is completely resorbed *in-vivo* in 5 to 7 weeks[4; 5]. It does not cause inflammation, foreign body reaction or rejection of the implant. Calcium sulfate is an osteoconductive and angiogenic material, which makes it a good candidate for use in bone scaffolds[4; 6-8]. It has been reported that when $CaSO_4$ is used *in-vivo* as bone regeneration implant, it reduces the local pH and makes the environment more acidic by releasing sulfate ions. This causes the adjacent bone to demineralize and release matrix-bound bone growth factor, which stimulates the growth of new bone[9].

Bioactive glasses were discovered in 1971[10]. The most used bioactive glass, 45S5, is a silicate glass with a low silica content (compared to other more durable silicate glasses) and a high calcium to phosphorus ratio (~10). It is biocompatible as well as bioactive *in-vivo*. It bonds to adjacent bone via a carbonated hydroxyapatite layer on the glass surface. Over the last 40 years the mechanism of how Bioglass® reacts with body fluid and bonds to bone have been studied in detail[11-13].

Recently it has been shown that other glass forming systems like borate glasses are also bioactive[14-17]. Borate glasses, like silicate glasses, convert to hydroxyapatite (HA) either

in-vitro or *in-vivo* but convert 3-5 times more rapidly[12; 13; 18; 19]. The conversion rate can be controlled by changing the composition of the glass i.e. adding SiO_2, alkali, and/or alkaline earth.

Studying the release of ionic dissolution products from inorganic materials plays an important role in understanding their bioactivity as well as their angiogenic and antimicrobial behavior[20]. For instance ionic dissolution products of 45S5 and other silicate glasses have been shown to stimulate the expression of several genes of osteoblastic cells[21].

Bioactive glasses have the ability to contain several different inorganic ions in their structure and release them while converting to HA. By altering the composition of a bioactive glass, it is possible to deliver different ions that have anabolic effects on bone metabolism like Cu, Zn, Sr, etc.[22-25]. Several studies have investigated the effect of such elements on bone and tissue regeneration[25]. Several promising results indicate that scaffolds made from bioactive glasses have the potential to deliver, in a controlled manner, elements that are required for bone regeneration.

Although calcium sulfate has a long history in bone regeneration, doping a glass with sulfur for biological purposes has never been reported, nor has the effect of sulfur *in-vitro* or *in-vivo* on the glass degradation rate, conversion products, and body response. In the present work, two calcium lithium borate glasses were doped with sulfur by using $CaSO_4$ to supply a quarter of the CaO in the glass composition and the remainder from $CaCO_3$.

Since this is the first time (to the authors knowledge) that a glass doped with sulfur was tested *in-vivo* any evidence of toxicity such as tissue necrosis or mast cell, was also of interest in the present work.

Based on previous work (evaluation of sulfur-doped borate glasses *in-vitro*) it was expected that adding sulfur to the glass would also affect its reaction *in-vivo*. The effect of sulfur on the conversion rate, the conversion products, and the structure of the reacted materials were investigated by implanting these glasses subcutaneously in rats for up to 12 weeks.

Histological studies were done to investigate the possible toxicity or inflammatory response in the animal. In this study, the effect of sulfur on the formation of new micro vessels was studied by evaluating tissue sections stained with H&E and CD31 staining. Collagen formation is important either in soft or hard tissue repair and regeneration so the sulfur-containing glasses were compared with sulfur-free glasses in terms of collagen formation by evaluating histology sections stained with Masson's Trichrome.

II. Experimental Procedure

(1) Glass Compositions and Preparation

The compositions of the bioactive glasses investigated are shown in Table 1. The raw materials used were reagent grade H_3BO_3, $CaCO_3$, $CaSO_4$, Li_2CO_3, K_2CO_3, Na_2CO_3, $MgCO_3$, and $NH_4H_2PO_4$. Calcium sulfate was the source of sulfur in the sulfur-containing glasses. One quarter of the CaO content in the CaLB glass and 93-B3 glass was supplied by $CaSO_4$, and the remainder by $CaCO_3$. The glasses were melted in a platinum crucible

in an electric furnace for 1 hour at 1100°C, for the CaLB glasses and at 1050°C for the 93-B3 glasses. Each melt was then poured and quenched between two copper plates. Cylindrical rods, 9mm in diameter were made from the 93B3-0 and 93B3-6 glasses.

(2) In-vivo Experiment

a. Implant Preparation and Sterilization

Rods, 9mm in diameter, were cast from the 93B3-0 and 93B3-6 melts, annealed at 550°C for 2.5 hour, and then cut with a diamond saw into 2mm thick discs. Small pieces of the quenched CaLB-0 and CaLB-12 glass were annealed at 595°C and 615°C, respectively, and then polished with SiC polishing papers (180, 320, 600 grit) to smooth the sharp edges and corners to form discs about 7mm in diameter and 2-3 mm thick. These discs were selected to be about the same size as the 93B3 discs but were not exactly the same shape. Each disc was washed with acetone and ethanol and then placed in glass vials covered with aluminum foil and sterilized in an oven at 300°C overnight.

b. Subcutaneous Implantation in Rats

Six female SD rats between the ages of 16 to 18 weeks were used in this experiment. Two rats (4 implants per animal) were used for each time period of 2, 4, and 12 weeks. Out of the two rats for each time period, the implants in one rat were used in histology studies and implants in the other rat were used for X-Ray Diffraction (XRD), Scanning Electron Microscopy (SEM), Energy Dispersive Spectroscopy (EDS), and micro-Raman. The implants used for histology analysis were decalcified (dissolved the glass completely) so they could not be used for XRD or similar analysis.

Each rat was pre-anesthetized with a mixture of CO_2/O_2 gas prior to an intraperitoneal injection of anesthetic (ketamine/xylazine 0.1 ml/100g). Each rat was shaved with a razor from the base of its tail to its neck and then cleaned with iodine solution to remove the hair and disinfected the incision sites. Four 1cm incisions were made on the back and a sample of each glass was implanted in the pocket under each incision, as shown in Fig 1.

After implantation, the incision was closed with 9mm wound clips and each rat received 0.2ml of penicillin intramuscular (0.1ml in each hind leg). After surgery, each rat was kept warm in a recovery cage until it regained complete consciousness whereupon it was moved to a separate cage. The glass implants remained in the rats for 2, 4 and 12 weeks.

c. Implant Removal and Processing

The rats were euthanized in a sealed container with CO_2 gas. The back of each rat was shaved and cleaned and the implants were then removed from the subcutaneous tissue. For each glass, the implant was put in 70% ethanol and then moved to 100% ethanol. These implants were evaluated by SEM, micro-Raman, and XRD. The other implant of each glass was fixed in a 10% formalin solution at 37°C for 3 days. Each implant was washed with running distilled water and then decalcified in 15ml of CalEx II (Fisher Scientific St. Louis MO) up to 12 hours. After decalcification each sample was washed with running distilled water again and then dehydrated with a series of ethanol solutions from 70% to 100% in a microwave tissue processor (EBSciences H2850 Microwave Processor) operating at 65% power for two and a half minutes. Each implant remained in the ethanol solution for 13 more minutes.

The implants were kept in xylene for another hour and then placed in warm tissue paraffin at 65°C for 3 hours. To complete the paraffin infiltration, tissues were infiltrated with the warm paraffin under vacuum.

The scaffold was then mounted in a parrafin block for histological sectioning with a paraffin mounting system (Leica EG 1150H).

Sections 10μm and 5μm thick were cut with a low profile microtome blade (Thermo Scientific MB35) and floated on a water bath (Lipshaw Electric Tissue Float, model number 375, Detroit MI) at 45°C prior to mounting on a glass slide (Fisher Brand Superfrost microscope slides, St. Louis MO). Three or four tissue sections were placed on each slide, and dried overnight on a slide dryer (Fisher Scientific slide warmer, St. Louis MO).

(3) Sample Analysis

a. X-Ray Diffraction

All phase identification of *in-vivo* implants (one sample for each glass for each time period) was done with either a Panalytical X'Pert Pro (MPD) or a Panalytical X'Pert Materials Research Diffractometer (MRD). Both diffractometers used Cu Kα radiation. The MPD used a minimum step size of 0.026° while the MRD had the incident angle fixed at one degree and a step size 0f 0.03° with a counting time of 1.5 seconds. The MPD was usually used for a bulk sample while the MRD was used for thin films and the surface of the samples. The XRD patterns obtained from each instrument were compared and the pattern with the most distinguishable and sharper peaks was chosen.

The spectra were collected from 10 to 80 degrees (2θ), but only the spectra from 25 to 70 degrees (2θ) are shown herein.

b. Micro-Raman

To identify the different phases across the cross-section of the disc implants the micro-Raman (LabRAM ARAMIS, Horiba Jobin Yvon) spectra were measured from 200 to 2000 cm^{-1} at several points using a diode laser (585 nm). The device was calibrated prior to measuring the spectra for each sample with a piece of a silicon wafer.

c. Scanning Electron Microscopy (SEM) and Energy Dispersive Spectroscopy (EDS)

A field emission Hitachi S-4700 SEM was used for microstructural analysis. This microscope was equipped with a Silicon Drift Detector (SDD) (EDAX Inc. Mahwah, NJ) which was used for elemental and phase mapping. The uncertainty in EDS analysis could be considered as ±5% through out this work.

Each implant was put in xylene for 1 hour and then infiltrated with Poly(methyl methacrylate), PMMA. The samples were then polished with SiC polishing papers (180 to 1200 grit). The cross-section of each implant was analyzed by SEM.

Elemental mapping of the reacted layer was collected to distinguish between the different phases that formed from the *in-vivo* conversion of the glass disc.

The thickness of the reacted layer was measured by ImageJ software and the average thickness value of at least 10 measurements is reported while standard deviation of the data set is calculated as the uncertainty. The thickness of the reacted layer was measured

around the center of the disc where the thickness is relatively uniform as opposed to the corners where the thickness varies (see Fig 2).

d. Histology

The tissue sections were stained by Hematoxylin and Eosin (H&E), immunohistochemical CD31, and Trichrome, at the Pathology Laboratory at the Phelps County Regional Medical Center (PCRMC), Rolla MO.

(4) In-vitro Experiment

In order to compare the *in-vivo* results with the *in-vitro* environment, discs of each glass were reacted in simulated body fluid (nSBF) for one week. The formulation of the different SBF solutions and blood ion concentration are given in Table 2. The nSBF has a composition slightly different from that of the commonly used SBF solution[26] in terms of ion concentration. The difference between these two SBF compositions is mostly in the carbonate concentration. The new SBF (nSBF) contains 127 mM of CO_3^{2-}, which is not only more than the Kokubo SBF[27], but it matches the carbonate concentration in human blood. After one week, the glass discs were washed with DI water and ethanol and dried at 90°C. The reaction products that formed on the surface of the disc were identified by XRD.

III. Results

(1) Implant Recovery and Tissue Examination

All six animals were in good general health and showed no outward sign of distress before euthanizing. The tissue around each implant was visually assessed at the time of removal and its general appearance before and after surgery is shown in Fig 3 and 4. No change in the size or shape of the implant was obvious after 2, 4, or 12 weeks of implantation. There was also no visual sign of necrosis, or any type of adverse reaction.

Comparing the 2 week column in Fig 3 with the 4 week column and the 12 week column indicates no significant difference in the redness at the surface of the implants, probably due to vascularity, for the CaLB-0 and CaLB-12 implants. However in Fig 4, the 93B3-0 implants show more redness after two weeks, which diminishes at four weeks and vanishes at 12 weeks (last column). In contrast, in the 93B3-6 implants, the redness remains even after 12 weeks.

(2) SEM and EDS

A schematic of a glass disc reacted inside a rat is shown in Fig 2. The glass disc was partially reacted and the subcutaneous tissue was attached to it. The cross-section was examined using SEM and micro-Raman spectroscopy to identify the different elements present and the phases formed in the reacted layer.

a. Backscattered Electron Microscopy

The implant cross-section was examined by SEM and the reaction layer thickness was measured after 2, 4, and 12 weeks *in-vivo*. The average reaction rate was calculated for each glass and is reported in Table 3. The reaction rate of the 93B3 glasses, sulfur-free or sulfur-containing, was 4 to 10 times greater than that for the comparable CaLB glasses. The reaction rate for all of the glasses decreased with the time *in-vivo*.

The reaction rate for the sulfur-containing CaLB-12 glass was not significantly different from that for the sulfur-free CaLB-0 glass. However, the sulfur-containing 93B3-6 glass reacted about 3 times faster than the sulfur-free 93B3-0 glass in the first 2 weeks. The reaction rate decreased for both 93B3 glasses after 4 and 12 weeks, but the sulfur-containing 93B3-6 glass still reacted faster than sulfur-free 93B3-0 glass.

Figure 5 shows the reacted layers that formed *in-vivo* on the CaLB and 93B3 implants. A thin solid reacted layer formed on both of the CaLB implants when they reacted with the body fluids *in-vivo* (Fig 5 A and B). However, the reacted layer on the 93B3 implants was a layered structure, which was highly porous since the PMMA was able to penetrate to the space between the layers, all the way to the unreacted glass (See Fig 5 C, D, E, and F). This type of structure was more distinct for the 93B3-6 implant (Fig 5 D and F) than for the 93B3-0 implant.

b. Elemental Mapping Analysis

All four implants exhibit the same behavior in terms of elemental mapping over the 12 week experiment. The results presented here are for the implants after 12 weeks in the

subcutaneous site and the remainder of the elemental mapping data are given in Figures 1 and 2 in the Appendix.

Elemental mapping analysis of CaLB-0 and CaLB-12 glass implants after 12 weeks *in-vivo* are shown in Fig 6. The elements that were identified by elemental mapping analysis of these implants are: Calcium (Ca), Phosphorus (P), Oxygen (O), Sulfur (S), and Carbon (C). Boron and lithium were not detected because of their low atomic number. Calcium was found in the unreacted glass (G) and the reacted layer (RL). As expected, phosphorus was only found in the reacted layer while sulfur was detected in the unreacted CaLB-12 glass only. Carbon was an indication of PMMA (PM). No map for oxygen is shown since oxygen was found everywhere as expected, in the unreacted glass, reacted layer, and PMMA.

Figures 7 and 8 show the elemental maps for the 93B3-0 and 93B3-6 implants, respectively, after 12 weeks in the subcutaneous site in a rat. Elemental mapping analysis of these glasses identified Ca, P, S, Na, K, Mg, O, and C. Boron was not detected because of its low atomic number. The reacted layer contains calcium and phosphorus as expected. The phosphorus was more concentrated in the extreme outer surface of the reacted layer in both 93B3-0 and 93B3-6 implants. Sodium (Na) and K were detected in the unreacted 93B3-0 and 93B3-6 glass while Mg was detected in both the unreacted glass and the reacted layer, see Figures 7 and 8. Sulfur only detected in the unreacted 93B3-6 glass, see Fig 8.

The molar calcium to phosphorus ratio was measured at several points in the reacted layer of each glass after 12 weeks *in-vivo*. As already mentioned, the most outer surface

of the reacted layer of the 93B3 implants was richer in phosphorus. The Ca/P ratio of the most outer, phosphorus-rich layer for the 93B3-0 and 93B3-6 implants was 1.7 and 1.6, respectively (Ca/P ratio for stoichiometric HA is 1.67). The Ca/P ratio for the reacted layer containing less phosphorus for the 93B3-0 and 93B3-6 glasses was about 4 compared to 6.3 and 6.5, respectively, for the as-melted glasses. The Ca/P ratio for the reacted layer on both of the CaLB glasses was ~1.7, but it increased to about 10 to 11 very close to the unreacted glass.

(3) Micro-Raman Analysis

The micro-Raman spectra of the reacted layer formed on the CaLB-0 implant after 12 weeks *in-vivo* are shown in Fig 9. The spectra at four selected points, which included the reacted layer (RL), are shown in Fig 9. The spectrum for point #1 is that for the unreacted glass, which matches the spectrum for the as-made CaLB-0 glass (Part I of this thesis).

Point #2, which is within the reacted layer close to the glass, represents material that is newer than that at point #3, which corresponds to the older material at the outer surface of the reacted layer. The phosphate peaks at 960, 570, and 420 cm^{-1} are more intense at point #3, while the carbonate peaks at 1085 and 711 cm^{-1} are more intense at point #2.

Similar results for the sulfur-containing CaLB-12 glass are shown in Fig 10. The main difference in the spectra for the CaLB-0 and CaLB-12 implants is that even the older material (point #3), which is farther from the unreacted glass surface, appears to be more carbonated compared to the same region (point #3 in Fig 9) of the reacted layer of the sulfur-free, CaLB-0, implant. The micro-Raman spectra for the 93B3 implants are given in Figures 3 and 4 in the Appendix.

(4) XRD

The XRD patterns for the implants after 12 weeks *in-vivo* are shown in Fig 11. Hydroxyapatite and calcite ($CaCO_3$) were identified in all the implants after 12 weeks *in-vivo*. The peaks for the CaLB implants are more intense and more easily distinguishable than those for the 93B3 implants. The XRD pattern for CaLB-12 (second curve from the bottom in Fig 11) shows that the primary phase is calcite (peaks for calcite ($CaCO_3$) are more intense than those for HA).

Prior to this *in-vivo* experiments a similar *in-vivo* study was performed as a pilot study in which CaLB-0 and CaLB-12 glass discs were implanted subcutaneously in a rat for 2 weeks. The XRD patterns showed that the sulfur-free CaLB-0 glass converted to hydroxyapatite while the sulfur-containing glass (CaLB-12) transformed to calcite (see the spectra in Fig 5 in the Appendix). The CaLB and 93B3 glasses were also reacted in the nSBF solution for 1 week at 37°C. The XRD patterns in Fig 12 show that the CaLB glasses reacted to form calcite ($CaCO_3$), whereas, the 93B3 glasses reacted to form an amorphous material.

(5) Histology- Stained Tissue Sections

Due to over decalcification of the 12 week implants, the quality of the tissue sections was poor so no histology results for the 12 week implants are presented in this work.

a. H&E Staining

i. CaLB Glasses

Figure 13 shows the tissue sections stained with H&E for the CaLB-0 and CaLB-12 implants after 4 weeks *in-vivo*. H&E staining is helpful in differentiating different cells by staining the nuclei and the cytoplasm. The attached (red/pink) tissue consists of connective tissue close to the unreacted glass along with connective tissue and adipose (fat) tissue farther from the unreacted glass, which may or may not contain micro blood vessels.

In the H&E stained sections of the sulfur-free glass (CaLB-0), reacted for 2 weeks *in-vivo* (see Fig 13 (A)) there was no sign of blood vessels; only a narrow band of connective tissue about 50-100μm thick surrounded the unreacted glass. After 4 weeks *in-vivo*, the surrounding tissue was about 60μm thick (see Fig 13 (B)) and no blood vessels were observed.

For the sulfur-containing glass (CaLB-12) several blood vessels were observed in the surrounding tissue, after both two (Fig 13 (C)) and four weeks (Fig 13 (D)) *in-vivo*. The connective tissue layer was also thicker (~300μm) compared to that for the sulfur-free CaLB-0 glass.

ii. 93B3 Glasses

Figure 14 shows representative H&E stained tissue sections for the 93B3-0 ((A) and (B)) and 93B3-6 ((C) and (D)) implants. The sulfur-free 93B3 glass has been reported to be angiogenic[28]. The H&E stained sections in Fig 14 (AA), (BB), (CC) are magnified

images of the area in the black box in (A), (B), and (C), respectively. Several blood vessels were observed in the tissue surrounding the implant after 4 weeks *in-vivo*.

The tissue surrounding the sulfur-containing 93B3-6 implant at 2 and 4 weeks *in-vivo* appeared similar to that for the sulfur-free 93B3-0 implant. Several micro vessels surrounded the implant after 2 or 4 weeks *in-vivo*, see Fig 14 (C, CC, D).

b. CD31 Staining

To confirm the presence of blood vessels, tissue sections were stained with CD31, which is an immunohistochemistry staining for endothelial cells that is used to detect endothelium tissue. Endothelium is the first interior layer (thin layer) of a blood vessel, which in CD31 sections is stained brown as where the connective tissue is stained blue.

In the present work, human antibodies in the staining materials are used against rat tissue (antigen). Antibodies from humans cross-link with rat antigens and make an antibody-antigen bond, which stains brown in the CD31 staining.

Figure 15 shows a CD31 stained section from a sulfur-free 93B3-0 implant, along with a tissue section from the same spot stained by H&E. As can be seen, the points denoted by the arrows in the H&E stained section are stained brown in the CD31 section, confirming that blood vessels are present at these points.

The CD31 stained sections of all 4 compositions had a visible brown layer adjacent to the unreacted glass. As an example, a CD31 stained section of all 4 glasses implanted *in-vivo* for 4 weeks is shown in Fig 16. This brown layer does not have the morphology of the endothelium (thin circular shape) and it is more like a sheath surrounding the implant.

c. Trichrome

To detect collagen formation, selected sections were stained with Masson Trichrome. In this stain, cell nuclei are stained black, keratin and muscle fibers are stained red, and collagen is stained blue.

There was no sign of collagen around any of the implants at 2 weeks, but after 4 weeks *in-vivo* collagen (blue) was present in the tissue adjacent to all of the implant as shown in Fig 17. There was more collagen surrounding the 93B3 implants than the CaLB implants.

The tissue surrounding the 93B3-0 and 93B3-6 implants contains similar amount of collagen, but the tissue surrounding the CaLB-12 implants appeared to contain more collagen than the tissue surrounding the CaLB-0 implant.

IV. Discussion

(1) Reaction of Glasses In-Vivo

a. Reaction Rate and Reacted Layer Structure

The reaction rate of borate glasses *in-vivo* and *in-vitro* (part one of this thesis) depends on the composition of the glass as well as the structure of the reacted layer (dense or onion-skin layered) or the experimental conditions like glass to solution ratio could affect the reaction rate. The effect of these parameters on the reaction rate of the CaLB and 93B3 glass implants *in-vivo* will be discussed in this section.

The reaction rate for the two 93B3 glasses was 4 to 10 times higher than for the CaLB glasses (see Table 3). This difference in reaction rate was expected since the CaLB

glasses contain twice as much CaO as the 93B3 glasses, while both glasses contain almost the same amount of B_2O_3. The reaction rate of borate glasses *in-vitro* in phosphate-containing solutions such as SBF was reported to increase by decreasing the Ca content of the glass[29]. The amount of CaO is important because as the Ca^{2+} ions dissolve from the glass they react with any nearby phosphate to form an amorphous or crystalline calcium phosphate precipitate.

Assuming that the reaction rate *in-vivo* also increases by decreasing the Ca content of the glass it was expected that the 93B3 glass implants (~20 wt% CaO) would react faster than the CaLB glass implants (35-40 wt% CaO).

The average *in-vivo* reaction rate decreased for all of the glasses from 2 to 12 weeks. The average reaction rate for the CaLB glasses decreased 4 to 5 times in 12 weeks, whereas it decreased only 2 times for the 93B3-0 glass and ~3 times for the 93B3-6 glass. The decrease in reaction rate is attributed to the composition of the glasses and/or the structure of the reacted layer. The CaLB glass implants contains 35-40 wt% CaO and they developed a single, relatively dense reacted layer on their surface that could slow the body fluids from reaching the unreacted glass (see Fig 5 (A,B)). In contrast, the 93B3 glass implants contained ~20 wt% CaO and the reacted layer was a more open (onion-skin) structure (see Fig 5 (E,F)) that could allow the body fluids to reach the unreacted glass easier. In bone repair and regeneration (especially in load bearing bones), the structure of the reacted layer on the CaLB glasses is expected to be mechanically stronger compared to the reacted layer of the 93B3 glasses.

The CaLB-12 glass reacted ~4 times faster than the CaLB-0 glass *in-vitro* in a 0.5M K_2HPO_4 phosphate solution at 37°C (Part I of this thesis Fig 3). However, the average reaction rate of the CaLB-12 glass is roughly the same as that for the CaLB-0 glass *in-vivo* (see Table 3).

The difference between the *in-vitro* and *in-vivo* reaction rate could be due to the difference in the glass to available solution ratio. The glass to solution ratio was much less (5mg/ml) *in-vitro* compared to *in-vivo* (~12mg/ml, estimated from the weight of the implanted glasses and total amount of extra cellular fluids in a 400g rat). Also, the phosphorus content of the K_2HPO_4 solution (0.25M or 0.5M) was 250 or 500 times greater than the phosphorus content of the body fluids (0.001M) in the rat. In addition, the denser reacted layer (~ 15μm thick) could limit the flow of body fluids to the implant and thus slow the reaction.

b. Effect of Sulfur

Sulfur did affect three parameters, (a) the reaction rate of the 93B3 implants, (b) the pH of the body fluids, and (c) the composition of the reacted layer. In the next few paragraphs the effect of sulfur on these parameters will be discussed.

Sulfur did not affect the average reaction rate of the CaLB glasses but it had a large effect on the 93B3 glasses. The sulfur-containing 93B3-6 implants reacted 2 to 3 times faster than the sulfur-free 93B3-0 implants. During the 12 week period, the average reaction rate for the sulfur-containing 93B3-6 implants decreased less (one-third after 12 weeks) than that for the sulfur-free 93B3-0 implants (one-half after 12 weeks).

The pH of the body fluids was not measured directly in the present work but it was assumed that the sulfur that was released from the sulfur-containing glasses (see Figures 6 and 8), locally decreased the pH of the body fluids based on the *in-vitro* experiments, which were explained in part one of this thesis.

In part one of this thesis (Figure 3), it was also shown that the pH of the K_2HPO_4 solution decreases slightly *in-vitro*, which is consistent with the presence of sulfate in the solution. Assuming that the release of sulfur *in-vivo* reduces the pH of the body fluids slightly, then sulfur in bioactive glasses could be beneficial by counteracting the increase in pH which can occur when bioactive glasses such as 45S5, 1393, CaLB, and 93B3 glasses react with body fluids and release alkali ions like Na^+, K^+, and Mg^{2+}.

Calcite ($CaCO_3$) was formed in the CaLB-12 implant after 12 weeks *in-vivo* (Fig 11). The inhibition of hydroxyapatite formation and the formation of calcite could be due to several factors. Certain proteins, such as Osteopontin, inhibit the nucleation and growth of hydroxyapatite crystals[30]. Chondroitin sulfate (sulfated glycosaminoglycan), which is mostly found in cartilage and extracellular tissue, is also known to inhibit the formation of hydroxyapatite[31; 32].

Calcite was also formed in the CaLB-0 and CaLB-12 glasses *in-vitro* after 1 week in the nSBF solution. While formation of HA is mostly reported for the bioactive glasses reacted in a phosphate solution like SBF, formation of calcite *in-vitro*, has been also reported previously[33; 34], due to (a) the depletion of phosphorus in the solution, (b) the saturation of the solution with Ca^{2+} ions due to the dissolution of a glass with high (> 35 mol%) CaO content and/or the glass to solution ratio (wt/vol), or (c) the increasing the carbonate content of the solution could favor calcite formation.

The localized depletion of phosphorus due to the reaction of the CaLB-12 glass with the body fluids and the high content (~38 mol%) of CaO in the CaLB-12 glass could explain the calcite that is formed instead of HA. The role of any biological species or specific proteins on the inhibition of HA formation was not studied in the present work and cannot be determined at this time.

While calcite formed for the sulfur-containing CaLB-12 implants after 12 weeks *in-vivo*, the XRD pattern of the other sulfur-containing 93B3-6 glass showed no sign of calcite formation *in-vivo* (Fig 11). This might be due to the lower sulfate content (~6 wt%) and/or the lower CaO content of this glass compared to the CaLB-12 glass. However, micro-Raman analysis of the sulfur-containing 93B33-6 implants showed that the reacted layer formed on the surface of the implant was more carbonated than that of the sulfur-free 93B3-0 implants (see Figures 3 and 4 in the Appendix).

c. Role of Phosphorus

Phosphorus has been present in bioactive glasses from the beginning. Bioglass® (45S5) and 1393 glass, which are both FDA approved and used in bioactive glass research

contain 6 wt% and 4 wt% P_2O_5, respectively. These glasses convert to HA *in-vivo* where the source of phosphorus in the conversion process could be either from the glass or from the body fluids (blood contains 27 mM HPO_4^{2-} ions). To the authors' knowledge, the role that the phosphorus in the conventionally melted bioactive glass may play in the formation of HA or other Ca-P compounds has not been investigated *in-vivo*.

In the present work, the 93B3 borate glasses contain 4 wt% P_2O_5, while P_2O_5 is absent in the CaLB glasses. The presence or absence of phosphate is not the only difference in the composition of these glasses, but the data for the phosphorus-free CaLB glasses provide an opportunity to evaluate how they react in comparison to the phosphorus-containing 93B3 glasses. The only source of phosphorus available to form calcium phosphate from CaLB glasses is from the body fluids.

In another effort to analyze the phosphorus distribution in the glass implant using EDS, a straight line was scanned for calcium and phosphorus over the cross-section of each implant, from the adjacent soft tissue to the unreacted glass. This analysis yielded a better understanding of how the present glass compositions react *in-vivo* plus how phosphorus may affect the reaction process. The data for the sulfur-free glasses is similar to the sulfur-containing glasses so only the sulfur-free CaLB-0 and 93B3-0glasses will be discussed. The calcium and phosphorus spectra for each sulfur-free glass are shown in Fig 18 along with the SEM image of the region where the spectra were collected along the white horizontal line shown in each SEM image in Fig 18. Figure 18 (B) (93B3-0 implant) is the same spot that was shown in Fig 7.

Phosphorus content varied across the calcium phosphate reacted layer for both phosphorus-free CaLB and phosphorus-containing 93B3 implants. The reacted layer for these implants has two regions; the most outer region/layer was richer in phosphorus while the inner region contained less phosphorus, see Fig 18. The variation of the phosphorus content across the reacted layer (Ca/P molar ratio of 1.3-1.6 near the outer edge and Ca/P molar ratio of 2.0-3.0 in the inner layers) was reported for scaffolds of randomly oriented 93B3-0 glass fibers doped with Cu, Sr, Zn, and Fe that were implanted in the subcutaneous site of a rat for 4 and 6 weeks[28].

For the phosphorus-free CaLB-0 glass there are two distinct regions in the reacted layer; a layer farthest from the glass (region 2 in Fig 18 (A)) which contains both phosphorus and calcium with molar Ca/P ratio of 1.8±0.2. Region 3, closest to the unreacted glass in Fig 18 (A), contains mostly calcium and the molar Ca/P ratio is 11.7±5.3, see circled numbers in Fig 18 (A).

For the phosphorus-containing 93B3-0 glass, the reacted layer also contains two regions; a layer farthest from the glass (region 2 in Fig 18 (B)) with a Ca/P ratio of 1.6±0.2, and the layer closer to the glass (region 3 in Fig 18 (B)) which contains significantly less phosphorus and has a molar Ca/P ratio of 4.3±1.5. As shown by the phosphorus spectrum in Fig 18 (B), each peak (usually broad) in the reacted layer region corresponds to one of the calcium phosphate layers (onion-skin layer), that were shown in Fig 7 as well.

The Ca/P ratio was measured at least 10 times for each region and the average value is shown in the circles inside each region in the SEM image in Fig 18. EDS cannot measure

the Ca/P ratio for the unreacted 93B3 glasses because B in the glass is not detectable so EDS cannot provide the right composition. The Ca/P ratio of 6.3 for the unreacted 93B3 glass in Fig 18 was calculated from the starting glass composition. Since the CaLB-0 glass did not contain phosphorus, no Ca/P value is given in Fig 18 (A). The PMMA (region 1) did not contain any calcium or phosphorus so no value is given for this region.

Region 2, which represents the older material (first formed), in the CaLB-0 and 93B3-0 implants (also the same for sulfur-containing glasses) has a molar Ca/P ratio of about 1.6-1.8 ± 0.2, which is close to that of stoichiometric HA (1.67). The material in region 3 for both glasses had a higher Ca/P ratio, 4.3 and 11.7 for the 93B3-0 and CaLB-0 glasses, respectively.

The Ca/P ratio for region 3 could be used to estimate how much phosphorus this region contains and how much of it could be provided by the body fluids. Based on the calcium content of each glass, see Table 1, and arbitrarily assuming 100 mol of glass, the phosphorus-free CaLB-0 glass contains 41.5 mol of calcium and the phosphorus-containing 93B3-0 glass contains 23.9 mol of Ca. Total amount of phosphorus can be calculated by dividing the calcium content by the Ca/P ratio (measured for the HA layer (region 2) in Fig 18 (A,B)) for each glass, see Fig 19.

The phosphorus-containing glass (93B3-0) contains 3.8 mol of phosphorus (in 100 mol of glass) and the phosphorus-free CaLB-0 does not have any phosphorus. So the total amount of phosphorus in the reacted layer of the implants was divided into the amount that the glass contains and what the body provided. Since the 93B3-0 glass contains 3.8 mol of phosphorus (in 100 mol of glass), it is assumed that 3.8 mol of the total

phosphorus (14.9 mol) came from the glass and the rest (11.1 mol) came from the body fluids. All of the phosphorus in the reacted layer of the CaLB-0 implant had to be provided from the body. The phosphorus absorbed from the body fluids in the reacted layer of the CaLB-0 implant was about two times more than that absorbed by the 93B3-0 implant (see the last row in Fig 19).

The 93B3-0 glass reacted 10 times faster than the CaLB-0 glass after 12 weeks *in-vivo*. It is also important to point out that the thin HA layer with molar Ca/P of 1.6-1.8 (see region 2 in Fig 18 (A,B)) is almost the same thickness (10-15μm) for both CaLB-0 and 93B3-0 implants. By dividing the amount of phosphorus absorbed from the body by the average reaction rate at 12 weeks, the amount of phosphorus absorbed by the body per μm per week of reacted material would be 11.5 (mol/(μm/week)) for the CaLB-0 implant and 0.75 (mol/(μm/week)) for the 93B3-0 implant. This value, along with the amount of phosphorus absorbed from the body, represents the effect of phosphorus between these two glasses.

As can be seen, the phosphorus-containing 93B3-0 glass needed only about one half as much phosphorus from the body fluids (11.1 mol) than that of phosphorus-free CaLB-0 glass (23.0 mol). Also, the rate of phosphorus absorption (0.75 mol/(μm/week)) for the phosphorus-containing 93B3-0 glass from the body fluids was about 15 times less than that of the phosphorus-free CaLB-0 glass (11.5 mol/(μm/week)).

(2) Biological Response

The biological response of all four glasses at 12 weeks *in-vivo* was considered satisfactory in terms of biocompatibility. There was no visual evidence of necrosis or

adverse reaction near the implants regardless of the presence or absence of sulfur in the two glasses. However, the attached connective tissue could be an inflammatory response to the implants.

Inflammatory response of the body to a foreign object could be first identified by presence of neutrophils and macrophages and then fibroblasts. Fibroblasts are the type of cells that synthesize extra-cellular matrix (ECM), collagen or basically the connective tissue. Attachment of the connective tissue to the implants could be an inflammatory response but no neutrophils, macrophages, mast cells, or any other type of cells that are responsible for an inflammation response were identified in any of the stained sections. Considering the possibility of inflammation in form of attached connective tissue when comparing the thickness of the attached tissue is advised to the reader.

Sulfur did affect the bioactivity of the borate glasses as well as formation of new blood vessels and new collagenous tissue. In the next few paragraphs the effect of sulfur on these aspects will be discussed.

Based on the thickness of the reacted layer and the thickness of the surrounding tissue the 93B3 glasses were more bioactive than the CaLB glasses. The reacted layer for the 93B3 implants was about 10 times thicker and the surrounding tissue was about 3 times thicker than that for the CaLB implants.

At 2 and 4 weeks *in-vivo*, the connective tissue around the sulfur-free CaLB-0 implant was not thicker than that around the sulfur-containing CaLB-12 implant, see Fig 13 (A,B)). There were also fewer blood vessels identified in the surrounding tissue of the CaLB-0 implants. The tissue surrounding the CaLB-12 implant, on the other hand, was

thicker and contained more blood vessels at 2 and 4 weeks *in-vivo* (see the black arrows in Fig 13 (C,D)).

Both 93B3-0 and 93B3-6 implants developed a thick layer (~600μm) of connective tissue that contained several blood vessels. Sulfur did not affect the 93B3 glasses in terms of connective tissue formation or formation blood vessels.

Sulfur showed an impact on the formation of collagen around the CaLB implants. It is important to see if the implants improve collagen formation. Also, it is essential to know how long it takes to form collagen and how much collagen forms with specific implants.

The extracellular matrix (ECM) is a part of tissue that holds cells and provides structural support for them. It also provides an environment for intercellular communication and supplies certain growth factors[35]. Proteins and glycosaminoglycans (GAGs) are the key components of the ECM. Collagen is the most abundant protein in the body and the most abundant protein that makes ECM[36; 37]. Collagen can be found in skin, tendon, ligament, cartilage, bone, blood vessels, and many other tissues. Collagen accounts for 90% of bone matrix protein[38] and gives bone its tensile strength. Collagen is biocompatible, biodegradable, and improves cellular penetration and wound repair[39]. As the key component of ECM, collagen is one the best candidates as a carrier for different variety of drugs, cells, and biological factors[40-47].

As shown in Fig 17 (blue represents collagen), the tissue adjacent to the sulfur-free CaLB-0 implant contains little if any collagen after 4 weeks *in-vivo* whereas the tissue attached to the sulfur-containing CaLB-12 implant contains noticeable collagen fibers after 4 weeks.

The biocompatibility, bioactivity, and angiogenic behavior of 93B3-0 glass was studied before but collagen formation was not investigated for these implants in the previous studies[29]. Trichrome stained sections of the 93B3 implants (Fig 17) showed that there was more collagenous tissue formed around the 93B3 implants compared to the CaLB implants. The higher bioactivity of the 93B3 implants could be the reason for the formation of the more collagen around these implants. However, there is no distinguishable difference between the sulfur-free 93B3-0 and sulfur-containing 93B3-6 implants in terms of collagen formation.

V. Conclusion

For the first time, a sulfur-containing bioactive glass has been implanted *in-vivo* to study the effect of sulfur in reaction materials, angiogenesis, and collagen formation. Solid glass discs of four different borate glass compositions, two of which contained sulfur, were implanted in subcutaneous tissue of rats and reacted with body fluids for 2, 4, and 12 weeks. Each rat remained healthy during the experiment and there were no sign of infection or adverse reaction at the implantation site.

As the sulfur-containing CaLB-12 and 93B3-6 reacted *in-vivo* the sulfur was released to the body fluids and was absent in the reacted carbonated HA layer.

The structure of the reacted materials varied for different glasses. The faster reacting 93B3 glass implants developed an onion-skin reacted layer structure while the slower reacting CaLB glass implants formed a denser but thinner calcium phosphate layer on their surface. The average reaction rates for the 93B3 implants were ~10 times faster than that of CaLB implants. While the sulfur did not affect the reaction rate of the two CaLB

glasses, the reaction rate for sulfur-containing 93B3-6 glass was 2 to 3 times faster than that of the sulfur-free 93B3-0 glass.

For CaLB implants, sulfur did not have much of an effect on the reaction rate and the structure of the reacted layer rather than formation of a more carbonated calcium phosphate layer around the sulfur-containing CaLB-12 implant. However, more collagenous tissue and more blood vessels were seen in the surrounding tissue of the sulfur-containing CaLB-12 glass implants compared to the sulfur-free CaLB-0 glass implants. Sulfur affected the reaction rate of the 93B3 glasses by increasing it for the sulfur-containing 93B3-6 glass implants but it did not have much of an effect on the thickness of the surrounding tissue, blood vessel and collagen formation.

In a comparison between phosphorus-free (CaLB) and phosphorus-containing (93B3) glass implants it was shown that the phosphorus-containing 93B3 implants absorbed half as much phosphorus from the body fluids than the phosphorus-free CaLB implants. Since these implants have a different reaction rate, in another comparison, it was shown that the phosphorus-containing 93B3 implants absorbed 15 times less phosphorus/(μm/week) than the phosphorus-free CaLB implants.

References

[1]D. H. Baker, "Utilization of Isomers and Analogs of Amino Acids and Other Sulfur-Containing Compounds," *Prog. Food Nutr. Sci.*, **10**[1-2] 133-78 (1986).

[2]A. N. Lin, R. J. Reimer, and D. M. Carter, "Sulfur Revisited," *J. Am. Acad. Dermatol.*, **18**[3] 553-58 (1988).

[3]N. Tarimci, S. Sener, and T. Kilinc, "Topical Sodium Sulfacetamide/Sulfur Lotion [1]," *J. Clin. Pharm. Ther.*, **22**[4] 301 (1997).

[4]W. H. Bell, "Resorption Characteristics of Bone and Bone Substitutes," *Oral Surg. Oral Med. Oral Pathol.*, **17** 650-7 (1964).

[5]R. Lillo and L. F. Peltier, "The Substitution of Plaster of Paris Rods for Portions of the Diaphysis of the Radius in Dogs," *Surg. Forum,* **6** 556-8 (1956).

[6]R. Strocchi, G. Orsini, G. Iezzi, A. Scarano, C. Rubini, G. Pecora, and A. Piattelli, "Bone Regeneration with Calcium Sulfate: Evidence for Increased Angiogenesis in Rabbits," *The Journal of oral implantology,* **28**[6] 273-78 (2002).

[7]W. S. Pietrzak and R. Ronk, "Calcium Sulfate Bone Void Filler: A Review and a Lock Ahead," *J. Craniofacial Surg.*, **11**[4] 327-33 (2000).

[8]M. J. S. Beuerlein and M. D. McKee, "Calcium Sulfates: What Is the Evidence?," *Journal of Orthopaedic Trauma,* **24**[SUPPL. 1] S46-S51 (2010).

[9]W. R. Walsh, P. Morberg, Y. Yu, J. L. Yang, W. Haggard, P. C. Sheath, M. Svehla, and W. J. Bruce, "Response of a Calcium Sulfate Bone Graft Substitute in a Confined Cancellous Defect," *Clin. Orthop. Relat. Res.*[406] 228-36 (2003).

[10]L. L. Hench, R. J. Splinter, W. C. Allen, and T. K. Greenlee, "Bonding Mechanisms at the Interface of Ceramic Prosthetic Materials," *J. Biomed. Mater. Res.*, **5**[6] 117-41 (1971).

[11]L. L. Hench, "Bioceramics," *J. Am. Ceram. Soc.*, **81**[7] 1705-27 (1998).

[12]W. Huang, D. E. Day, K. Kittiratanapiboon, and M. N. Rahaman, "Kinetics and Mechanisms of the Conversion of Silicate (45S5), Borate, and Borosilicate Glasses to Hydroxyapatite in Dilute Phosphate Solutions," *J. Mater. Sci.: Mater. Med.,* **17**[7] 583-96 (2006).

[13]W. Huang, M. N. Rahaman, D. E. Day, and Y. Li, "Mechanisms for Converting Bioactive Silicate, Borate, and Borosilicate Glasses to Hydroxyapatite in Dilute Phosphate Solution," *Phys. Chem. Glasses: Eur. J. Glass Sci. Technol., Part B,* **47**[6] 647-58 (2006).

[14]D. E. Day, J. E. White, R. F. Brown, and K. D. McMenamin, "Transformation of Borate Glasses into Biologically Useful Materials," *Glass Technol.,* **44**[2] 75-81 (2003).

[15]X. Han and D. E. Day, "Reaction of Sodium Calcium Borate Glasses to Form Hydroxyapatite," *J. Mater. Sci.: Mater. Med.,* **18**[9] 1837-47 (2007).

[16]D. Zhao, W. Huang, M. N. Rahaman, D. E. Day, and D. Wang, "Mechanism for Converting Al_2O_3-Containing Borate Glass to Hydroxyapatite in Aqueous Phosphate Solution," *Acta Biomater.,* **5**[4] 1265-73 (2009).

[17]H. B. Pan, X. L. Zhao, X. Zhang, K. B. Zhang, L. C. Li, Z. Y. Li, W. M. Lam, W. W. Lu, D. P. Wang, W. H. Huang, K. L. Lin, and J. Chang, "Strontium Borate Glass: Potential Biomaterial for Bone Regeneration," *J. R. Soc., Interface,* **7**[48] 1025-31 (2010).

[18]A. Yao, D. Wang, W. Huang, Q. Fu, M. N. Rahaman, and D. E. Day, "In Vitro Bioactive Characteristics of Borate-Based Glasses with Controllable Degradation Behavior," *J. Am. Ceram. Soc.,* **90**[1] 303-06 (2007).

[19]Q. Fu, M. N. Rahaman, H. Fu, and X. Liu, "Silicate, Borosilicate, and Borate Bioactive Glass Scaffolds with Controllable Degradation Rate for Bone Tissue Engineering Applications. I. Preparation and In Vitro Degradation," *J. Biomed. Mater. Res., Part A,* **95**[1] 164-71 (2010).

[20]M. N. Rahaman, D. E. Day, B. Sonny Bal, Q. Fu, S. B. Jung, L. F. Bonewald, and A. P. Tomsia, "Bioactive Glass in Tissue Engineering," *Acta Biomater.,* **7**[6] 2355-73 (2011).

[21]I. D. Xynos, A. J. Edgar, L. D. K. Buttery, L. L. Hench, and J. M. Polak, "Gene-Expression Profiling of Human Osteoblasts Following Treatment with the Ionic Products of Bioglass 45S5 Dissolution," *J. Biomed. Mater. Res.,* **55**[2] 151-57 (2001).

[22]P. D. Saltman and L. G. Strause, "The Role of Trace Minerals in Osteoporosis," *J. Am. Coll. Nutr.,* **12**[4] 384-89 (1993).

[23]J. H. Beattie and A. Avenell, "Trace Element Nutrition and Bone Metabolism," *Nutr Res Rev,* **5**[1] 167-88 (1992).

[24]F. H. Nielsen, "New Essential Trace Elements for the Life Sciences," *Biol. Trace Elem. Res.,* **26-27** 599-611 (1990).

[25]A. Hoppe, N. S. Guldal, and A. R. Boccaccini, "A Review of the Biological Response to Ionic Dissolution Products from Bioactive Glasses and Glass-Ceramics," *Biomaterials,* **32**[11] 2757-74 (2011).

[26]A. Cuneyt Tas, "Synthesis of Biomimetic Ca-Hydroxyapatite Powders at 37°C in Synthetic Body Fluids," *Biomaterials,* **21**[14] 1429-38 (2000).

[27]T. Kokubo and H. Takadama, "How Useful is SBF in Predicting In Vivo Bone Bioactivity?," *Biomaterials,* **27**[15] 2907-15 (2006).

[28]S. B. Jung, "Borate Based Bioactive Glass Scaffolds for Hard and Soft Tissue Engineering," Doctor of Philosophy Maerial Science and Engineering, Missouri S&T (2010).

[29]K. P. Fears, "Formation of Hollow Hydroxyapatite Microspheres " Master of Science, Materials Science & Engineering Department, University of Missouri-Rolla (2001).

[30]D. A. Pampena, K. A. Robertson, O. Litvinova, G. Lajoie, H. A. Goldberg, and G. K. Hunter, "Inhibition of Hydroxyapatite Formation by Osteopontin Phosphopeptides," *Biochem. J.,* **378**[3] 1083-87 (2004).

[31]C. C. Chen and A. L. Boskey, "Mechanisms of Proteoglycan Inhibition of Hydroxyapatite Growth," *Calcif. Tissue Int.,* **37**[4] 395-400 (1985).

[32]G. K. Hunter, B. L. Allen, M. D. Grynpas, and P. T. Cheng, "Inhibition of Hydroxyapatite Formation in Collagen Gels by Chondroitin Sulphate," *Biochem. J.,* **228**[2] 463-69 (1985).

[33]M. Mami, A. Lucas-Girot, H. Oudadesse, R. Dorbez-Sridi, F. Mezahi, and E. Dietrich, "Investigation of the Surface Reactivity of a Sol-Gel Derived Glass in the Ternary System SiO_2-CaO-P_2O_5," *Appl. Surf. Sci.,* **254**[22] 7386-93 (2008).

[34]V. J. Shirtliff and L. L. Hench, "Macroporous Bioactive Glasses," pp. 989-92. in, **Vol. 254-256.** *The Annual Meeting of the International Society for Ceramics in Medicine.* Edited by M. A. Barbosa, F. J. Monteiro, R. Correia, andB. Leon, Porto, 2004.

[35]V. Kumar, N. Fausto, and A. A., "Robbins & Cotran Pathologic Basis of Disease," 7th ed. Saunders, (2004).

[36]G. A. Di Lullo, S. M. Sweeney, J. Korkko, L. Ala-Kokko, and J. D. San Antonio, "Mapping the Ligand-Binding Sites and Disease-Associated Mutations on the Most Abundant Protein in the Human, Type I Collagen," *J. Biol. Chem.,* **277**[6] 4223-31 (2002).

[37]G. Karsenty and R. W. Park, "Regulation of Type I Collagen Genes Expression," *Int. Rev. Immunol.,* **12**[2-4] 177-85 (1995).

[38]B. Kern, J. Shen, M. Starbuck, and G. Karsenty, "Cbfa1 Contributes to the Osteoblast-Specific Expression of Type I Collagen Genes," *J. Biol. Chem.,* **276**[10] 7101-07 (2001).

[39]W. Friess, "Collagen - Biomaterial for Drug Delivery," *Eur. J. Pharm. Biopharm.,* **45**[2] 113-36 (1998).

[40]J. L. Chen, Z. Yin, W. L. Shen, X. Chen, B. C. Heng, X. H. Zou, and H. W. Ouyang, "Efficacy of hESC-MSCs in Knitted Silk-Collagen Scaffold for Tendon Tissue Engineering and Their Roles," *Biomaterials,* **31**[36] 9438-51 (2010).

[41]Z. Ruszczak, "Effect of Collagen Matrices on Dermal Wound Healing," *Adv. Drug Delivery Rev.,* **55**[12] 1595-611 (2003).

[42]Y. B. Lee, S. Polio, W. Lee, G. Dai, L. Menon, R. S. Carroll, and S. S. Yoo, "Bio-Printing of Collagen and VEGF-Releasing Fibrin Gel Scaffolds for Neural Stem Cell Culture," *Exp. Neurol.,* **223**[2] 645-52 (2010).

[43]Z. Chen, X. C. M. Lu, D. A. Shear, J. R. Dave, A. R. Davis, C. A. Evangelista, D. Duffy, and F. C. Tortella, "Synergism of Human Amnion-Derived Multipotent Progenitor (AMP) Cells and a Collagen Scaffold in Promoting Brain Wound Recovery: Pre-Clinical Studies in an Experimental Model of Penetrating Ballistic-Like Brain Injury," *Brain Res.,* **1368** 71-81 (2011).

[44]N. Davidenko, J. J. Campbell, E. S. Thian, C. J. Watson, and R. E. Cameron, "Collagen-Hyaluronic Acid Scaffolds for Adipose Tissue Engineering," *Acta Biomater.,* **6**[10] 3957-68 (2010).

[45]Y. Sumita, M. J. Honda, T. Ohara, S. Tsuchiya, H. Sagara, H. Kagami, and M. Ueda, "Performance of Collagen Sponge as a 3-D Scaffold for Tooth-Tissue Engineering," *Biomaterials,* **27**[17] 3238-48 (2006).

[46]Y. Zhang, X. Cheng, J. Wang, Y. Wang, B. Shi, C. Huang, X. Yang, and T. Liu, "Novel Chitosan/Collagen Scaffold Containing Transforming Growth Factor-B1 DNA for Periodontal Tissue Engineering," *Biochem. Biophys. Res. Commun.,* **344**[1] 362-69 (2006).

[47]I. V. Yannas and J. F. Burke, "Design of an Artificial Skin. I. Basic Design Principles," *J. Biomed. Mater. Res.,* **14**[1] 65-81 (1980).

Table 1. As-Batched composition for the CaLB and 93B3 glasses in wt%. The values in ( ) are in Mol%.

Glass Identifier	B_2O_3	CaO	Na_2O	K_2O	MgO	P_2O_5	Li_2O	SO_3
	wt% (mol%)							
CaLB-0	52.5 (43.9)	40 (41.5)	-	-	-	-	7.5 (14.6)	-
CaLB-12	45.9 (39.7)	35 (37.6)	-	-	-	-	6.6 (13.3)	12.5 (9.4)
93B3-0	53 (50.9)	20 (23.9)	6 (6.5)	12 (8.5)	5 (8.3)	4 (1.9)	-	-
93B3-6	49.5 (46.9)	18.7 (22)	5.6 (6)	11.2 (7.9)	4.7 (7.6)	3.7 (1.7)	-	6.7 (7.9)

Table 2. Ion concentration (mM) of human blood plasma, nSBF, and Kokubo-SBF.

Ion	Human Blood Plasma	nSBF	Kokubo-SBF
Na^+	142	142	142
K^+	5	5	5
Mg^{2+}	1.5	1.5	1.5
Ca^{2+}	2.5	2.5	2.5
HPO_4^{2-}	1	1	1
HCO_3^{2-}	27	27	4.2
Cl^-	103	125	147.8
SO_4^{2-}	0.5	0.5	0.5
Buffering Agent	-	Tris	Tris

Table 3. Reaction rate (μm/week) as calculated from the thickness of the reacted layer and time, *in-vivo*. The thickness of the reacted layer was measured on the flat surface of each implant where the thickness is relatively uniform as opposed to the corners where the thickness varies (see Fig 5).

Glass Identifier	2 weeks	4 weeks	12 weeks
	(μm/week)		
CaLB-0	9 ± 2	7 ± 2	2 ± <1
CaLB-12	11 ± 3	5 ± 2	2 ± <1
93B3-0	40 ± 2	34 ± 9	20 ± 3
93B3-6	125 ± 25	40 ± 10	36 ± 8

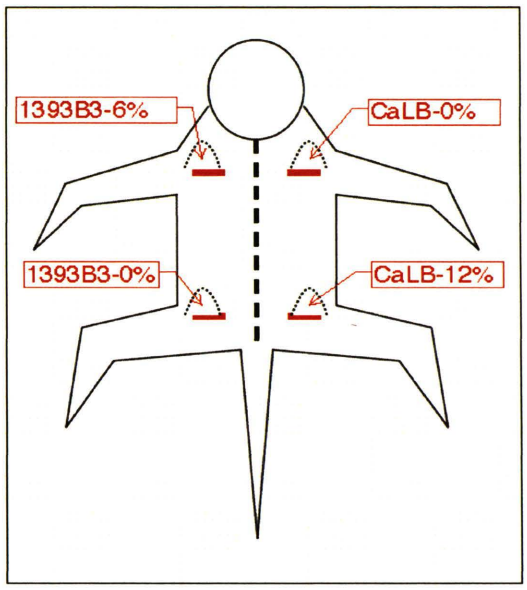

Figure 1. Schematic figure showing the subcutaneous site, where one sample of each glass was implanted in six rats.

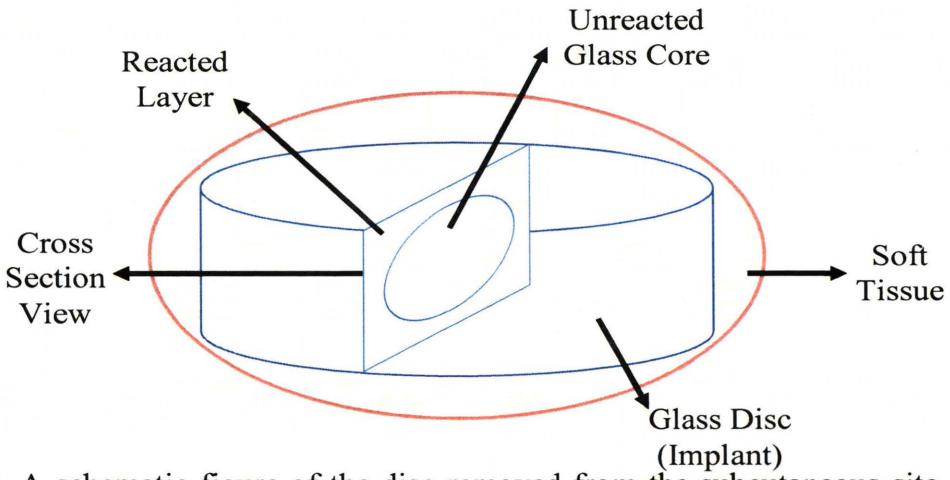

Figure 2. A schematic figure of the disc removed from the subcutaneous site of a rat showing the reacted surface layer and unreacted glass in the cross section of the disc.

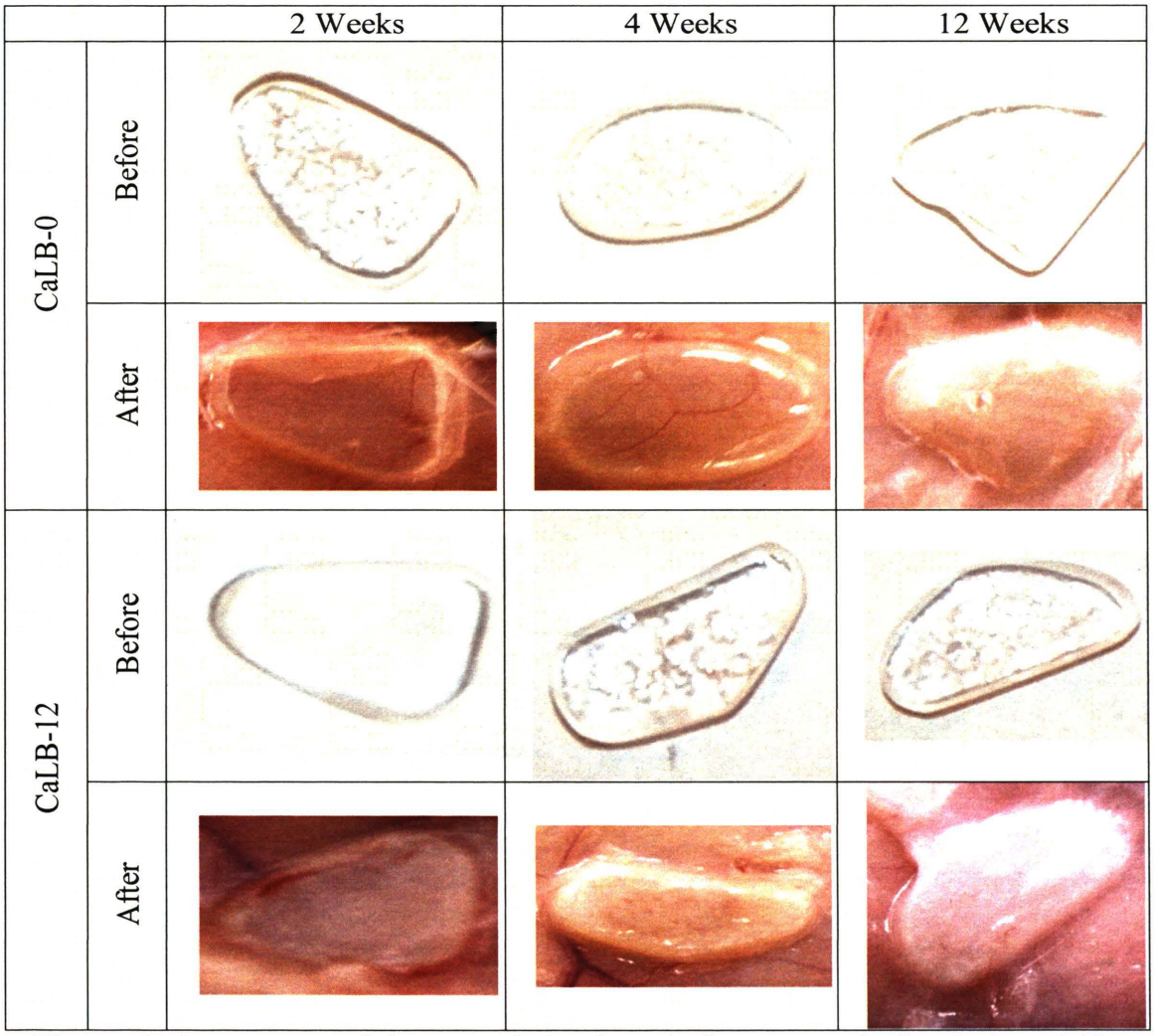

Figure 3. Appearance of the as made implants before removal after 2, 4, and 12 weeks in a subcutaneous site in a rat. The view shows the implant surface adjacent to the muscle tissue.

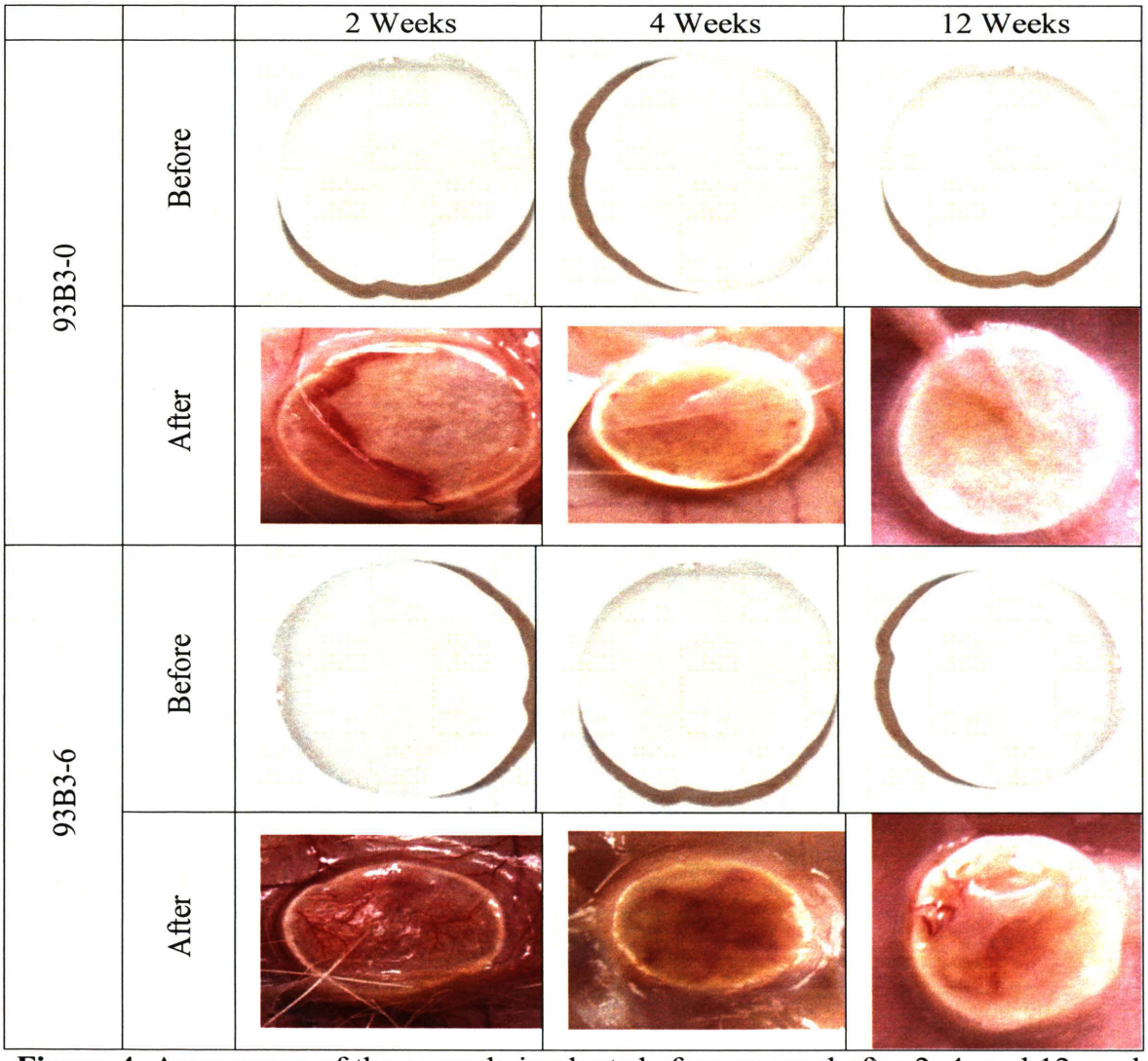

Figure 4. Appearance of the as made implants before removal after 2, 4, and 12 weeks in a subcutaneous site in a rat. The view shows the implant surface adjacent to the muscle tissue.

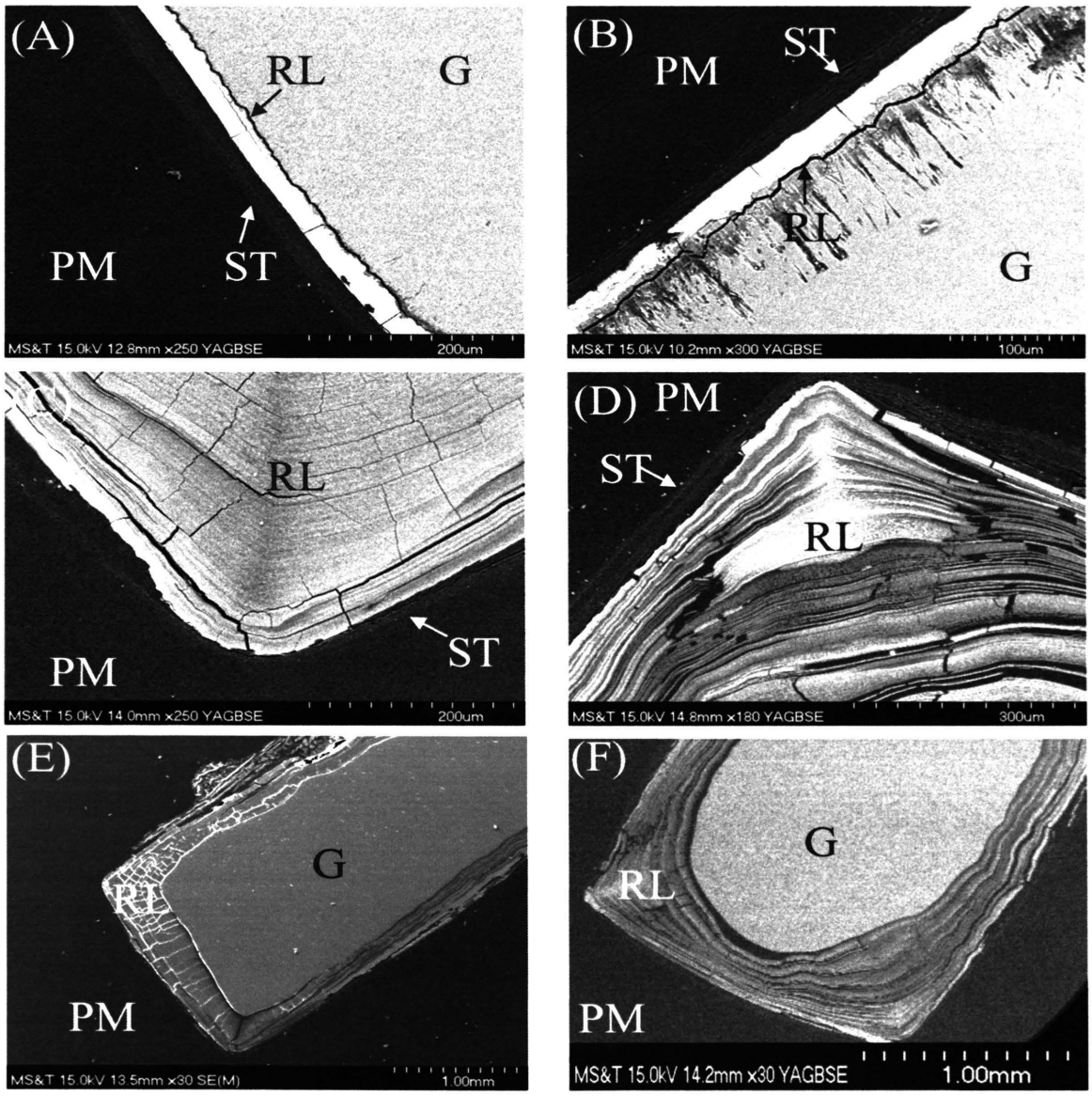

Figure 5. Backscattered SEM image of the cross section of the glass implants after 12 weeks in a rat. (A): CaLB-0, (B): CaLB-12, (C,E): 93B3-0, (D,F): 93B3-6. A thin layer of soft tissue (ST) is faintly visible between the reacted layer (RL) and the PMMA (PM). The unreacted glass is designated as G.

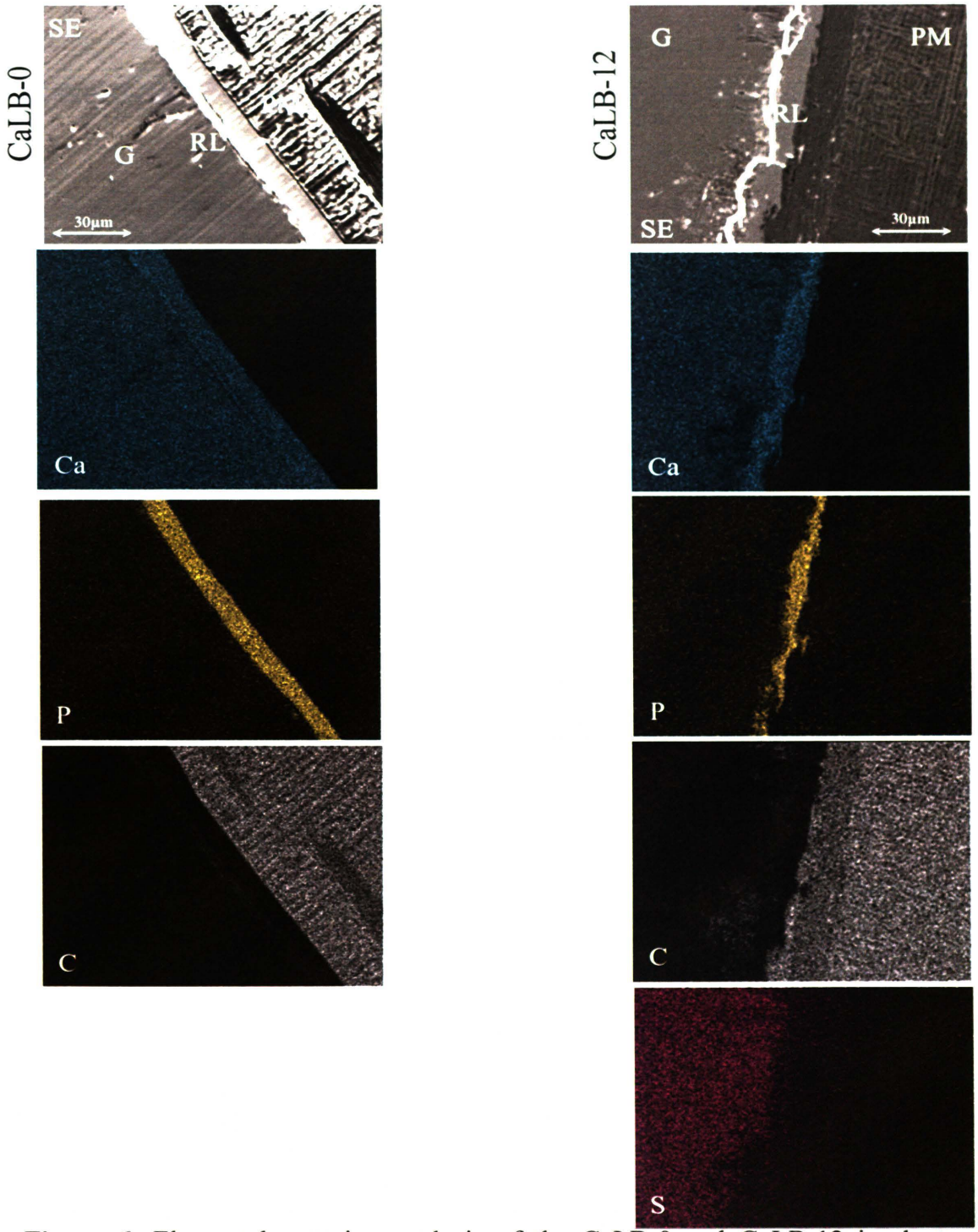

Figure 6. Elemental mapping analysis of the CaLB-0 and CaLB-12 implants after reaction in the subcutaneous site of a rat for 12 weeks and impregnated with PMMA (PM). SE= Secondary Electron, Ca= Calcium, P= Phosphorus, C= Carbon, S= Sulfur, RL= Reacted Layer, G= Unreacted Glass. Dark lines in PMMA regions are formed during the EDS scan due to degradation of PMMA.

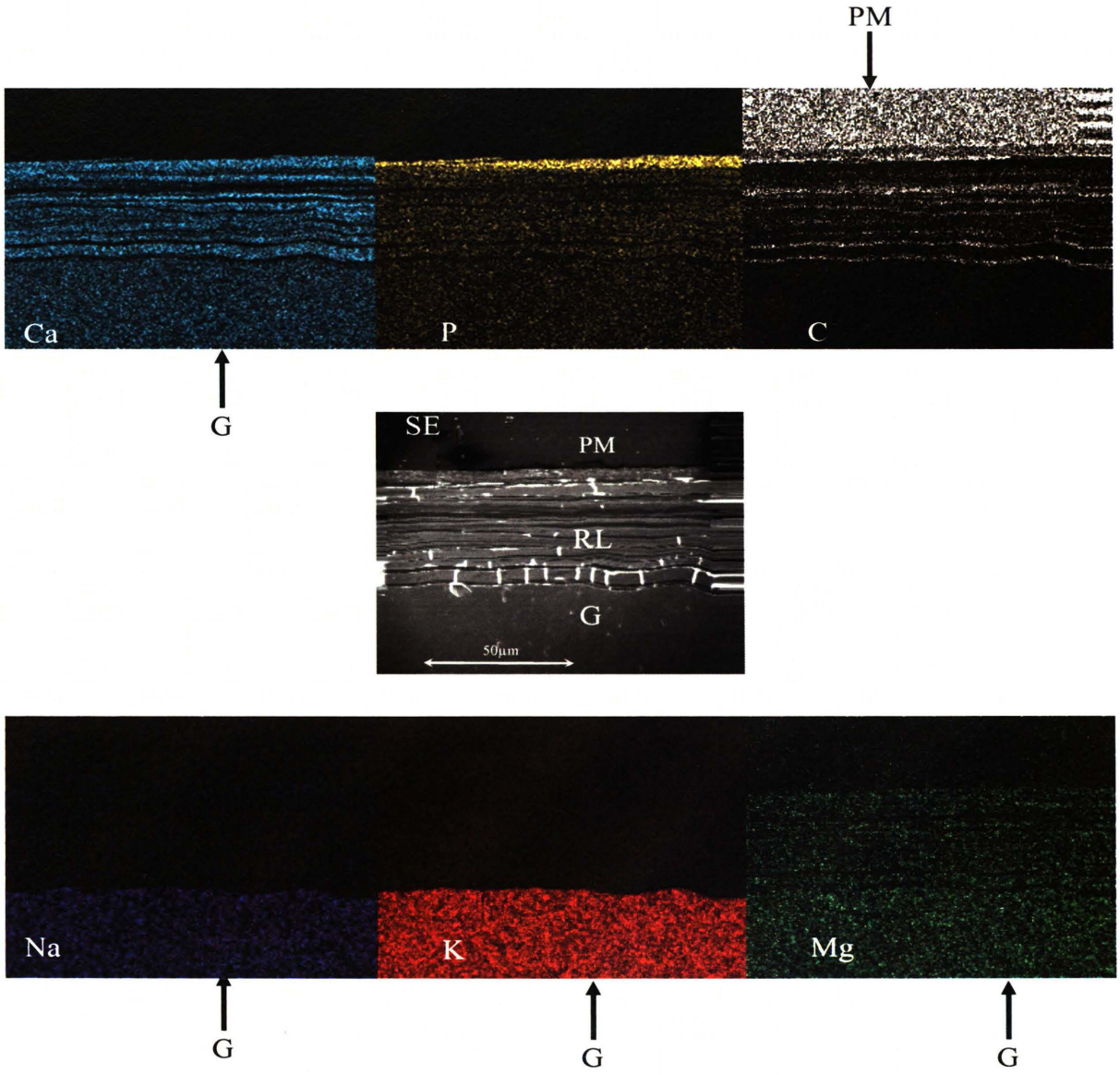

Figure 7. Elemental mapping analysis of 93B3-0 reacted in subcutaneous site of a rat for 12 weeks impregnated with PMMA (PM). SE= Secondary Electron, Ca= Calcium, P= Phosphorus, C= Carbon, Na= Sodium, K= Potassium, Mg= Magnesium, RL= Reacted Layer, and G= Unreacted Glass.

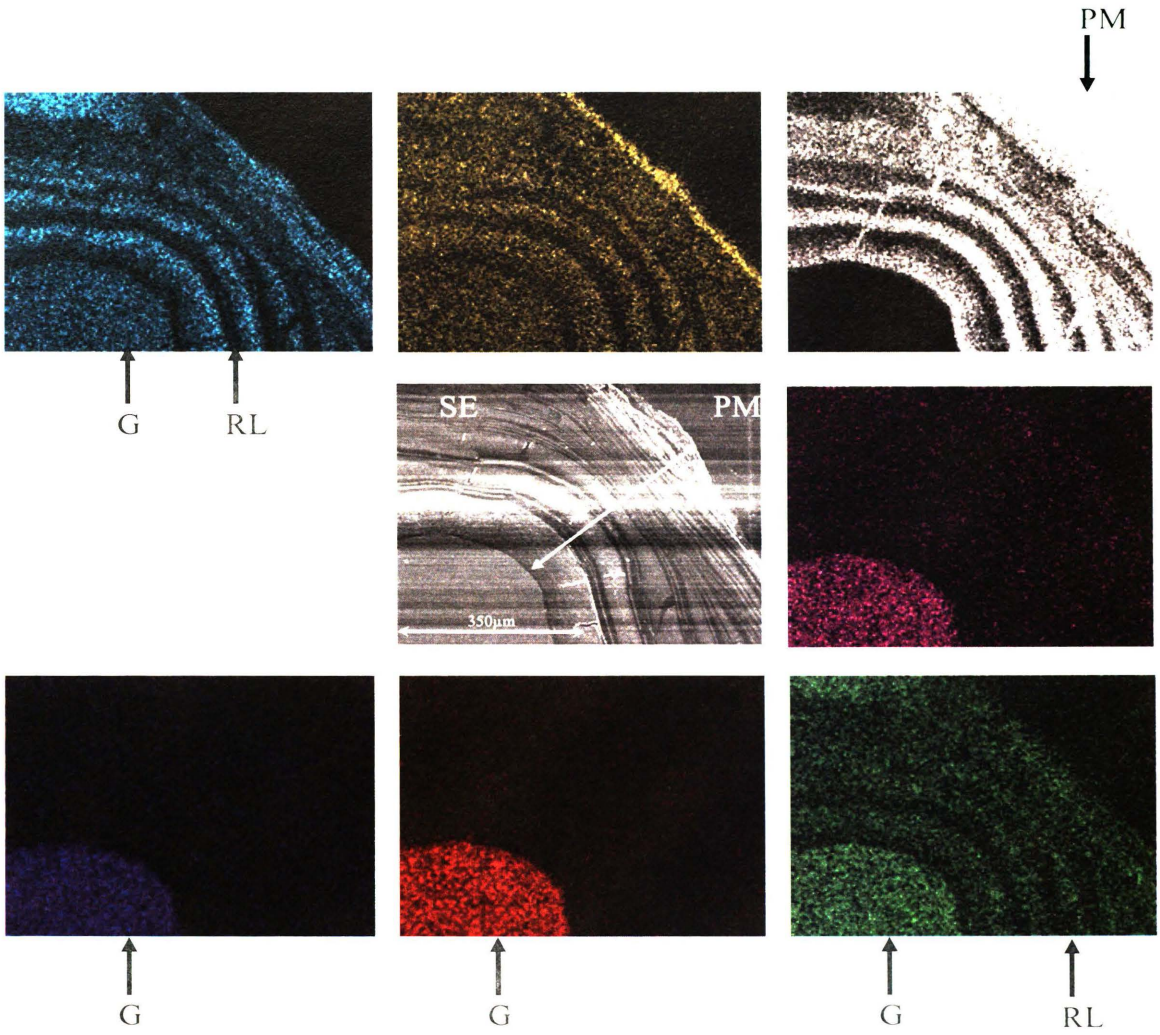

Figure 8. Elemental mapping analysis of 93B3-6 reacted in subcutaneous site of a rat for 12 weeks impregnated with PMMA (PM). SE: Secondary Electron, Ca: Calcium, P: Phosphorus, C: Carbon, Na: Sodium, K: Potassium, Mg: Magnesium, PM: PMMA, RL: Reacted Layer, and G: Unreacted Glass.

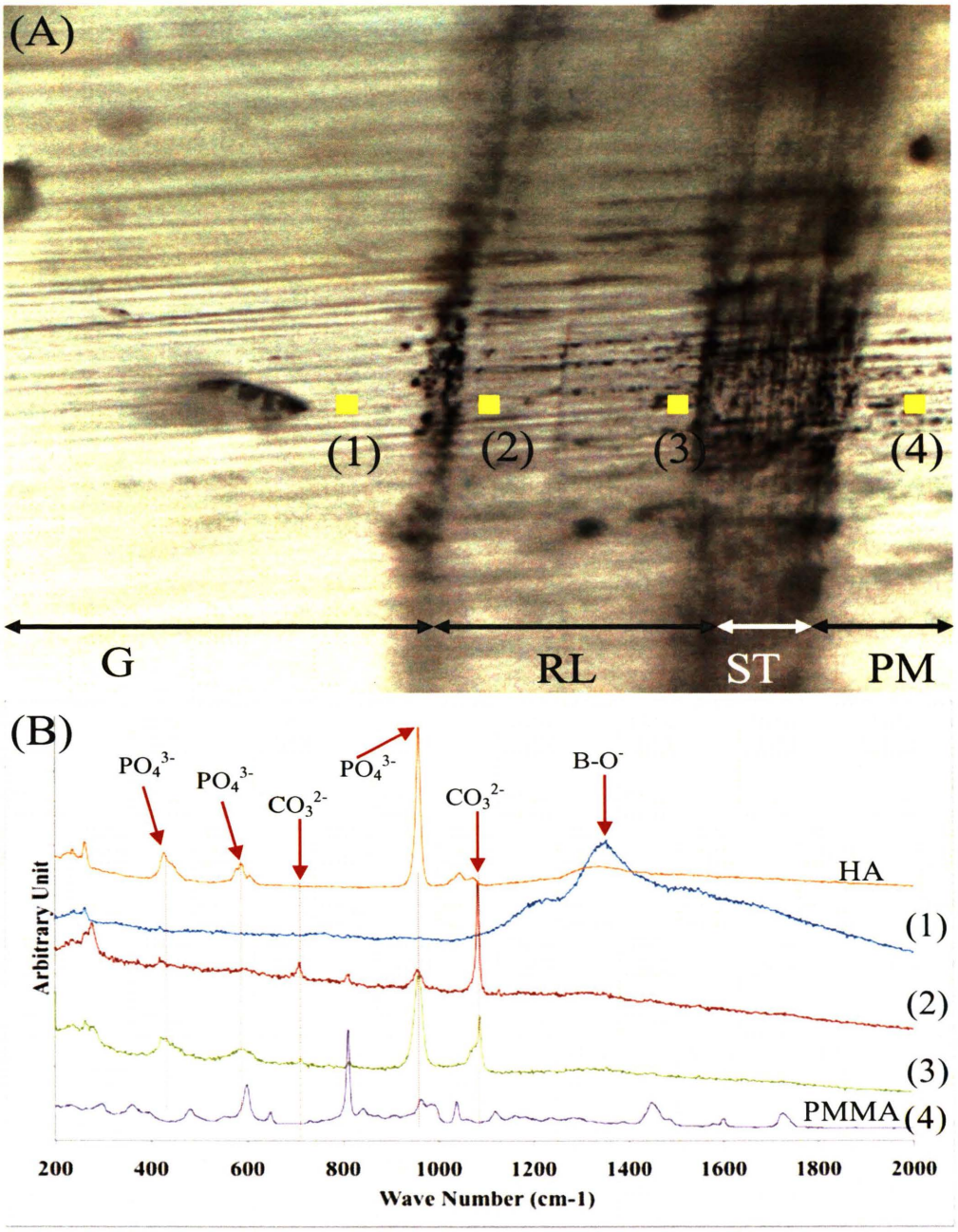

Figure 9. Optical micrograph (100X) of the polished cross-section of the CaLB-0 implanted subcutaneously in a rat for 12 weeks (A). Micro-Raman spectra (B) were collected for the point showed with squares. Carbonate ion (CO_3^{2-}) has 2 peaks at 711 cm^{-1} and 1085 cm^{-1}. Phosphate ion (PO_4^{3-}) represents HA which has 3 major peaks at 420 cm^{-1}, 570 cm^{-1}, and 960 cm^{-1}. The HA spectrum showed as a reference. The lines across the cross section are due to polishing. G: Unreacted Glass, RL: Reacted Layer, ST: Soft Tissue, PM: PMMA, HA: Hydroxyapatite

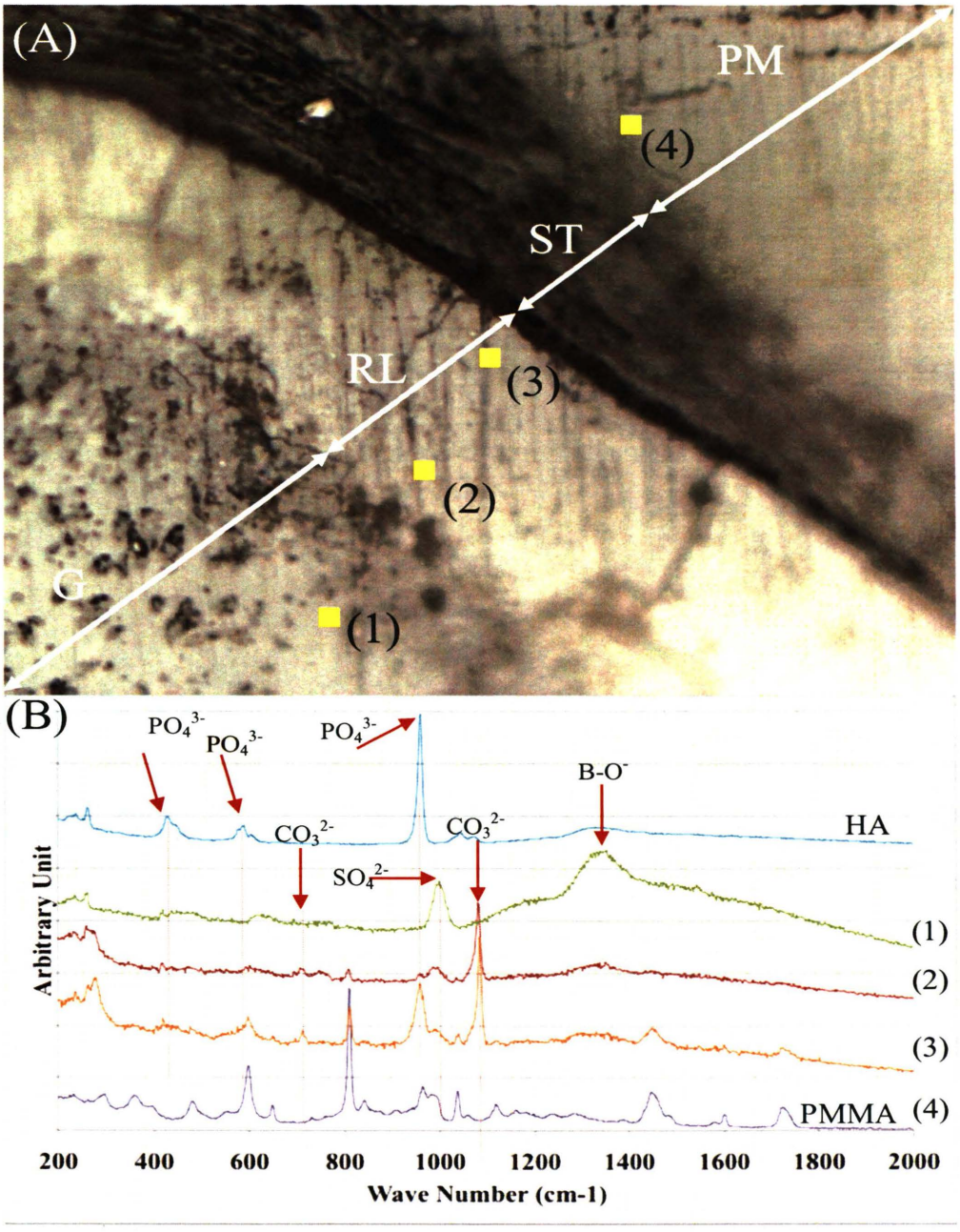

Figure 10. Optical micrograph (100X) of the polished cross-section of the CaLB-12 implanted subcutaneously in a rat for 12 weeks (A). Micro-Raman spectra (B) were collected for the point showed with squares. Carbonate ion (CO_3^{2-}) has 2 peaks at 711 cm^{-1} and 1085 cm^{-1}. Phosphate ion (PO_4^{3-}) represents HA which has 3 major peaks at 420 cm^{-1}, 570 cm^{-1}, and 960 cm^{-1}. The sulfate ion (SO_4^{2-}) has a primary peak at 1000 cm^{-1}. The HA spectrum showed as a reference. G: Unreacted Glass, RL: Reacted Layer, ST: Soft Tissue, PM: PMMA, HA: Hydroxyapatite

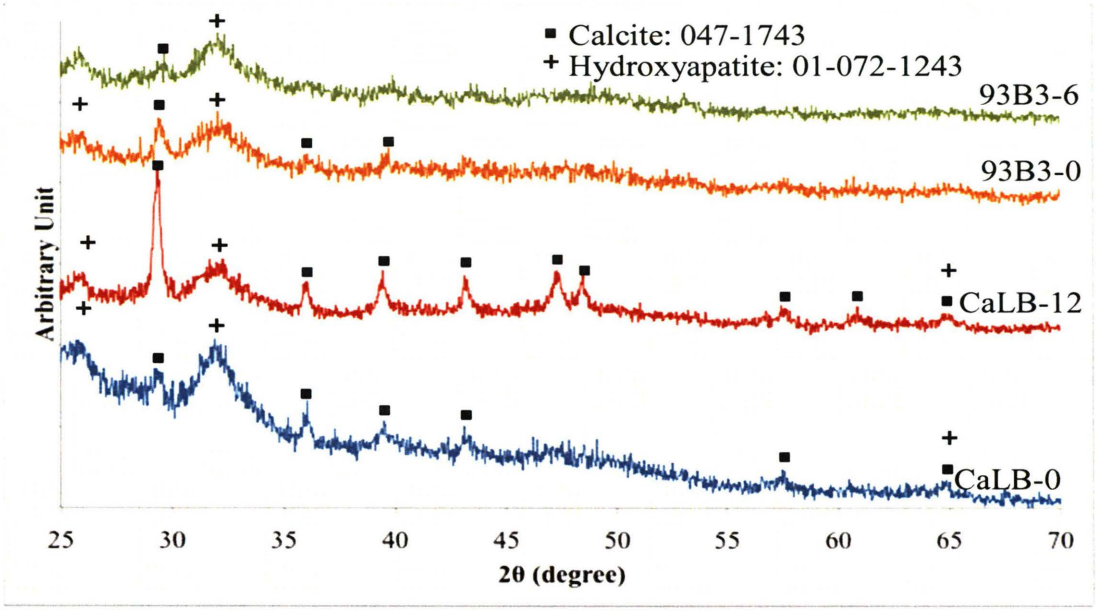

Figure 11. X-Ray diffraction patterns for the glass implants after 12 weeks in the subcutaneous site in a rat. The spectra were collected from 10 to 80 degrees, but only that portion from 25 to 70 degrees are presented here.

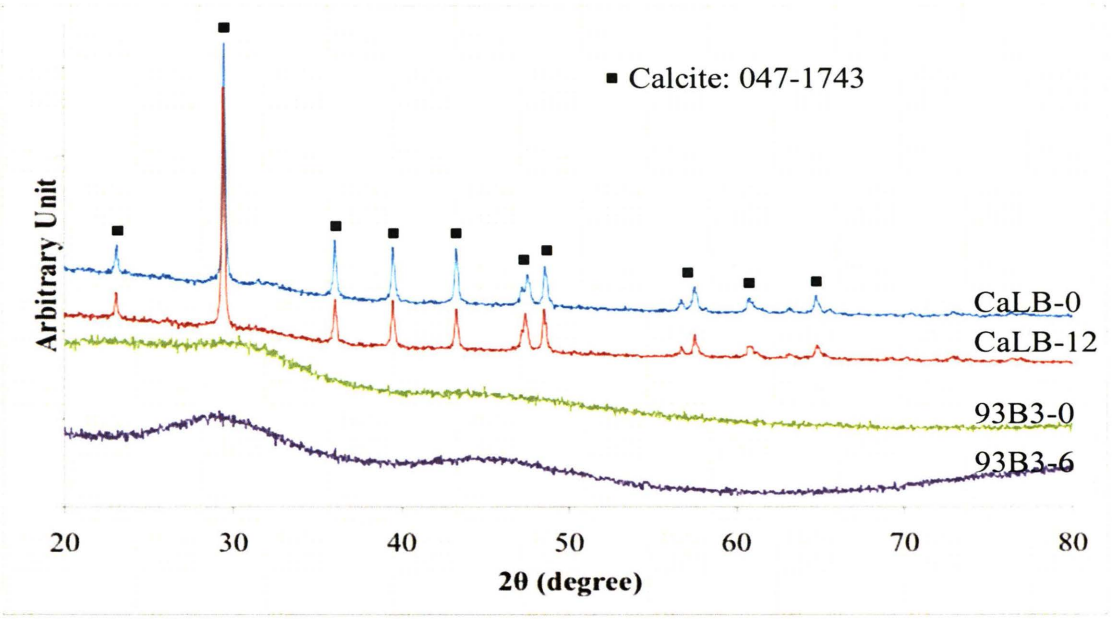

Figure 12. X-Ray diffraction patterns for glass discs reacted *in-vitro* in nSBF for 1 week at 37°C.

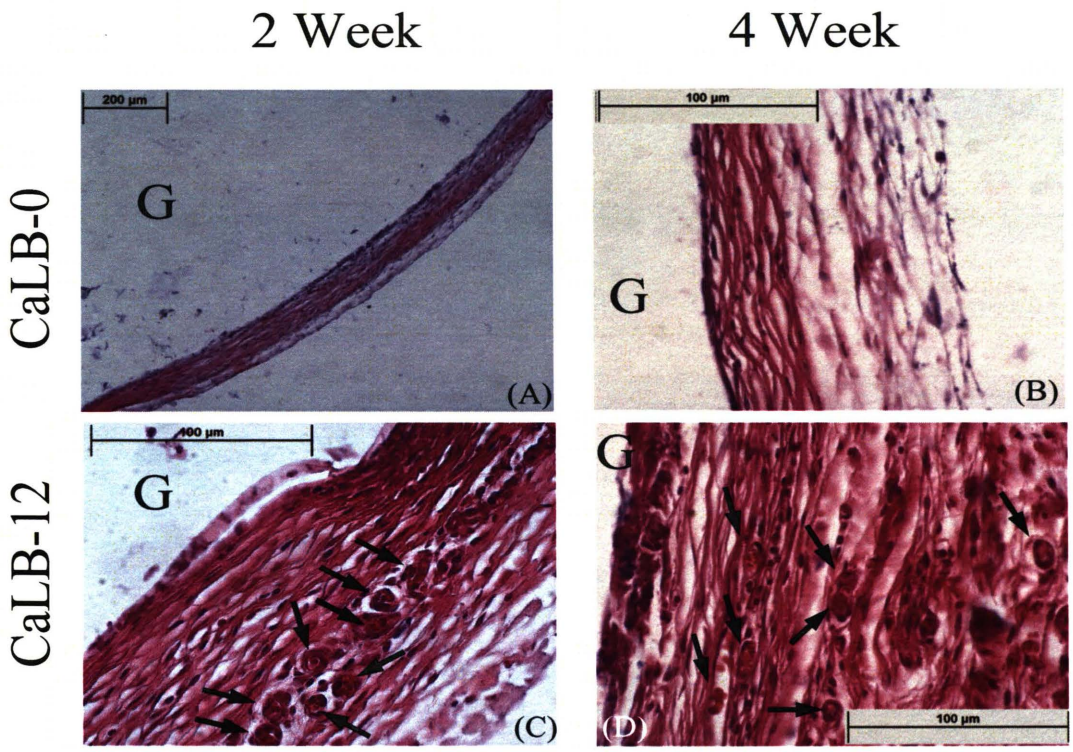

Figure 13. H&E stained sections of the tissue attached to a CaLB-0 and a CaLB-12 implant after 2 and 4 weeks in a rat. (A): CaLB-0, 2W, (B): CaLB-0, 4W, (C) CaLB-12, 2W, (D): CaLB-12, 4W. G: Unreacted (decalcified) Glass. Black arrows point to blood vessels.

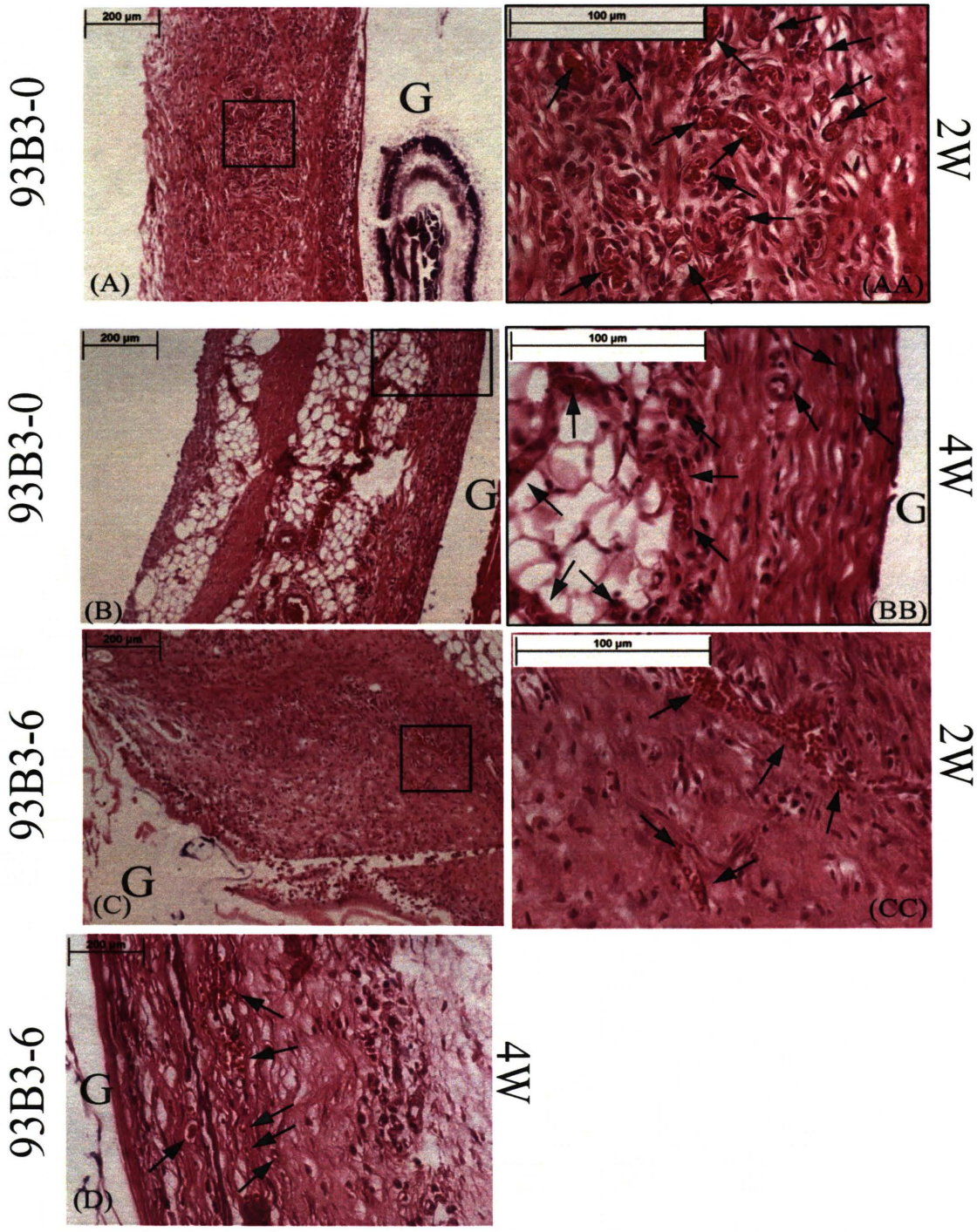

Figure 14. H&E stained sections of the tissue attached to 93B3-0 and 93B3-6 implants after 2 and 4 weeks in a rat. (A,AA): 93B3-0, 2W, (B,BB): 93B3-0, 4W, (C,CC): 93B3-6, 2W, (D): 93B3-6, 4W. G: Unreacted (decalcified) Glass. Black arrows point to blood vessels.

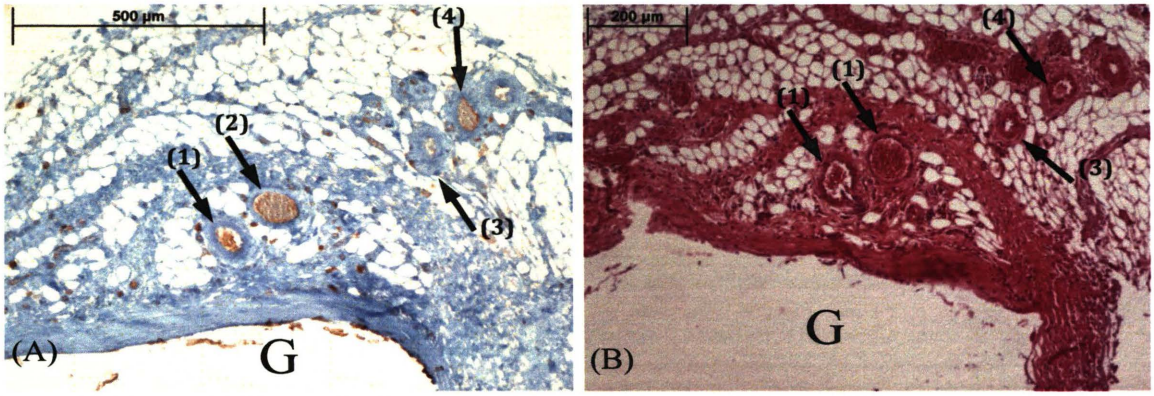

Figure 15. CD31 (A) and H&E (B) stained section of 93B3-0 after 4 weeks in a rat. A sample of 4 blood vessels selected and identified by arrows with assigned numbers. Brown in CD31 section shows platelets or endothelial cells. CD31 identified that these are blood vessels because they stained brown. This confirms that the regions marked with black arrows in the H&E stained section are indeed blood vessels. G= Unreacted (decalcified) Glass.

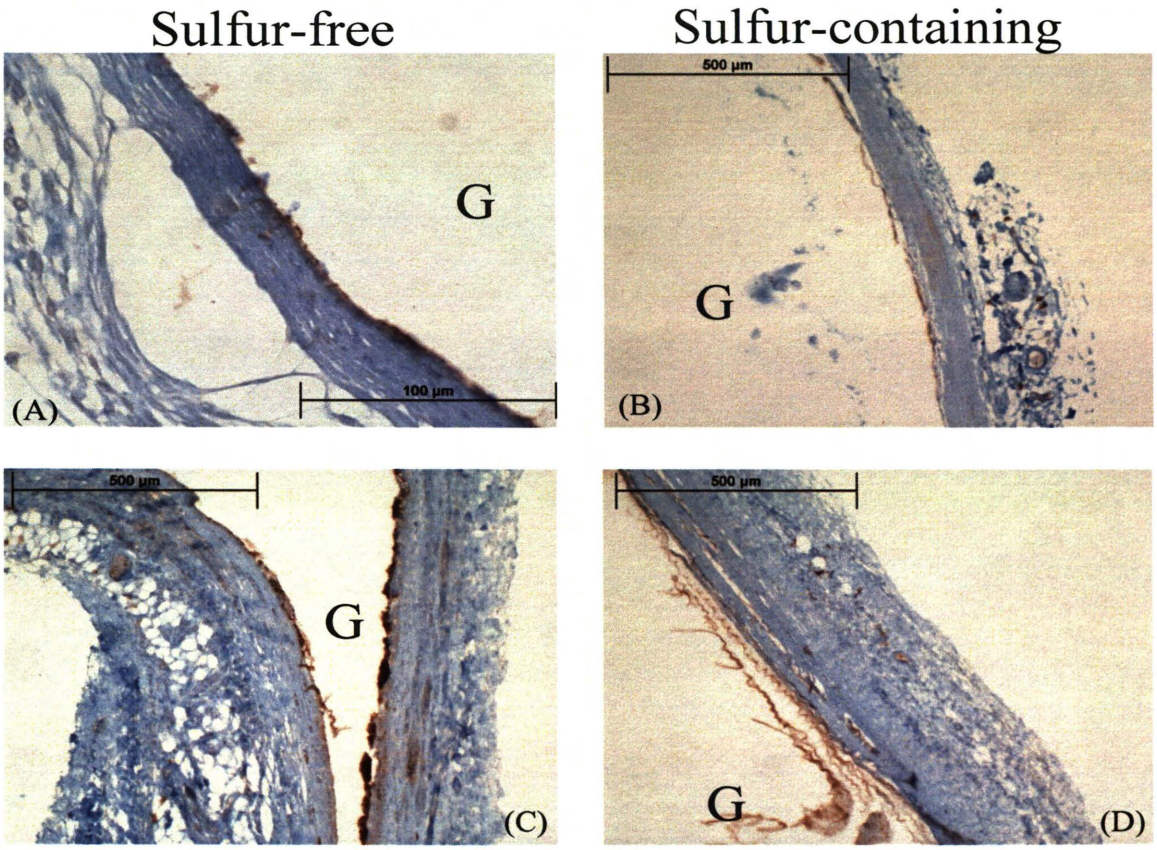

Figure 16. CD31 stained sections of CaLB and 93B3 glasses after 4 weeks in the subcutaneous site in a rat. (A): CaLB-0, (B): CaLB-12, (C): 93B3-0, (D): 93B3-6. Brown color denotes endothelial cells or platelets in CD31 staining and blue is connective tissue. G: Unreacted (decalcified) Glass.

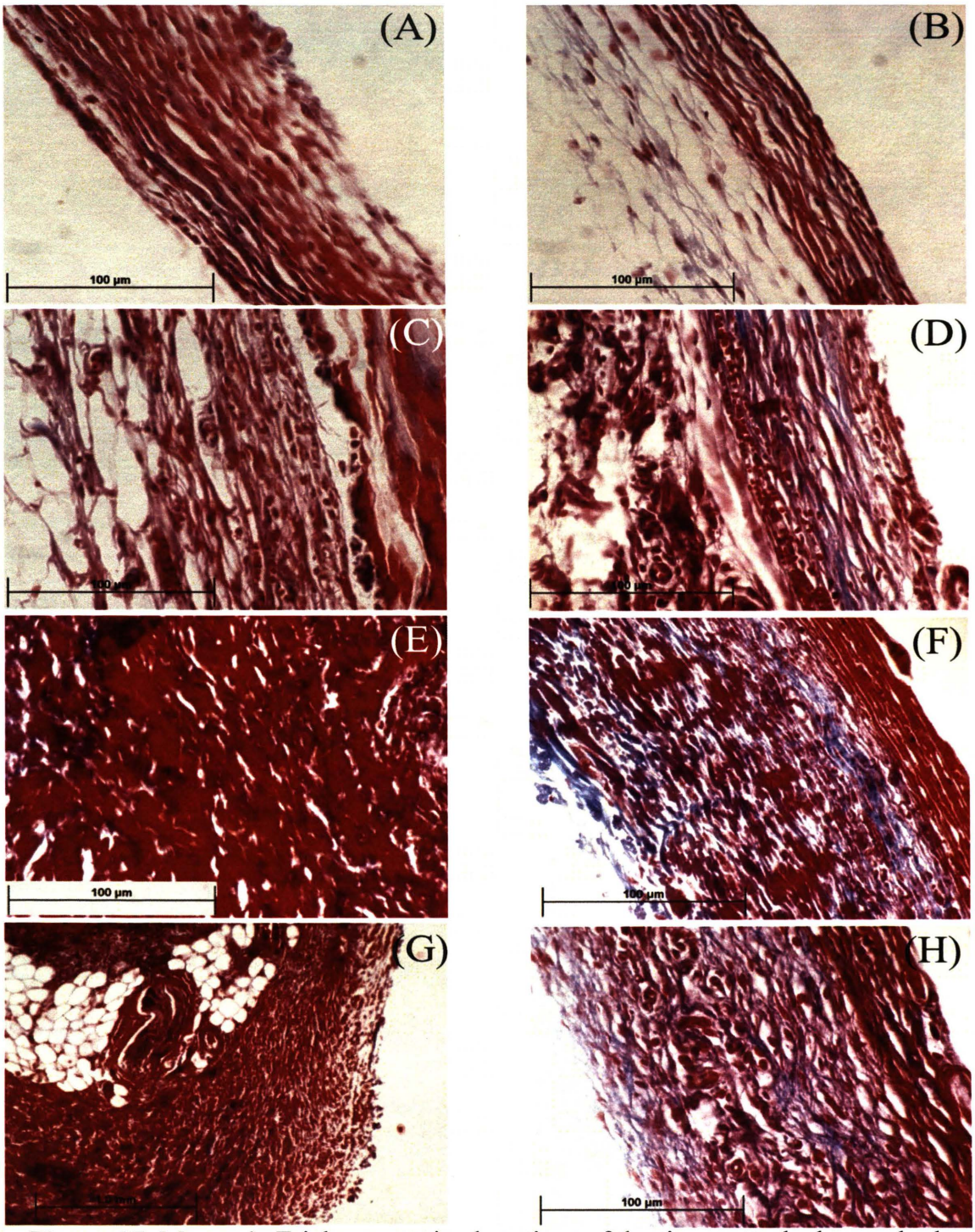

Figure 17. Masson's Trichrome stained sections of the tissue attached to each glass after 2 (left column) and 4 (right column) weeks in a subcutaneous site in a rat. (A,B): CaLB-0, (C,D): CaLB-12, (E,F): 93B3-0, (G,H): 93B3-6. Red= Keratin, Muscle Fibers, Cytoplasm, and Blue= Collagen

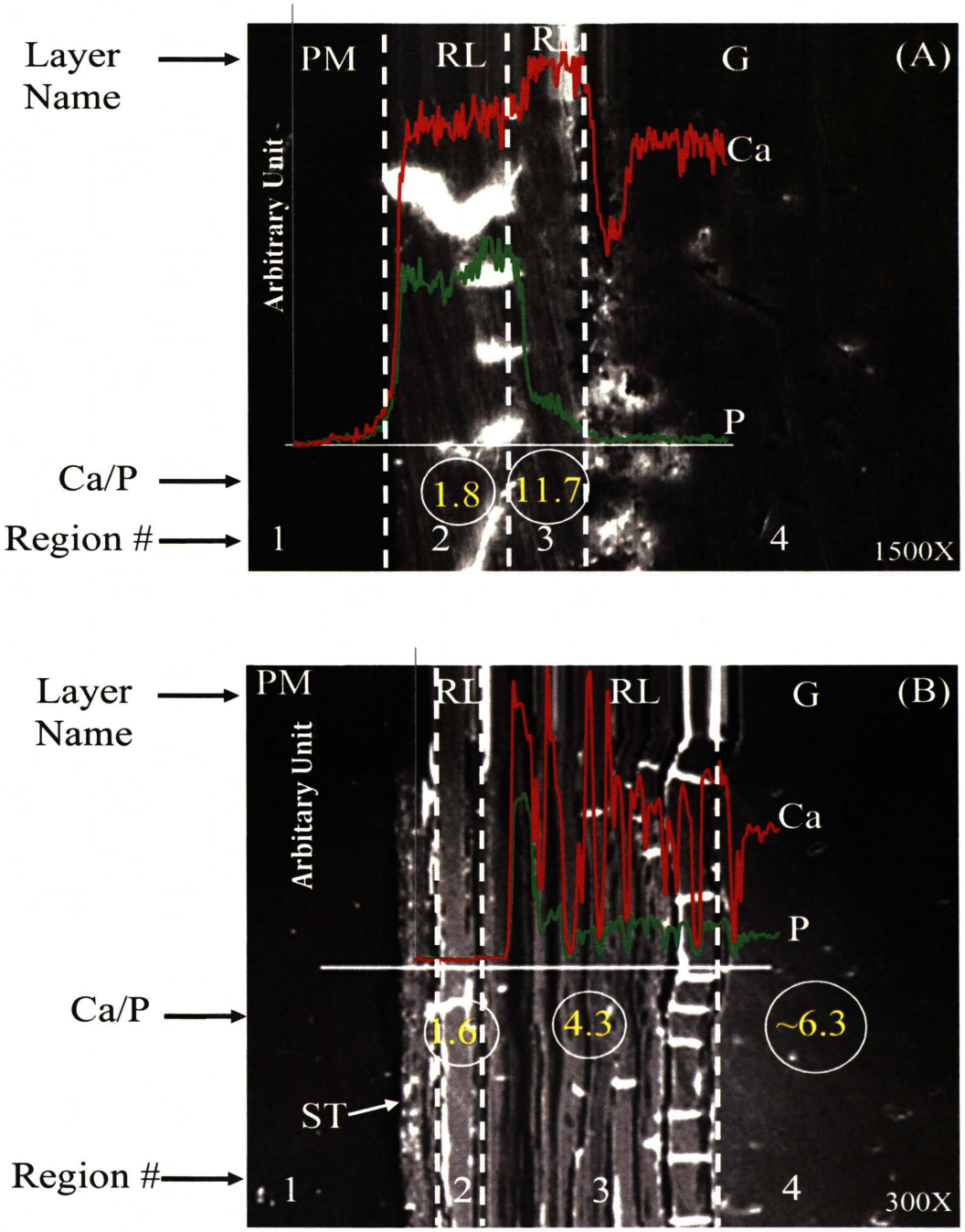

Figure 18. Line-scan (white line) EDS analysis for Ca (red) and P (green) across the reacted layer for a (A) CaLB-0 and (B) 93B3-0 glass implanted subcutaneously for 12 weeks in a rat. G= Unreacted Glass, RL= Reacted Layer, ST= Soft Tissue, and PM= PMMA. The figure shows the intensity of the signal for Ca and P is shown along the scanned line. Ca/P ratio for each region is shown in blue and circled.

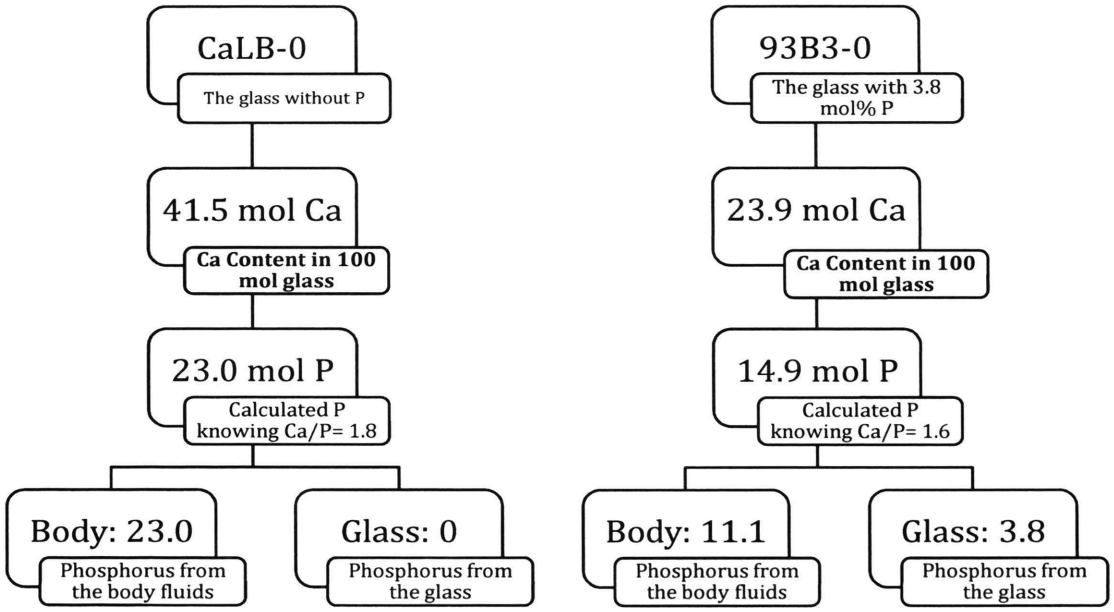

Figure 19. Proposed determination of the source and amount of phosphorus (P) in the reacted layer on CaLB-0 and 93B3-0 implants after subcutaneous implantation for 12 weeks in a rat.

APPENDIX: SUPPLEMENTARY DATA FOR PAPER 2

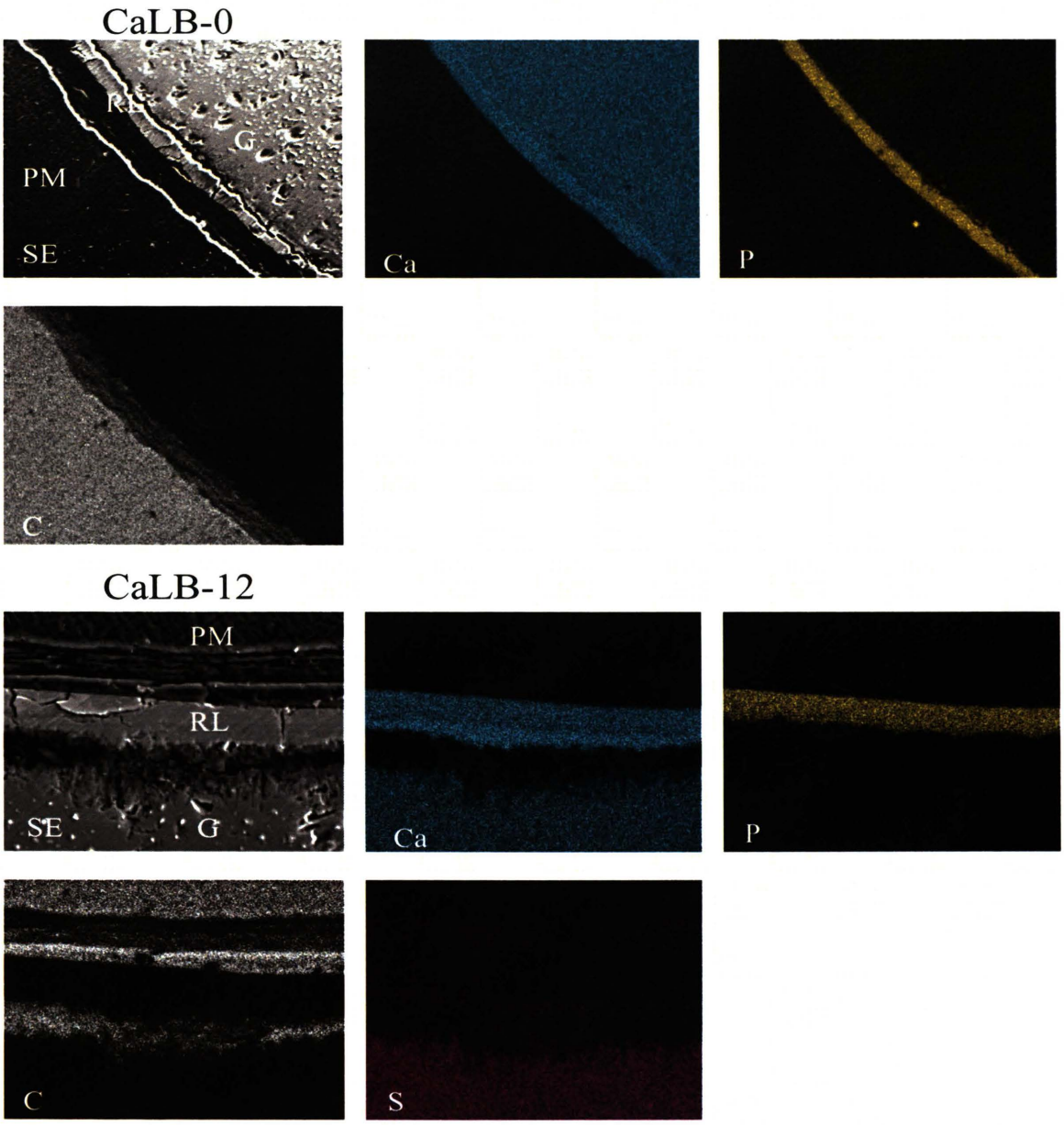

Figure 1. Elemental mapping analysis of the CaLB-0 and CaLB-12 implants after reaction in the subcutaneous site of a rat for 4 weeks and impregnated with PMMA (PM). SE= Secondary Electron, Ca= Calcium, P= Phosphorus, C= Carbon, S= Sulfur, RL= Reacted Layer, G= Unreacted Glass. Dark lines in PMMA regions are formed during the EDS scan due to degradation of PMMA.

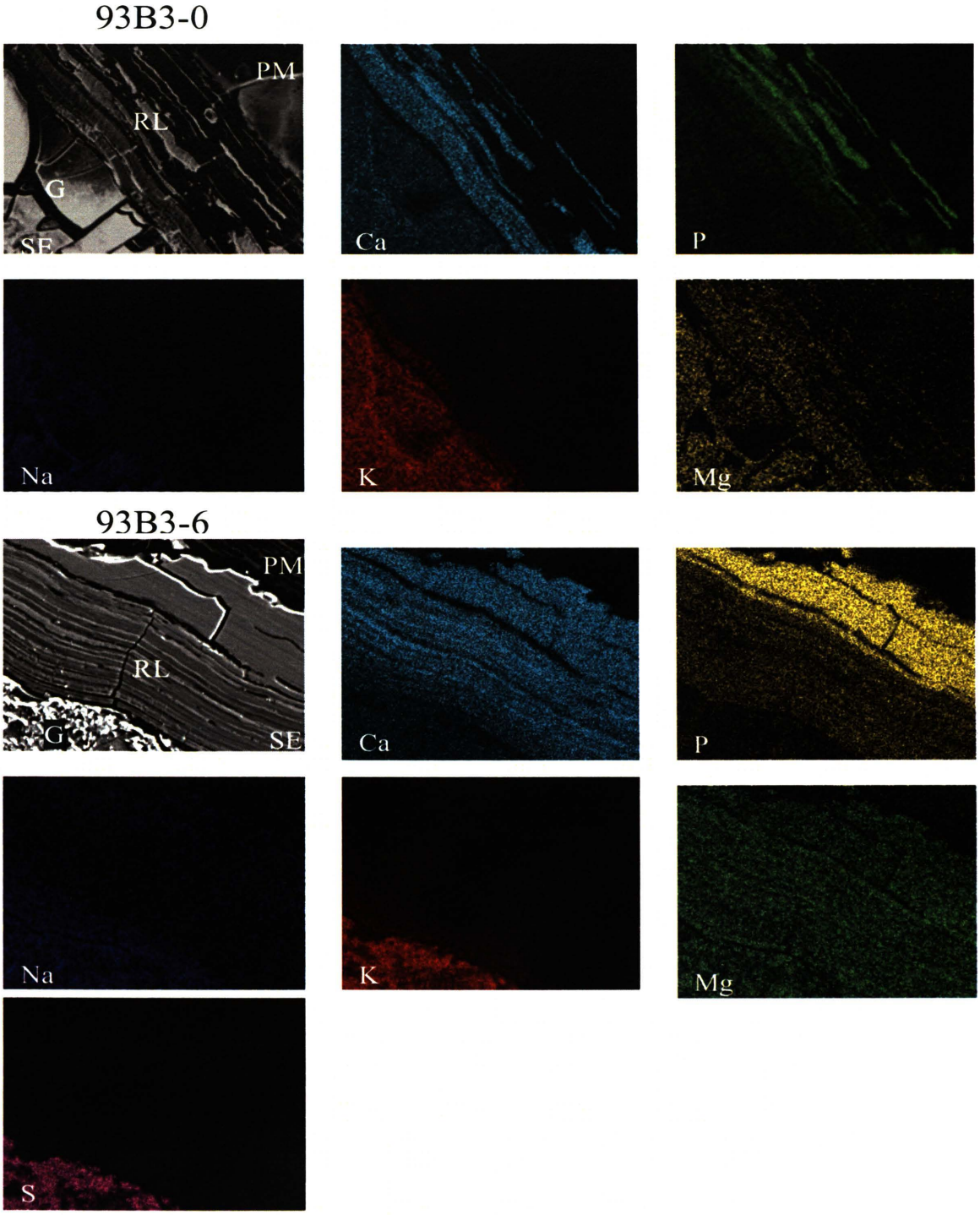

Figure 2. Elemental mapping analysis of 93B3-0 and 93B3-6 reacted in subcutaneous site of a rat for 4 weeks impregnated with PMMA (PM). SE: Secondary Electron, Ca: Calcium, P: Phosphorus, C: Carbon, Na: Sodium, K: Potassium, Mg: Magnesium, PM: PMMA, RL: Reacted Layer, and G: Unreacted Glass.

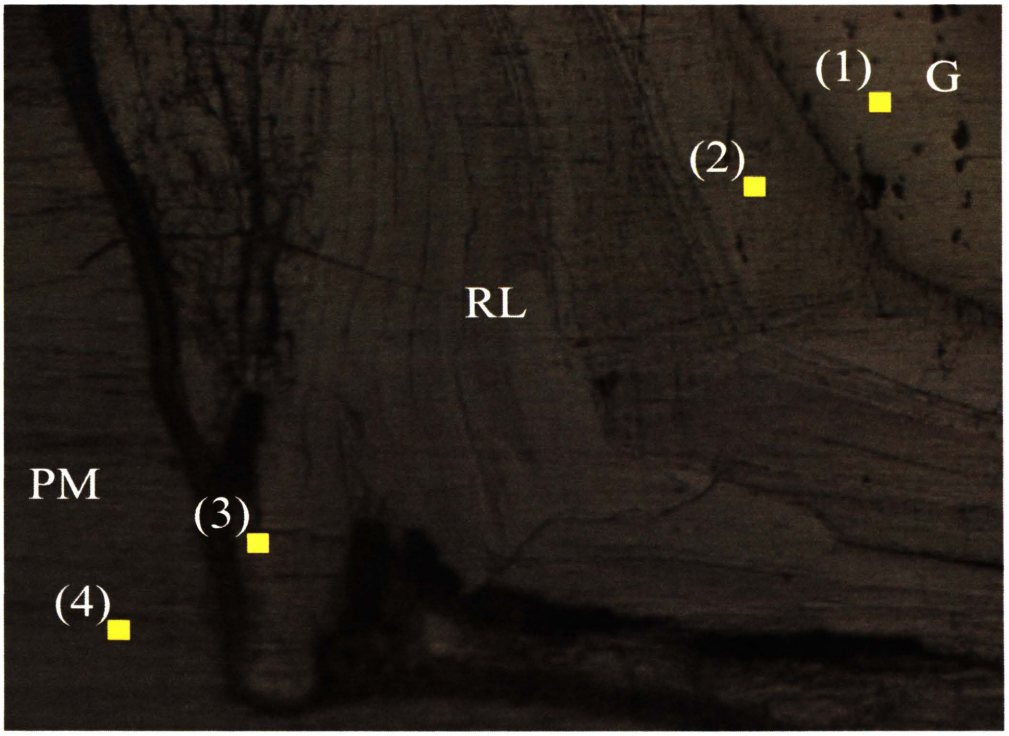

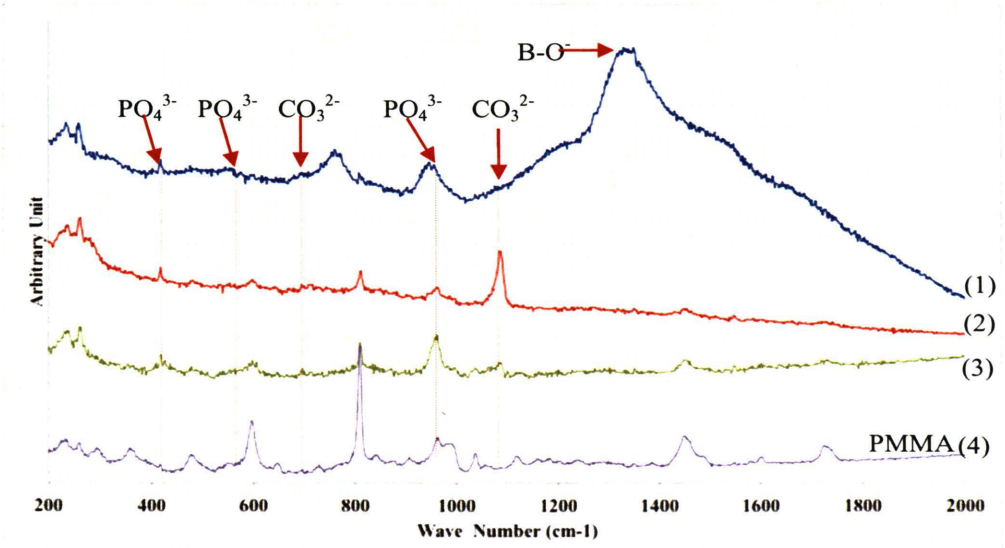

Figure 3. Optical micrograph (10X) of the polished cross-section of the 93B3-0 implanted subcutaneously in a rat for 12 weeks (A). Micro-Raman spectra (B) were collected for the point showed with squares. Carbonate ion (CO_3^{2-}) has 2 peaks at 711 cm^{-1} and 1085 cm^{-1}. Phosphate ion (PO_4^{3-}) represents HA which has 3 major peaks at 420 cm^{-1}, 570 cm^{-1}, and 960 cm^{-1}. G: Unreacted Glass, RL: Reacted Layer, PM: PMMA, HA: Hydroxyapatite.

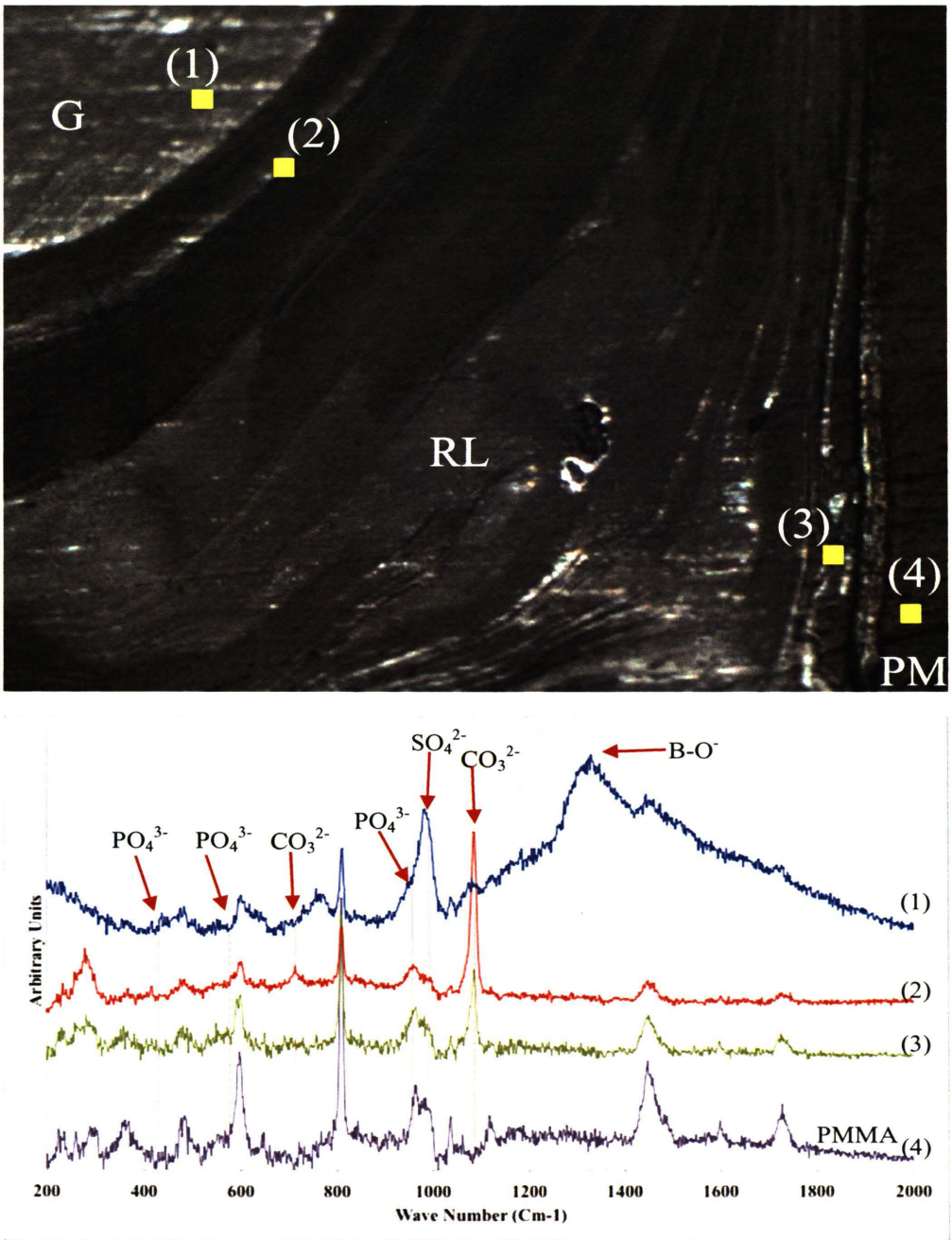

Figure 4. Optical micrograph (10X) of the polished cross-section of the CaLB-12 implanted subcutaneously in a rat for 12 weeks (A). Micro-Raman spectra (B) were collected for the point showed with squares. Carbonate ion (CO_3^{2-}) has 2 peaks at 711 cm^{-1} and 1085 cm^{-1}. Phosphate ion (PO_4^{3-}) represents HA which has 3 major peaks at 420 cm^{-1}, 570 cm^{-1}, and 960 cm^{-1}. The sulfate ion (SO_4^{2-}) has a primary peak at 1000 cm^{-1}. G: Unreacted Glass, RL: Reacted Layer, PM: PMMA, HA: Hydroxyapatite

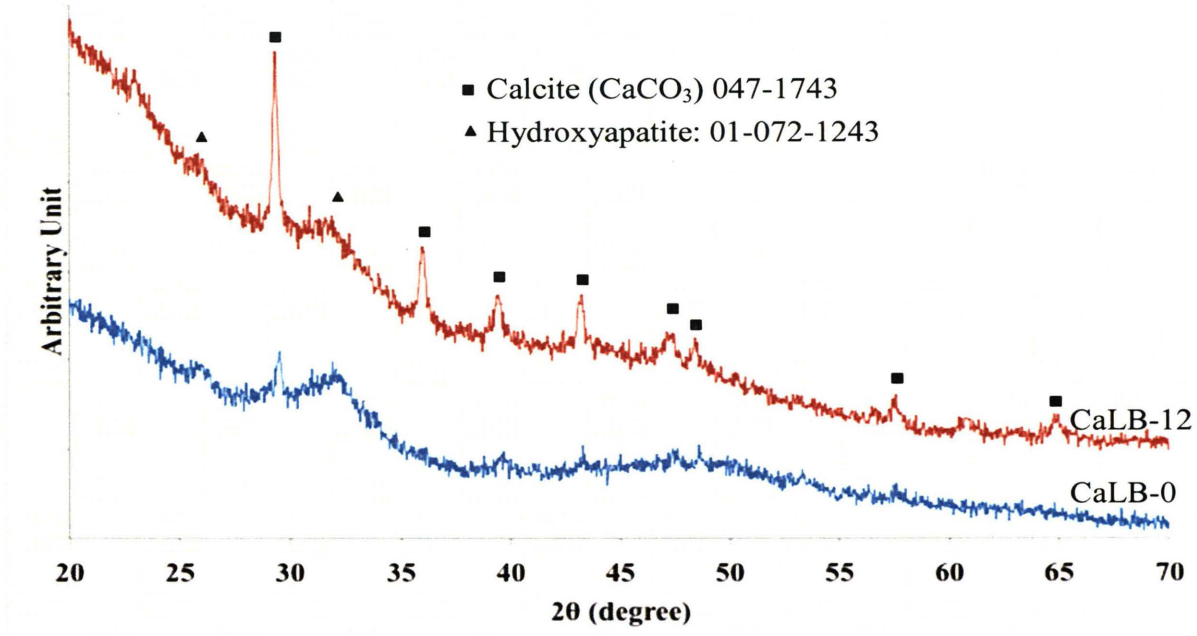

Figure 5. X-Ray diffraction patterns for the CaLB-0 and CaLB-12 glass implants after 2 weeks in the subcutaneous site in a rat. The spectra were collected from 10 to 80 degrees, but only that portion from 20 to 70 degrees are presented here.

VITA

Ali Mohammadkhah was born in Tehran, Iran on September 19, 1987. He earned his bachelor's degree in Chemical Engineering from the University of Tehran in June 2009. In the same year (August 2009) he was accepted at Missouri S&T to pursue his graduate studies in the Material Science and Engineering department under the supervision of Professor Delbert Day, Curators' Professor Emeritus of Materials Science and Engineering.

As a research assistant in The Center of Bone and Tissue Repair and Regeneration (CBTRR) he chose bioactive glasses for bone repair as the subject for his master's degree. During his master's studies he worked to develop a borate glass containing sulfur. Studying the effect of sulfur on the conversion of these glasses in-vitro (in phosphate solution) and (in rats) was the major part of his research. Ali earned his master's degree in Material Science and Engineering in May 2012.